EFFECTS OF PHYSICO-CHEMICAL PROPERTIES OF SODIUM EXCHANGED ZEOLITES ON THE FATE OF MALATHION IN WASTE WATER

BY

ELLY TETY OSEWE

A THESIS SUBMITTED IN FULFILLMENT OF THE

REQUIREMENTS FOR THE DEGREE OF DOCTOR OF PHILOSOPHY IN CHEMISTRY

SCHOOL OF BIOLOGICAL AND PHYSICAL SCIENCES

MASENO UNIVERSITY

©2017

ABSTRACT

Adsorbents are applied in the removal of organic pollutants from wastewaters. One of the main adsorbents that have been widely used is activated carbon. However, activated carbon is associated with high operational costs, hence the need to design low cost alternatives. Various materials such as magnetic nanoparticles and zeolites have been used in the purification of polluted waters with varied merits and demerits. Among the well-studied water pollutants are pesticide residues. Considering the great potential of zeolites, this study examined its utility for the removal of a model pesticide, malathion, from wastewaters. The overall objective of this study was to explore the effects of physico-chemical properties of sodium exchanged zeolites on the fate of malathion in fresh waters. The effects of Si/Al ratio, diffusion dimensionality, pore/channel size and particle size of the zeolites mordenite (MOR), ferrierite (FER), ZSM-5 (MFI) and USY (FAU) on the adsorption and degradation kinetics of malathion were studied. Water samples for treatments were collected from Monjolinho River in Brazil. The zeolites were characterized by XRD, FTIR, AAS, SEM, and ^{27}Al-MAS-NMR, and then used to treat 500 mL of water sample in the ratio of one unit cell of zeolite to one molecule of pesticide in triplicates in the laboratory and analyses done at selected intervals up to 72 h. The concentrations of the remaining pesticides and their metabolites in solutions were determined using a GC-MS while the means and standard deviations were obtained by SPSS. Malathion degradation was enhanced in Na-zeolites with half-life (t½) in fresh water of 49.5 h. Additionally, the t½ of 16.5, 30.3, 24.8, and 29.7 h were realized in faujasite, mordenite, ZSM and ferrierite, respectively. The degradation kinetics of malathion in fresh water was pseudo-first order (R^2=0.996) with rate constant of -0.144±0.010 h^{-1} compared to other zeolites. Na-faujasite had the highest percentage degradation of malathion. High Si/Al ratio encouraged degradation of malathion. Effectiveness of dimensionality decreased in the order of 3D, 2D 1D. Larger channeled zeolites enhanced the dissipation of malathion in water. Major degradation products of malathion in water were malathion mono and dicarboxylic acids and upon introduction of zeolite were eliminated. Analysis of the zeolites after adsorption by XRD showed enhanced stability and crystallinity of the zeolite structure. The decrease in weight below 500°C observed from TGA curves was as a result of malathion thermal decomposition and desorption. The FTIR, NMR, SEM and EDS detected interaction of malathion molecules with the zeolite structure without formation of new chemical bonds between malathion and zeolites.

CHAPTER ONE

INTRODUCTION
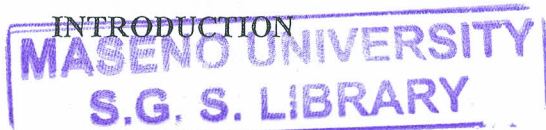
1.1 Background of the study

The removal of hazardous materials from wastewater is one of the most important environmental issues to be solved today. Since 1960s, molecular sieve zeolites have substantially impacted adsorption and catalytic process technologies throughout the chemical process industries; provided timely solutions to energy and environmental problems such as air and water purifications; and grown to over a hundred million dollar industry worldwide. Materials with very narrow pores in the nano-scale range, that is, from ca. 0.1 to 100 nm, are commonly referred to as nanoporous materials. Notably, the lower end of this range from ca. 0.1 to 1 nm, coincides with the dimensions of the vast majority of environmental pollutant molecules. The similarity of molecular dimensions and pore widths forms the basis for some unique and most striking applications of nanoporous materials in modern separation processes and heterogeneous catalysis (Shoumkova, 2011).

The evolution of zeolite materials with improved or novel properties has strongly influenced the expansion of their applications, and provided new flexibility in the design of products and processes (Flanigen, 1980). However, zeolites and catalyst-coated membranes face challenges as have always faced ceramic water treatment membranes, that is, high manufacturing cost and low packing densities. Specifically, the target solutes can be those which require complete removal due to high influent concentrations and/or strict effluent regulations, or which show poor removal with other adsorbents (Kowenje &Osewe 2015).Notably, due to its selective nature, adsorption on zeolites should only be considered as an additional treatment step to existing water purification plant processes, dedicated for the removal of specific organic micro-pollutants. Literature reports how zeolites that differ only by their cages, channels or cavity dimensionalities (1, 2, or 3 dimensional) and "door" openings, their Si/Al ratios, and unit cell sizes have shown varied successes in removal and abstraction of selected molecule(Shoumkova, 2011, Kowenje &Osewe 2015).Likewise, different molecules that poses similar functional groups though differ in their molecular sizes have also shown varied interaction by a given zeolite (Junghoet al., 2011, Wilkinson, 2014). However, the observed interplay between the zeolite physico-chemical properties and the

1

adsorbates molecular properties is yet to be better understood. This study with zeolitic adsorbents and catalysis could represent a simple solution to the problem of cleaning up industrial wastewater as well as recovering valuable chemicals at relatively low costs. Thus due to its branched chemical structure and intermediate molecular size malathion was a model pesticide in this study. The interactions of the extensively branched chemical structure of malathion with the various channels and cages of mordenite, (MOR), ferrierite (FER),ZSM-5(MFI) and USY(FAU) zeolites is not yet documented

1.2 Statement of the problem

Due to heavy agricultural industrialization in Sao Carlos area, River Monjolinho is bound to be heavily polluted by malathion pesticide. Malathion is a general purpose organophosphorus contact insecticide employed in controlling insects of household, home, garden, stored grains, greenhouse, agriculture, forestry and public health. It is among the main pesticides found in waste water. Technologies that are currently being employed in water purification lack the capacity and efficacy to eliminate pesticides and their degradation products from waters. The zeolites that are touted as the panacea to this deficit are also limited by the interactions of their physical and chemical properties with the target adsorbate pollutants. Thus, specific adsorbates would only be effectively adsorbed or degraded by zeolites of specific physico-chemical characteristics. However, the matching of that specific zeolite to the specific adsorbate is still a challenge. The individual effects of the cages, channels or cavity dimensionalities (1, 2, or 3 dimensional), "door" openings, their Si/Al ratios, and unit cell sizes of zeolites and the resultant solution pH on fate of malathion dissipation in waste water is not well understood.

In this work, six zeolites of varied structural dimensions and Si/Al ratios, *viz.* mordenite (MOR), ferrierite (FER), ZSM-5 (MFI) and USY (FAU), were utilized for abstraction of malathion from water under laboratory conditions. The effects of cage, channel, and cavity dimensionality, resultant solution pH, and the Si/Al ration of the zeolite types and their time-dependency kinetics and adsorption equilibrium behavior modelized using Langmuir and Freundlich isotherm models are discussed.

2

1.3 Objectives of the Study

1.3.1 Broad Objective

To explore effects of some physico-chemical properties of sodium exchanged zeolite on the removal of malathion in waste water.

1.3.2 Specific Objectives

To help facilitate the broad objective, there were five specific objectives:

i. To determine the effects of zeolite Si/Al on the water pH;
ii. To determine the effects of Si/Al and water pH on malathion dissipation half-life;
iii. To determine the effects of zeolite channel opening and dimensionality on malathion dissipation half-life;
iv. To identify the metabolites produced and the kinetics of the reaction;
v. To determine impacts of malathion exposure on zeolite structure.

1.4 Hypothesis

The rate of degradation and the possible breakdown products of pesticides are affected by the channels, cages and Si/Al ratios of the adsorbent zeolites and the resultant pH of the reaction medium.

1.5 Null hypotheses

i. There is no effect of zeolite Si/Al on the solution pH;
ii. Si/Al and solution pH does not affect dissipation half-life of malathion;
iii. Channel opening and dimensionality has no effect on malathion dissipation half-life;
iv. It is not possible to identify the metabolites produced in this reaction
v. Structure of zeolite is not affected by exposure of malathion.

1.6 Justification of the study

Pesticides and pesticide residues are a problem in drinking water treatments and use of zeolites to trap and degrade the hazardous pesticides from the environment is vital. It has been noted that the degradation products of pesticides depend on the type of zeolites used. Therefore comparison study should be done with other types of zeolites of different cage dimensionalities and silicon-aluminum ratio to establish which one is more effective with the

3

model malathion pesticide. Finally, scientific data on degradation kinetics of pesticides as affected by physico-chemical properties of zeolite is lacking.

CHAPTER TWO

LITERATURE REVIEW

2.1 Introduction

The removal of hazardous materials from wastewater is one of the most important environmental issues to be solved today. Since 1960s, molecular sieve zeolites have substantially impacted adsorption and catalytic process technology throughout the chemical process industries; provided timely solutions to energy and environmental problems such as air and water purifications; and grown to over a hundred million dollar industry worldwide. Materials with very narrow pores in the nano-scale range, that is, from ca. 0.1 to 100 nm, are commonly referred to as nanoporous materials. Notably, the lower end of this range from ca. 0.1 to 1 nm coincides with the dimensions of the vast majority of environmental pollutant molecules. The similarity of molecular dimensions and pore widths forms the basis for some unique and most striking applications of nanoporous materials in modern separation processes and heterogeneous catalysis (Shoumkova, 2011)

The evolution in zeolite materials with improved or novel properties has strongly influenced the expansion of their applications, and provided new flexibility in the design of products and processes (Flanigen, 1980). However, zeolites and catalyst-coated membranes face challenges as have always faced ceramic water treatment membranes, that is, high manufacturing cost and low packing densities. Specifically, the target solutes can be solutes which require high removal due to high influent concentrations and/or strict effluent regulations, or which show poor removal with other adsorbents (Kowenje &Osewe 2015).Notably, due to their selective nature, adsorption on zeolites should only be considered as an additional treatment step to existing processes, dedicated for the removal of specific organic micro-pollutants. The approach with zeolitic adsorbents and catalysis could represent a simple solution to the problem of cleaning up industrial wastewater as well as recovering valuable chemicals at relatively low costs. This section will therefore discuss the development and the applications of zeolites and the nature and interactive properties of pesticides and to lay ground for the study on these very zeolitic properties with malathion.

2.2 Identification and development of nano- materials

The development in process catalysts during the last few decades have been mandated mainly by considerations related to the abatement and prevention of pollution, conservation of raw materials and eco-friendly production of fine chemicals. With growing ecological concern, chemical procedures have been subjected to increasing pressure to minimize the dispersion of waste chemical (Gadekar, Katkar, Vidhate, Arbad, & Lande, 2008).Zeolites in particular and nanoporous materials in general play an important role in chemical processing in which they can be successfully used as adsorbents, catalysts, catalyst supports and membranes and form the basis of new technologies (new, more efficient and environmentally fully acceptable processes) mainly due to their unique structural and surface properties(Shoumkova, 2011). Among the unique features of zeolites compared to more conventional solid catalysts or catalyst supports are (i) their strictly uniform pore diameters and, (ii) pore widths in the order of molecular dimensions. Bearing in mind the pertinent IUPAC classification for: micropores: 2.0 nm $\geq$ dp, mesopores: 2.0 nm < d $\geq$ 50 nm and, micropores: dp> 50 nm, where with dp being the pore diameter, zeolites are typical microporous materials (Weitkamp, 2000).

Jungh et al.(2011) asserted that for nanoparticles, shape and size of the openings are very important. In a study on production of aromatic compounds from glucose, the aromatic yield was a function of the pore size of the zeolite catalyst. In addition to pore window size, internal pore space and steric hindrance play a major role for aromatic production. The kinetic diameters of the products and reactants were estimated to determine whether the reactions occur inside the pores or at external surface sites for the different zeolite catalysts. The different pore window size of zeolites ranging from 5 Å to 12 Å causes a mass transfer effect excluding certain reactant molecules based on size relative to the zeolite pore window size. In a similar manner, zeolites limit the formation of products (i.e. high mass-transfer-limited products) larger than the pore size of the zeolite.

Shape selectivity is also related to confined spaces within the pores (that is, pore intersections). Such a confined space restricts certain transition states and influences the course of reaction. Zeolite chemistry can also be further complicated due to reactions on the exterior of the zeolite surface. In addition, zeolites can cause a ''confinement effect'' or ''solvent effect'' where the concentration of different reactants is higher inside the zeolite pores than in the gas phase. Therefore, the role of pore size and shape on the catalytic

chemistry must be better understood if zeolites are to be designed for improved environmental remediation applications.

2.2.1 Zeolites

The name "zeolite" originated from the union of two Greek words, zeo which means boi l and lithos which means stone. This designation was assigned by Baron Cronsted 1756, a Swedish Mineralogist, a group of natural minerals that after the rapid heating skipped as the water evaporated(Occelli & Robson, 1989).Zeolites are known for over 250 years and are form ed in different geological environments. Zeolites are hydrated aluminosilicates of a crystalline structure with precise geometry and uniform size of nanopores, forming channels of molecular dimensions with special properties to be used as molecular sieve, ion exchanger and selective adsorbent (Breck, 1974; Kazemimoghadam& Mohammadi, 2007). Currently, these minerals are of great interest in catalysis, but in its natural form have limitations due to the presence of impurities and variations in chemical composition in different deposits, or even in the same deposit. A major event was the introduction of faujasite (zeolite X and Y) in industrial scale, the process of fluidized catalytic cracking (FCC) (Weitkamp, 2000).The fluidized catalytic cracking is one of the most important industrial catalytic processes as well as the most important oil refining process(Kowenje &Osewe 2015).

Besides applications in catalysis, zeolites are being applied in various fields. In separation processes, zeolites are used as drying agents in gas purification, separation of paraffins from branched linear, separation of xylene isomers. The greater use of zeolite is related to the manufacture of detergents. In this application we use the zeolite entering in the formulation of detergents as a sequestering agent to replace phosphates. Because of its cation-exchange properties, the zeolite acts in detergent removing ions contained in water that may hinder foam production. Zeolites are used in the treatment of effluents containing radioactive materials, as a supplement to animal and soil improvements (Kowenje &Osewe 2015). These materials are synthesized with the aid of surfactant molecules, and, although not having the crystal structure, show regular distribution of pores, whose size can vary between 15 and 200 Å (Vartuli, Shih, Kresge, & Beck, 1998).The primary family is the M41S mesoporous sieves discovered by Mobil MCM-41 is a member more extensively investigated (Weitkamp, 2000).

7

2.2.1.1 Structure of zeolites

A zeolite is a crystalline aluminosilicate with a framework based on an extensive three-dimensional network of oxygen ions. Situated within the tetrahedral sites formed by oxygen may be an ion Si^{4+} or Al^{3+} (Meier & Olson, 1970). The AlO_2^- determines the load of the structure. This is balanced by cations in positions outside the structure. Equation 01 shows a representative empirical formula for a zeolite can be written as: $M_2/NO. Al_2O_3. x SiO_2. yH_2O$ Where M represents an exchangeable cation, generally, ions of Group I or II, although other metals, non-metals and organic cations may also be used to balance the load of the structure, while N represents the valence of the cation. These cations are inserted into the structure during the synthesis or by ion exchange after the synthesis. The value of x must be greater than or equal to 2, because Al^{3+} does not occupy adjacent tetrahedral sites. The crystal structure contains voids (cavities and channels) of mild size, unlike molecular sieves micro porous charcoal, which have a pore distribution in a bigger range, and sometimes quite irregular. Water molecules present in the structure are located in these channels and cavities, as well as cations which neutralize the negative charge created by the presence in the structure of AlO_2^-. Cations which normally may be placed within the micro porous channels of zeolites are: alkali (Li^+, Na^+, K^+, Rb^+, Cs^+), alkaline earth (Mg^{2+}, $Ca^{2+,}$ Ba^{2+}), NH_4^+, H_3O^+ (H^+), tetra methyl ammonium (TMA^+), other nitrogen-containing organic cations, rare earth ions and noble metals(Zhao et al., 1988).

In an attempt to formulate how these complex structures crystallize, scholars have proposed a model based on construction units. These units were called secondary building units (SBU's). The secondary building units are based on the Parsimosy Pauling rule. Based on this rule, the structures of zeolites can be constructed from a type of SBU's (Szostak, 1998). As every rule has an exception, there are structures that require more than one type of SBU's. Figure 1 presents some types of SBU's, with T atoms (T = Si or Al) located at the vertices and each edge represents a link T-O-T. Currently, 23 types are used in SBU's to describe the structures of zeolites (Baerlocher, McCusker, & Olson, 2007).
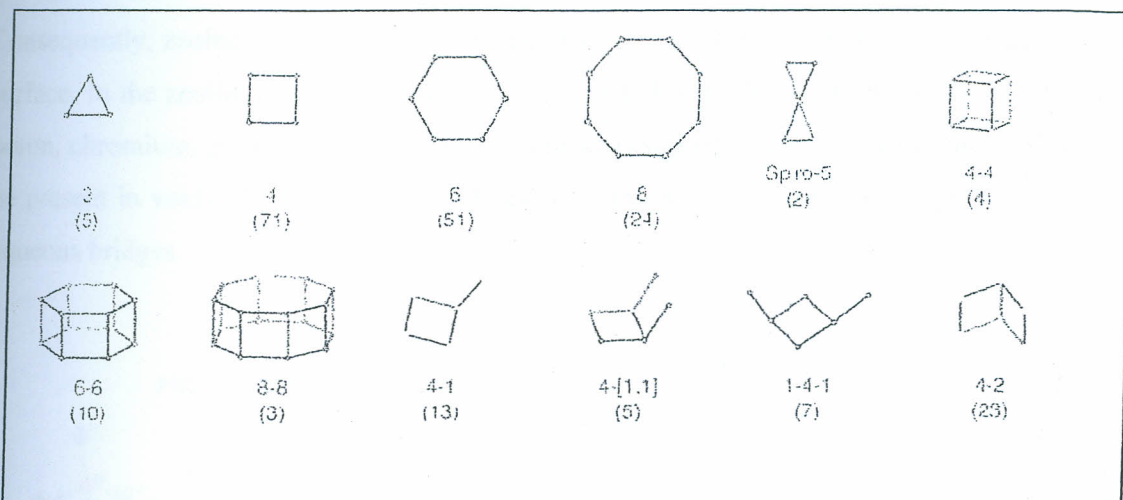
Figure 1: Secondary building units (Baerlocher, McCusker, & Olson, 2007)

After analyzing the pore size consider the pore system of a zeolite. This level of classification takes into account two important features: the dimensionality of the channel system and the format of opening pores.

The pore size is very important in catalytic applications. The clogging of the zeolite pores caused by stacking faults or accumulation of hydrocarbons within the pores decreases their adsorption and catalytic properties (Zhao*et al.,* 1988).The porous system of a zeolite can be one, two or three dimensional. Structures that have channels in three directions allow greater mobility of chemical species within it, and thus are less susceptible to deactivation(Luna, Ukawa, Wallau, & Schuchardt, 1997), it is important to classify a zeolite in terms of the volume of voids it is having, that is, the accessible space for the molecules to be adsorbed. The adsorption capacity of a zeolite can be expressed in terms of the density of the structure. The density of a structure is defined as the number of T atoms per 1000 $Å^3$. Structures with lower densities have greater void volume (Zhao*et al.,* 1988).

2.2.1.2 Zeolite Framework

According to (Karmen, Nataša, Šiljeg, & Farkaš, 2013), the structure of zeolite is very interesting and complex. The primary building units (PBU) of zeolites are the SiO_4 and AlO_4tetrahedra, generally referred to as TO_4tetrahedra. They connect via oxygen atoms into secondary building units (SBU), which are then linked into a three-dimensional crystalline structure to form zeolite framework. Substitution of Si by Al generates the negative charge of

the zeolite framework, which is compensated by alkaline or earth alkaline metal cations. Consequently, zeolites appear as cation exchangers because they have negative charge on the surface. In the zeolite lattice, substitution is not limited to Si-Al substitution. Atoms of iron, boron, chromium, germanium, and titanium may also substitute silicon. Water molecules can be present in voids of large cavities and held to framework ions and exchangeable ions via aqueous bridges.
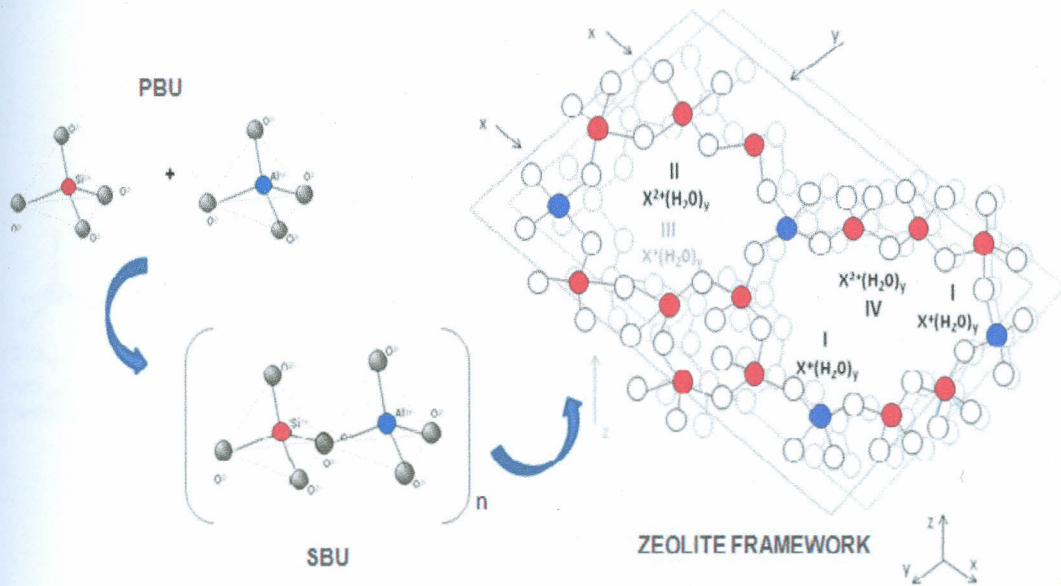

Figure2: Binding of building units (PBU and SBU) in three-dimensional zeolite- clinoptilolite structure (Karmen *et al.*, 2013).

According to the rule Lowenstein, the centers of TO_4 tetrahedra are occupied by silicon atoms and aluminum in a Si: Al ratio which can vary from 1:1 to ∞: 1.The acidity in the aluminosilicate can be controlled by manipulating the Si: Al ratio, it is possible to obtain zeolites with Bronsted acidity comparable to that of sulfuric acid. Other properties which are influenced by the concentration of aluminum in the structure are the density, the ion exchange capacity, thermal stability, hydrophilic and hydrophobic properties and dimensions of the unit cell (Smith, 1993).

The general empirical formula, which represents a zeolite chemical structure, is shown below:
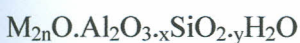
$M_{2n}O.Al_2O_3._xSiO_2._yH_2O$ [1]

Where, M represents any alkali or alkaline earth cation, n the valence of the cation, x varies between two and ten, and y varies between two and seven(Weitkamp, 2000).Several framework types; pore-caged, channelled, zigzag channelled, etc. of zeolites which originate by the scheme in Fig. 3 are recognized.
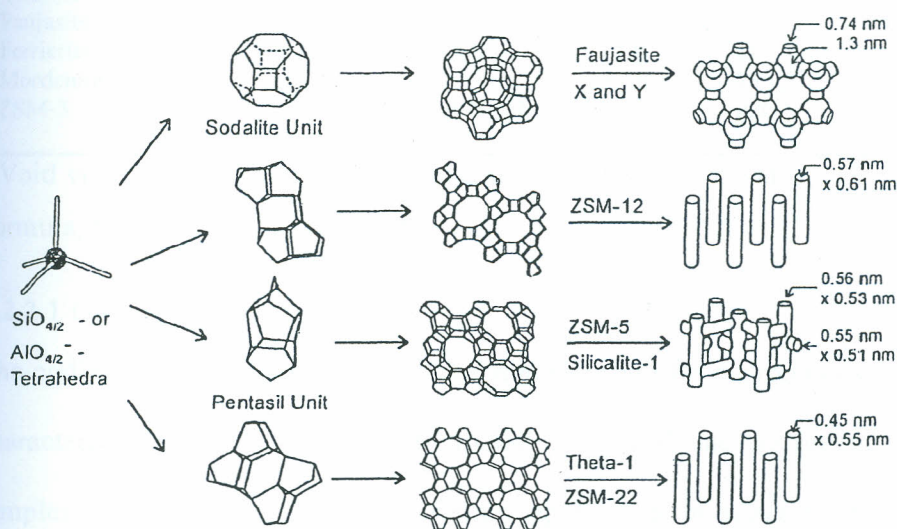

Figure 3: The structure of four selected zeolite (from top to bottom, faujasite or zeolite Y or X, ZSM-12, ZSM-5 (silicate-1), and ZSM-22 (Theta-1) (Weitkamp, 2000)

2.2.2 Categorization and characterization of zeolites

Each time a new zeolite framework structure is reported, it is examined by the Structure Commission of the International Zeolite Association (IZA-SC), and if it is found to be unique, it is assigned a 3-letter framework type code, like CLI, MOR, ANA etc. Zeolites are divided into several groups (Table 1) according to their crystal structure, based on morphology, their physical properties, different ways of binding secondary units in the three-dimensional framework, the free pore volume and types of exchangeable cations (Cation Exchange Capacity - CEC) in zeolites structure (Karmen *et al.,* 2013). Such diverse types of zeolite are a reflection of the fascinating structures of these microporous materials.

Table 1: Typical formulae, structure type and selected physical properties of some natural zeolites (adapted from Shoumkova, 2011; Jungho et al, 2011).
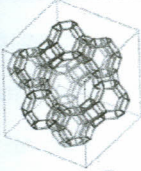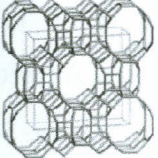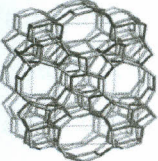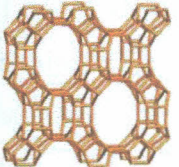
Zeolite	Representative unit-cell formula	Structure Type	Void volume, % *	Channel dimensions, Å	CEC, meq g^{-1} **
Analcime	$(Na_{10})(Al_{16}Si_{32}O_{96}).16H_2O$	ANA	18	2.6	4.54
Chabazite	$(Na_2Ca)_6(Al_{12}Si_{24}O_{72}).40H_2O$	CHA	47	3.7 x 4.2	3.84
Clinoptilolite	$(Na_3K_3)(Al_6Si_{30}O_{72}).24H_2O$	HEU	34	3.9 x 5.4	2.16
Erionite	$(NaCa_{0.5}K)_9(Al_9Si_{27}O_{72}).27H_2O$	ERI	35	3.6 x 5.2	3.12
Faujasite	$(Na_{58})(Al_{58}Si_{134}O_{384}).24H_2O$	FAU	47	7.4	3.39
Ferrierite	$(Na_2Mg_2)(Al_6Si_{30}O_{72}).18H_2O$	FER	28	4.3 x 5.5	2.33
Mordenite	$(Na_8)(Al_8Si_{40}O_{96}).24H_2O$	MOR	28	2.9 x 5.7	2.29
ZSM-5	$Na_nAl_nSi_{96-n}O_{192}.16H_2O, 0<n<27$	MFI	n.d	5.3 x 5.6; 5.1 x 5.5	2.07

*Void volume determined from water content. **Theoretical value, calculated from unit-cell formula, ***, n.d = not determined.

2.2.2.1 Coding for natural zeolites

The coding is part of the official IUPAC nomenclature for microporous materials. However, characterizations of natural zeolites include chemical and instrumental analyses of the samples and are crucial for their further application in water treatment. The chemical composition, usually determined by several different methods: classical chemical analysis – gravimetric method, Atomic Absorption Spectrometry or X-ray Fluorescence Spectrometry, is very important for the efficiency of the water treatment processes and provides insight into the main amount of basic oxide components (SiO_2 and Al_2O_3), exchangeable cations (Na^+, K^+, Ca^{2+}, Mg^{2+}, Ba^{2+}, Sr^{2+}) and other elements present in smaller concentrations (like Ti atoms). According to the proportion of exchangeable cations, the type of zeolite can be determined. However, the proportion of the oxide components in natural zeolite materials depends on the geological deposits (Karmen et al., 2013). Zeolites can also be categorized based on dimensional framework (table 2). Since Kenya is in a very volcanic active region, varieties of natural zeolites are present. However, at the time of this work, none of them had been fully characterized therefore was not available to use in this work. This is because their Si/Al and dimensionalities would not be available.

12

Table 2: Zeolite types and their dimensionality details

Zeolite	Structure	Dimensionality	Dimensions	Si/Al
Faujasite		3D	7.4 (window)	2.77
ZSM-5		3D	5.3 x 5.6	12.75, 23.59
Ferrierite		2D	4.3 x 5.5	10.71
Mordenite		1D	2.9 x 5.7	6.83, 10.72

Source: Structure Commission of the International Zeolite Association (IZA-SC), Ridder, 2012; Shoumkova, 2011, and Jungho *et al.,* 2011.

2.2.2.2 Chemical modification of the zeolites

It has been found that the modified zeolites have more efficient catalytic properties as compared to original samples (Gadekar et al., 2008). Owing to a large internal surface area and considerable costs than synthetic counterparts such as mordenite, scolecite, erionite, phillipsite, clinoptilolite and chabazite, in recent past the natural and modified zeolites have attracted researchers working in the area of catalysis, all over the world. However, most researchers recognize the primary determinant is the interplay between the molecular size and the zeolitic window opening.

2.2.3 Properties of zeolites

Zeolites are widely used in industry due to the acidity, the hydrothermal stability, the large surface area and porosity well defined; they present (Corma, Corell, & Pérez-Pariente, 1995).

2.2.3.1 Charge development

When Al^{3+} is substituted for Si^{4+}, an extra positive charge is required in the vicinity to maintain charge balance with the O^{2-}. The most obvious source of this charge is hydrogen H^+ or H_3O^+ from water, which makes the Al^{3+} site very acidic (able to provide H^+ and oxidise materials). The catalytic activity of zeolites is in part due to this acidity and in part to the size and shape of the channels which hold the intercalated molecules. The crystal structure contains voids (cavities and channels) of medium size unlike molecular sieves, the microporous charcoal which have a bigger range of pore distributions, are sometimes quite irregular. Water molecules present in the structure are located in these channels and cavities, as well as cations which neutralize the negative charge created by the presence in the structure of AlO_2. Cations which may be placed within the microporous channels of zeolites are: alkali (Li^+, Na^+, K^+, Rb^+, Cs^+), alkaline earth (Mg^{2+}, Ca^{2+}, Ba^{2+}), NH_4^+, H_3O^+, H^+), tetra methyl-ammonium (TMA^+), other nitrogen-containing organic cations, rare earth ions and noble metals(Barrer, 1985).

2.2.3.2 Acidity

Zeolites have a structure that allows the creation of active sites, such as acid sites, whose strength and concentration can be controlled according to the desired application (Gates & Schuit, 1979). The concentration of Al in the structure plays a crucial role in the acidity of zeolites. Purely siliceous zeolites, materials not containing Al^{3+} or another trivalent metal are not acidic. The Bronsted acid sites in zeolites occur when the negative charge of the crystal structure is balanced by a hydrogen ion (Smith, 1993). This property would impact on the resulting acidity of solution and hence affect subsequent zeolite molecule reaction.

14

2.2.3.3 Effects of Si/Al ratio

The Si/Al ratio of a zeolite cage is the most important factor affecting its chemical stability, hydrophilic properties, and occurrence of inter-crystalline defects. Zeolites have a structure that allows the creation of active sites, such as acid sites, whose strength and concentration can be controlled according to the desired application (Gates & Schuit, 1979). The concentration of Al in the structure plays a crucial role in the acidity of zeolites. Purely siliceous zeolites, materials not containing Al^{3+} or other trivalent metals are not acidic. The Bronsted acid sites in zeolites occur when the negative charge of the crystal structure is balanced by a hydrogen ion (Smith, 1993). This property will have eventually effect on the acidity or alkalinity of the reaction sites. How this property impacts on malathion removal is not yet well documented.

Table 3: Classification of zeolites in terms of Si/Al ratios

Si/Al ≤ 2 Low silica	2 < Si/Al ≤ 5 Intermediate silica	5 < Si/Al High silica	Phosphates and other elements
ABW, Li-A(BW)	BPH, linde Q	ASV, ASU-7	ACO, ACP-1
AFG, afghanite[a]	BOG, boggsite[a]	BEA, zeolite β	AEI, AlPO-18
ANA, analcime[a]	BRE, brewsterite[a]	CFI, CIT-5	AEL, AlPO-11
BIK, bikitaite[a]	CAS, Cs-aluminosilicate	CON, CIT-1	AEN, AlPO-EN3
CAN, cancrinite[a]	CHA, chabazite[a]	DDR, dreadodecasil 3R	AET, AlPO-8
EDI, edingtonite[a]	CHI, chiavennite[b]	DOH, dodecasil 1H	AFI, AlPO-5
FAU, NaX	DAC, dachiardite[a]	DON, UTD-1F	AFN, AlPO-14
FRA, franzinite	EAB, EAB	ESV, ERS-7	AFO, AlPO-41
GIS, gismondine[x]	EMT, hexagonal faujasite	EUO, EU-1	AFR, SAPO-40
GME, gmelinite[a]	EPI, epistilbite[b]	FER, ferrierite[a]	AFS, MAPSO-46
JBW, NaJ	ERI, erionite[a]	GON, GUS-1	AFT, AlPO-52
LAU, laumontite[a]	FAU, faujasite[a], NaY	IFR, ITQ-4	AFX, SAPO-56
LEV, lewyne[a]	FER, ferrierite[a]	ISV, ITQ-7	AFY, CoAPO-50
LIO, liottite[b]	GOO, goosecreekite[a]	ITE, ITQ-3	AHT, AlPO-H2
LOS, losod	HEU, heulandite[a]	LEV, NU-3	APC, AlPO-C
LTA, linde Type A	KFI, ZK-5	MEL, ZSM-11	APD, AlPO-D
LTN, NaZ-21	LOV, lovdarite[b]	MEP, melanophlogite[a]	AST, AlPO-16
NAT, natrolite[a]	LTA, ZK-4	MFI, ZSM-5	ATE, AlPO-25
PAR, partheite[a]	LTL, linde L	MFS, ZSM-57	ATN, MAPO-39
PHI, phillipsite[a]	MAZ, mazzite[a]	MSO, MCM-61	ATO, AlPO-31
ROG, roggianite[a]	MEI, ZSM-18	MTF, MCM-35	ATS, MAPO-36
SOD, sodalite	MER, merlinoite[a]	MTN, dodecasil 3C	ATT, AlPO-12, TAMU
WEN, wenkite[a]	MON, montesommaite[a]	MTT, ZSM-23	ATV, AlPO-25
THO, thomsonite[a]	MOR, mordenite[a]	MTW, ZSM-12	AWO, AlPO-21
TSC, tschortnerite	OFF, offretite[a]	MWW, MCM-22	AWW, AlPO-22
	PAU, paulingite[a]	NON, nonasil	BPH, beryllophosphate-H
	RHO, rho	NES, NU-87	CAN, tiptopite[a]
	SOD, sodalite	RSN, RUB-17	CGF, Co-Ga-phosphate-5
	STI, stilbite[a]	RTE, RUB-3	CGS, Co-Ga-phosphate-6
	YUG, yugawaralite[a]	RTH, RUB-13	CHA, SAPO-47
		RUT, RUB-10	CLO, cloverite
		SFE, SSZ-48	CZP, chiral zincophosphate
		SFF, SSZ-44	ERI, AlPO-17
		SGT, sigma-2	DFO, DAF-1
		SOD, sodalite	DFT, DAF-2
		STF, SSZ-35	FAU, SAPO-37
		STT, SSZ-23	GIS, MgAPO-43
		TER, terranovaite	OSI, UiO-6
		TON, theta-1	RHO, pahasapaite[a]
		ZSM-48	SAO, STA-1
		VET, VPI-8	SAS, STA-6
		VNI, VPI-9	SAT, STA-2
		VSV, VPI-7	SAV, Mg-STA-7
			SBE, UCSB-8Co
			SBS, UCSB-6GaCo
			SOD, AlPO-20
			SBT, UCSB-10GaZn
			VFI, VPI-5
			WEI, weinebeneite
			ZON, ZAPO-M1

2.2.3.4 Selectivity form.

The phenomenon of selectivity in zeolites can be used to drive a catalytic reaction toward the desired product while avoiding unwanted side reactions. Zeolites have a complex network of channels which gives them different types of shape selectivity, as sketched in Figure 4. The selectivity of reagent occurs due to limitation of access of some types of reactants to the interior of the pores. In this case, at least two reactants with different molecular dimensions exist, and the diffusion of molecules less bulky for the pores occurs preferentially.
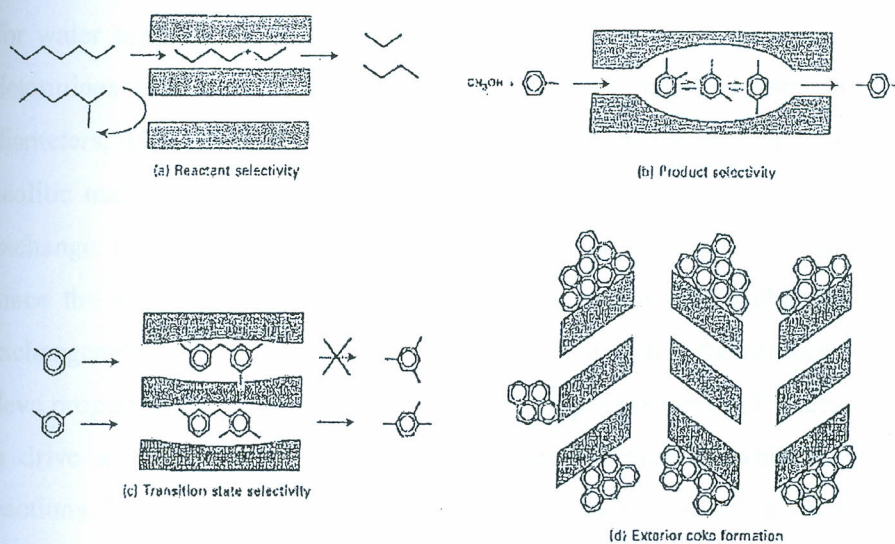

(a) Reactant selectivity

(b) Product selectivity

(c) Transition state selectivity

(d) Exterior coke formation

Figure 4: Effects of shape, size of molecule and channel dimensionality molecular sieving (Wilkinson, 2014).

When there is the limitation of the diffusion of products outside the crystal lattice, this result in the selectivity of products. In this type of selectivity at least two products with different molecular dimensions may form parallel or consecutive reactions. In this case, a reaction occurs at the expense of another. The concentration of molecules less bulky decreases rapidly within the pore structure for a reaction. In some instances, the selectivity is independent of the size of the crystals. When the restrictions are determined by transition states, a consideration is taken to the selectivity of the transition state. The selectivity of the transition state is intrinsically chemical effects, since a single molecule can react in a certain transition state and not in another (Barrer, 1985). In this case, one of the reactions is suppressed. It is not known how the property for mordenite (MOR), ferrierite (FER), ZSM-5 (MFI) and USY (FAU) zeolites will impact on adsorption of malathion pesticide.

17

2.2.3.5 Thermal Stability analysis.

Zeolites have high thermal stability which varies in a wide range of temperature depending on the chemical composition. The decomposition temperature of the materials with low silica content is about 700°C, whereas the high silica zeolites of this value can reach 1300 °C (Payra& Dutta, 2003).This property is relevant in ascertaining that the selected zeolites remain structurally stable after activation.

2.2.3.6 Molecular sieve effects

Pore size and framework density are the primary factors of concern when considering zeolites for water separations; pore size determines ion selectivity and framework density, in turn, determines water permeability. Furthermore, zeolite channel diameters are close to molecule diameters, which results in strong van der Waals interaction. Thus in general, separations in zeolitic materials occur primarily through molecular sieving, competitive adsorption or ion exchange. Ions with small hydrated radii diffuse more quickly through zeolite pore structures. Since the ability to act as a molecular sieve is due to the channel widths, changing the exchangeable or framework atoms of the zeolite, and thus the channel widths, will change the sieve properties (Kowenje &Osewe 2015). The phenomenon of selectivity in zeolites is used to drive a catalytic reaction toward the desired product while avoiding unwanted side reactions. Zeolites have a complex network of channels which gives them different types of shape selectivity, as sketched in Figure 4. The selectivity of reagent occurs due to limitation of access of some types of reactants to the interior of the pores.

Upon increasing the crystal size, the diffusional paths of the molecules inside the pores are lengthened, and this may, under certain circumstances, affect the selectivity in a desirable manner (Weitkamp, 2000). In addition, zeolites with high Si/Al ratio can be used as selective adsorbents in water treatment, targeting organic micro pollutants which are poorly removed by activated carbon. Due to size exclusion, many Natural Organic Matter (NOM) components cannot access the pores, thus limiting adsorption competition between organic micro pollutant and NOM. It is not known whether Malathion pesticide will be internally or externally attached to the zeolite.

2.2.3.7 Hydrophobicity and hydrophilicity of the zeolites

Organic contaminants are important pollutants in water and their removal in an economic way remains a significant problem, although various methods have been developed. Owing to

18

their native negative surface charge, zeolites are able to capture organic cations by ion exchange. However, both natural and synthetic zeolites exhibit little adsorption of organics in aqueous solution due to their surface hydrophilics. Several factors dictate whether zeolite framework will be hydrophilic or hydrophobic and chief among them is the presence of silanol group ($\equiv SiOH$) or a cation associated with the aluminum site (Chen, McDonald, & Newton, 1976) and other hydrophilic defect sites (Humlik et al., 2014). Zeolites with high Silanol groups, low Si/Al ratio (Chen et al., 1976), and more defect sites tend to be more hydrophilic (Humplik et al., 2014). The modification of zeolite by suitable surfactant can change the surface functionality by adding hydrophobic groups and thus to enhance the adsorption of various organics, including non-polar species (Shoumkova, 2011). The localized electrostatic poles between the positively charged cations and the negatively charged zeolitic framework strongly attract highly polar molecules, resulting in a hydrophilic structure.

Hydrophobic or hydrophilic nature of zeolites also appears to depend on their framework structure and pure siliceous zeolite beta has been reported to be much more hydrophobic than silicalite-1 and the other siliceous 12-numbered ring zeolites, even though they contain almost no aluminum (Blagica et al., 2006).For zeolites to be good adsorbents for organic pollutants, their hydrophilicity must be low. Humplik et al. (2014) observed that molecules move within the adsorbents by capillarity type of motion and therefore the concept of like adsorbing like would apply. This means hydrophilic zeolites would best adsorb polar or protic substances while hydrophobic zeolites will be best for non-polar or aprotic substances. In particular, when zeolite was coated with octadecyltrichlorosilane (C18) to change its surface properties, active carbon content was realized resulting in efficient sorption of o-xylene and naphthalene(ATSDR, 2005,Kowenje &Osewe 2015).

Moreover, because of its unique physical properties, solvent control systems using hydrophobic zeolite, when applied to many solvent mixes, exhibit separation capacity equal to or better than systems using activated carbon without requiring much of the support equipment. However, due to its homogenous pores, hydrophobic zeolite exhibits limited performance for some common solvents (Blocki, 1993).Blagica et al. (2006) reported that regular Si/Al-zeolites have adsorption capacities for alcohols/water in the following order H_2O >MeOH>EtOH>PrOH, whereas silicalites or hydrophobic ones are expected to give the reversed order of adsorption. Specifically, the amounts of PrOH and acetone adsorbed on

19

silicalite corresponded to approximately 71% of the pore volume and for PrOH on F-silicalite approximately 61 %, showing that these sorbents preferably adsorb these compounds from water. In contrast to the "low" and "intermediate" silica zeolites, representing heterogeneous hydrophilic surfaces within a porous crystal, the surface of the high silica zeolites approaches a more homogeneous characteristic with an organo – philic hydrophobic selectivity. They more strongly adsorb the less polar organic molecules and only weakly interact with water and other strongly polar molecules (Flanigen, 1980). In the last decade SMZ zeolite was extensively been researched as sorbents of benzene, toluene, ethyl benzene, xylenes, phenols, pesticides, herbicides, dyes, humic acids, etc. from aqueous solutions (Shoumkova, 2011).

In another study, the MOR-200 and ZSM-5, the two most hydrophobic zeolites, showed the highest removal of neutral nitrosamines in demineralised water, with higher efficacy than activated carbon. DAY and MOR-30, which were relatively hydrophilic zeolites, did not show appreciable removal of any of the nitrosamines. When nitrosamines were adsorbed from surface water, there was no influence of competition with, or pore blockage by, NOM components on nitrosamine removal for ZSM-5 zeolite, in contrast to activated carbon. Generally, the removal of organic micropollutants from aqueous solution is enhanced when zeolites with high Si/Al ratio (that is hydrophobic zeolites) are used. However, it was found that above a Si/Al ratio of 90, the removal of MTBE on ZSM-5 zeolite did not improve (Kowenje &Osewe 2015).For our case the interplay between the river water, the pesticide and the zeolite is not yet documented.

2.3 Water treatment applications of zeolites

2.3.1 Water softening

Zeolite NaA finds its use in laundry detergents, and nowadays, most of the commercial washing powders, contain zeolite, instead of harmful phosphates, banned in many parts of the world because of the risk of water eutrophication. Zeolite NaA does not contribute to the eutrophication potential of surface waters and is nontoxic to freshwater and marine aquatic communities. The largest commercial market of synthetic zeolites, estimated of about 1.3 million tons per annum, is as water softening "builder" in detergent formulations. In 1973 the German company "Henkel" patented formulations incorporating zeolite NaA as a water softener. In 1978 "Procter and Gamble" introduced zeolites in as water softener in detergent formulations, is that since zeolites are insoluble in water they lead to increase in sewage sludge mass (Shoumkova, 2011).

2.3.2 Ammonia removal

Another industrial application of zeolites is for separation of ammonia from drinking or wastewater. The term ammonia includes the non-ionized (NH_3) and ionized (NH_4^+) species. Ammonia in the environment originates from metabolic, agricultural and industrial processes and from water disinfection with chloramine. Ammonia in water is an indicator of possible bacterial, sewage and animal waste pollution. Ammonia may have harmful effect on human and animal health; it contributes to the eutrophication and oxygen depletion in receiving waters, and in addition attacks the rubber components of water plumbing systems (Shoumkova, 2011).

2.3.3 Heavy metals removal

Heavy metals are generally considered to be those whose density exceeds 5 g cm^{-3}. A large number of elements fall into this category, but the ones of relevance in the environmental context are Cd, Cr, Cu, Ni, Zn, Pb and Hg. Heavy metals are well known of their toxicity. It is known that the immobilization of heavy metal ions from aqueous solutions by zeolites is quite a complicated process, consisting of ion exchange and adsorption and is likely to be accompanied by precipitation of metal hydroxide complexes on active sites of the particle surface. Similarly to the sorption of ammonia, the heavy metal cations removal efficiency depends upon the type, dose and grain size of zeolite used, contact time, pH, temperature, initial metal concentration and to a significant extent to the presence of competitive ions (Shoumkova, 2011).

2.3.4 Radioactive species removal

Various processes used in the nuclear fuel cycle and in the application of radio nuclides in industry, medicine, and research generate low or intermediate level liquid wastes, containing radioactive isotopes (such as ^{137}Cs, ^{90}Sr, ^{60}Co, ^{45}Ca, ^{51}Cr, ^{111m}Cd, ^{110m}Ag). Such effluents usually require treatment to remove radioactive contaminants or to reduce them to levels, which allow safe discharge. One of the first publications on the utilization of zeolites for the sorption of radioactive species was probably the patent of Ames, who proposed a method for removal of caesium from aqueous solutions by sorption with clinoptilolite (Shoumkova, 2011).

2.3.5 Removal of inorganic anions

Nitrates, phosphates, arsenates, chromates and fluorides are among the most common anionic water contaminants. As it has been mentioned, raw zeolites are negatively charged, and thus

have no affinity for sorption of anionic species. However, some cation-modified zeolites, having positive net charge, are able to adsorb anions by means of electrostatic interaction. There are a number of regions where arsenic may be present in drinking-water sources, particularly groundwater, at elevated concentrations. Arsenic is considered to be a high-priority substance for screening in drinking-water sources, as is a recognized carcinogen for human and other living organisms. The inorganic arsenic is more toxic than organic arsenic. Conventional precipitation methods for arsenic removals using iron and aluminum salts have not been successful to meet drinking and effluent standards for As due to limitation of solubility of the resultant product. As an alternative, adsorption was found to be one of the promising methods for removal of arsenic from water (Shoumkova, 2011).

2.3.6 Organic compounds removal

Organic contaminants are important pollutants in water and their removal in an economic way remains a significant problem, although various methods have been developed. Owing to their native negative surface charge, zeolites are able to capture organic cations by ion exchange.

However, both natural and synthetic zeolites exhibit little adsorption of organics in aqueous solution due to their surface hydrophilics. The modification of zeolite by suitable surfactant can change the surface functionality by adding hydrophobic groups and thus to enhance the adsorption of various organics, including non-polar species. In the last decade SMZ was extensively been researched as sorbents of benzene, toluene, ethyl benzene, xylene, phenols, pesticides, herbicides, dyes, humic acids, etc. from aqueous solutions (Shoumkova, 2011).

2.3.7 Dyes removal

Dyes in wastewater originate mainly from textile, printing, food and leather industries. In aqueous ecosystems dyes reduce sunlight penetration and thus affect photosynthesis. Some dyes, in addition, are toxic or carcinogenic. The most important types of water-soluble dyes are acid, basic (cationic), direct (anionic), and reactive dyes. The adsorption dyes by natural and modified clinoptilolites was recently documented (Shoumkova, 2011).

2.3.8 Humic substances removal

Humic substances (including humic acid, fulvic acid, and humin) make up about 80% of soil organic matters in dark soils. Their presence in surface and ground water may produce toxic

22

chemicals during disinfection processes and thus should be reduced. Some important studies on humic substances adsorption by natural zeolites were summarized recently (Shoumkova, 2011). It was demonstrated that the enrichment of tuff by monovalent cations slightly reduced the adsorption (down to 6.5-7.0 mg g^{-1}), whereas the enrichment by divalent cations significantly enhanced humic acid sorption. Ca and Mg enriched samples, yielded the best results - 21.5 and 22 mg g^{-1}, respectively. Thus it will be interesting to investigate how natural waters from river Monjolinho in Sao Paulo, Brazil imbedded with humic acids affect pesticide removal by zeolites.

2.3.9 Removal of other organics

Phenols are toxic compound coming from a variety of industrial sources, such as pesticides, dyes, and paper industries, coke and resin manufacturing, textile, plastic, rubber, pharmaceutical, and petroleum production. Bisphenol A uptake increased at alkaline pH conditions, which enabled the formation of bisphenolate anion. The zeolites having higher BET surface area showed greater retention for bisphenol A. The uptake of bisphenol A was improved slightly in the presence of NaCl, and was enhanced at a low temperature (Shoumkova, 2011).

2.4 Zeolites application in degrading of pesticides

It has been reported that the presence of some zeolites in the wastewater enhances the decomposition of pesticide contaminants (Ogunah, Kowenje, Osewe, Lalah, Jaoko, & Koigi, 2013) found that zeolites X degrade DDT faster. However, the extent and exact kinetics of such zeolitic action are not yet reported. Zeolites can absorb and chemically decompose both organo-phosphates such as dimethyl methylphosphonates (Yang, 2006) and organochlorines (Kanyi, 2006). Most pesticides with longer half-lives in the environment for instance malathion and DDT have phosphate and chloride functional groups, respectively, in their chemical makeup. Secondly, the tunable chemical properties of zeolites have been known to depend on their Si/Al ratio and levels of cation exchange (Kowenje, Jones, Doetschman, Yang, & Kanyi, 2006). In addition, systematic adsorption tests (Jonam, Diuna, Stanic, & Pfend, 2006) showed that organo-zeolites help remove atrazines, lindane and diazinones from waters. Elsewhere, Lalah, Yugi, Jumba and Wandiga, (2003) established that a reasonable amount of organochlorine pesticides exist in Kenyan river waters and elsewhere and the pesticides eventually end up in the lake/ oceans water bodies. Due to heavy agricultural industrialization in Sao Carlos area river Monjolinho is bound to be heavily polluted by

23

Malathion, there is need to treat domestic water from these water bodies to get rid from Malathion pesticides contaminants.

2.4.1 Why zeolites are suitable for water treatment

They have pores into which molecules can be incorporated and after dehydration the exchangeable cations can be modified by chemical treatment thus permitting control of chemical forces on the sorted molecules, which will favour them to be used as catalysts (Rabo, 1976).Natural zeolites are abundant in nature because of high percentage of aluminum and silicon in the earth crust (Arnold, 1996). Synthetic X and Y zeolites (faujasite) are pure and contain the sodalite units (β cages) interconnected as to result in large 3 dimensional pores(Rabo, 1976),their framework are very open and enclose a system of large cages (α supercages) and prefer lithium, sodium and potassium as counter cations. They also have a high mobility for cations due to their large pore diameter (Kowenje &Osewe 2015).Their occurrences are associated with vulcanicity and are very abundant in Kenya, hence would be cheaply available for use.

2.4.2 Applications of Zeolites on water purification

Zeolites in powdered form, as they are traditionally produced, are not very useful in water treatment applications as the zeolites have to be removed from the water somehow before it is used, and removal of a fine powder (especially one which is worth saving for reuse) would be cumbersome. Also, since the concentrations of pollutants are generally low in water being treated, a relatively small amount of the adsorbent would be sufficient to treat a large stream of water. Currently, the adsorbents used to remove contaminants from water are usually used in a packed tower, and this technology is very simple and suited to the task of water treatment (Spence, 2007).The technological sequence of porous materials for catalytic application generally follows the sequence below.
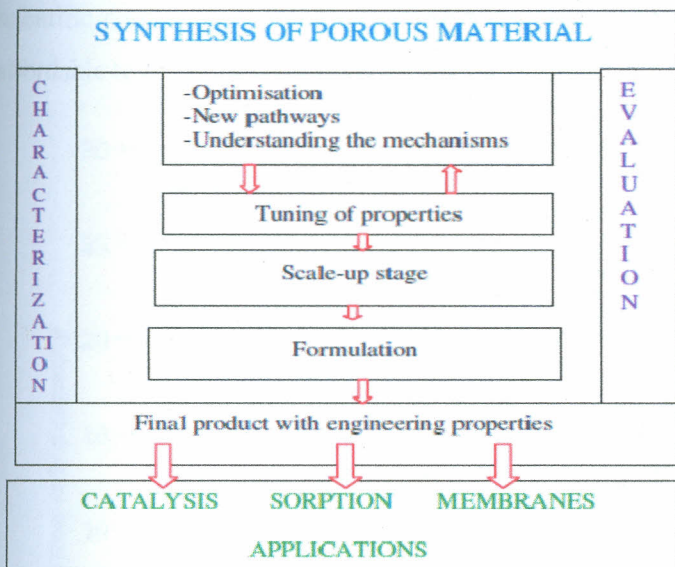
```
┌──────────────────────────────────────────────────────────────┐
│            SYNTHESIS OF POROUS MATERIAL                       │
│  ┌─┐ ┌──────────────────────────────────────────┐ ┌─┐        │
│  │C│ │ -Optimisation                            │ │E│        │
│  │H│ │ -New pathways                            │ │V│        │
│  │A│ │ -Understanding the mechanisms            │ │A│        │
│  │R│ └──────────────────────────────────────────┘ │L│        │
│  │A│        ⇓              ⇑                        │U│        │
│  │C│ ┌──────────────────────────────────────────┐ │A│        │
│  │T│ │         Tuning of properties             │ │T│        │
│  │E│ └──────────────────────────────────────────┘ │I│        │
│  │R│              ⇓                                │O│        │
│  │I│ ┌──────────────────────────────────────────┐ │N│        │
│  │Z│ │           Scale-up stage                 │ │ │        │
│  │A│ └──────────────────────────────────────────┘ │ │        │
│  │TI│             ⇓                                │ │        │
│  │O│ ┌──────────────────────────────────────────┐ │ │        │
│  │N│ │            Formulation                   │ │ │        │
│  └─┘ └──────────────────────────────────────────┘ └─┘        │
│                    ⇓                                          │
│        Final product with engineering properties             │
└──────────────────────────────────────────────────────────────┘
        ⇩              ⇩              ⇩
   CATALYSIS      SORPTION      MEMBRANES
                 APPLICATIONS
```

Figure 5: Technological progress in molecular sieves development (Source -Shoumkova, 2011).

Most current water purification methods either lack the capacity to get rid of most pesticides and pesticides decomposition products from the drinking water supply sources or are very expensive. Recent studies indicate that zeolite X is more effective in abstraction of malathion pesticide and its residues, and the degradation products depended on the type of zeolite used but more specifically, finally the mechanistic pathway depends on the silicon-aluminum ratio of the adsorbent (Ogunah*et al*., 2013). Work by Jonam *et al*. (2006), indicate that the presence of some zeolites in the waste-water enhances the degradation of pesticide contaminants. The zeolites more so have cages of different dimensions and since the pesticides also possess different molecular shapes, sizes and functional groups (organophosphate and organohalogens) there is, therefore, a need to find that unique zeolite most suitable for a specific environmental pollutant. In addition, it has been noted the degradation products of pesticides depend on the type of zeolites used therefore a discussion is needed to highlight which types of zeolites of different cage dimensionalities, Si/Al, hydro-phobicity or -philicity etc. is most fitted to be more effective in a particular situation.

2.4.3 Wastewater re-use by regions of the world.

For wastewater to be re-used, it implies that a complete purification according to the regional standards is met. Annual increase of installed capacities for re-use of wastewater is presented in Figure 6. From the graph, the less economically regions of the world of Africa, Asia and Latin America are at the bottom of percentage re-usability of water. It therefore behooves the

scientific community to come up with technologies which are not only sustainable but also affordable to the poorest of this world.
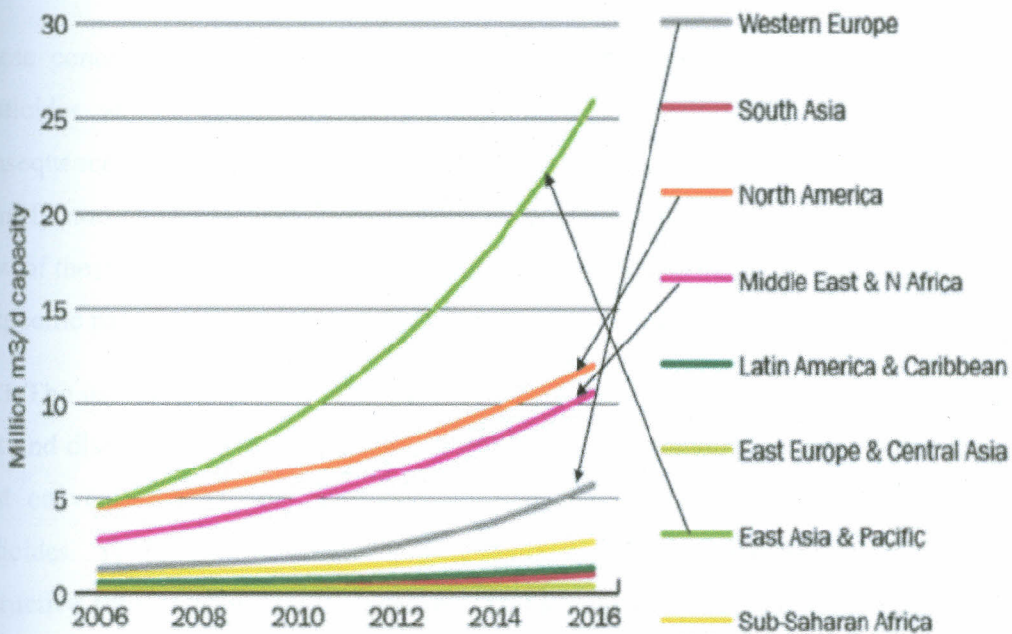

Figure 6: Regional water re use levels (Adopted from: Shoumkova, 2011).

Zeolites can be used from both synthetic and natural origin. The natural zeolites have been shown to be just as efficacious as their synthetic analogues in most chemical reactions. Besides, as Kowenje &Osewe (2015) observed, zeolites can be recycled. Recycle tests indicated that the zeolite could be used, cleaned and reused at least three times without significant reduction in treatment effectiveness.

2.5 Pesticide usage

Revolution in pest management occurred seven decades ago with the discovery and use of organochlorines, organophosphates, carbamates and more recently pyrethroids. These chemical pesticides became the main tool in pest management for public health, livestock and crop protection and their use led to substantial suppression of pests.

However, it was discovered over time that these chemicals are not entirely harmless to other forms of life. The pesticides would also kill non-target organisms such as beneficial insects' vertebrates both in aquatic and terrestrial ecosystems. Some were extremely persistent organic pollutants (POPs) and would undergo bio-accumulation through the food chain. Their active ingredients and metabolites were also found to impair mammalian endocrine system,

nervous systems and some were carcinogenic. Insects also quickly developed resistance to some of the pesticides.

These concerns finally led to strict restrictions and absolute banning of some chemical pesticides and a search for natural and environmentally friendly products began. In consequence, during the last two decades, a great deal of research has been undertaken to identify non-chemical pest control alternatives. Unfortunately, production, availability and flow of these products in Kenya have been constrained by a number of factors, including lack of specific national registration and lack of mass production protocol.

2.5.1 The use of pesticides in Kenya

Pest and diseases are responsible for 30-40% loss in agricultural produce in the tropics. The most conventional and common way of pest and disease control is through the use of pesticides. These pesticides are largely synthetic compounds which kill or deter the destructive activity of the target organism. Unfortunately, these compounds possess inherent toxicities that endanger the health of the farm operator, consumer and the environment.

2.5.1.1 Pesticide imports and exports

Approximately 7047 metric tonnes of the pesticides with a value of US$ 50 million (4.0 billion Kenya shillings) were imported into the country in 2005(Egerton, 2005). The major active substances imported during the year were glyphosate, mancozeb, amitraz, copper oxycholide, 1, 3-dichloropropene, 2, 4-D amine, sulphur, dimethoate and methyl bromide in order of decreasing volume. In the year, more insecticides were imported in comparison to the other pesticide groups. The pesticides value contributed to more than 50% of the total value of pesticides imported during the year.

In 2005, approximately 63 metric tonnes of pesticides worth US$ 700,000 (Kshs. 55 million) were exported from Kenya to the neighboring countries (mainly Seychelles, Burundi, Uganda and Tanzania) (Egerton, 2005). The pesticides exported were mainly cypermethrin, chorofenvinphos and permethrin + pirimiphos. These are mainly synthetic pyrethroid. These figures exclude exports of crude pyrethrin done by the pyrethrum board of Kenya which amount to 6000 tonnes annually. The export figure may be more because some dealers may be exporting pesticides without the board's knowledge.

27

2.5.1.2 Registration of synthetic pesticides and bio pesticides in Kenya

The registration of pesticides in Kenya is governed by the Pest Control Products Act, Cap 346 of the Laws of Kenya. Since the law was enacted in 1982, many conventional chemical pesticides and biopesticides have been registered for use in Kenya. In 2003, over 620 pest control agents had been registered, of which, 30 are derived from natural materials such as plants and microbes (Wabule, Ngaruiya, Kimmins, & Silverside, 2004).

Most of the biopesticides so far registered in Kenya are based on pyrethrum extracts and those derived from *bacillus thuringensis* (Bt). Over the last decade, applications for registration of biopesticides have increased with active ingredients derived from pyrethrin, warbugia and azadirachtin as well as micro-organisms such as *beauveriabussiana, bacillus thuringensis*, (insecticide), *pseudomonas fluorescens, trichodermaharzianum*(fungicide), *paecilomyceslilacinusspores* (nematocide) (Egerton, 2005).

2.5.1.3 Incidences of pesticide misuse in Kenya

Abuse and misuse of insecticides is common in Africa and, although the use of pesticides in Africa represents a small fraction of the global total, misuse is disproportionately high Factors that lead to these high rates include the high illiteracy levels and inaccessibility to reliable protective clothing. Smuggled products, unregistered products, open air sales, sale of banned product, cases of decanting and reweighing, faking of pest control products using counterfeit labels, sale of expired products with modified expiry dates are among the misuse cases that have been reported in Kenya. Spraying mistaken products has led to the death of hundreds of flock (Kowenje &Osewe 2015). The study of the two groups (organochlorides and organophosphates) as represented by DDT and malathion, respectively, is necessitated by the fact that water bodies act as a final reservoir of what remains after plants and soil accumulate the said pesticides and their breakdown products (Lalah, Acholla, & Wandiga, 1994).

2.5.1.4 Challenges facing the horticultural industry in Kenya

The Kenya horticultural industry is the second largest foreign exchange earner after tea. It earns US$300,000,000 annually. It creates employment to both the rural and the urban populations estimated at 500,000 and over 2 million people, respectively (Egerton, 2005). Kenya is the largest flower exporter to the EU, with 25% of the market share, where 50,000 tonnes of flowers are exported annually. The horticulture industry is the major consumer of pesticides and the export market customers now demand a reduction in pesticide use. Minimum residue limits (MRLs) has been enacted by the European Union which does not tolerate any detectable traces of residues. There are also strict phytosanitary regulations which do not tolerate pests or related damage to produce. It is therefore a challenge to Kenya to produce pest/damage free products, which are also pesticide residue free. The only way to come out of the puzzle is to adopt a cheaper and effective way to remove pesticides and their metabolites from water bodies which act as their final reservoir.

2.5.2 Malathion

Malathion, S-1, 2-bis (ethoxycarbonyl) ethyl O, O-dimethylphosphorodithioate(Worthing, 1979) was discovered in 1950 as a low mammalian toxic organophosphorus insecticide and was introduced in the same year by the American Cyanamid Company under the code number EL4B049 and protected by USP 2578652. Malathion is synthesized by addition of methanol to phosphorus pentasulphide, forming dimethyl phosphorodithioic acid. This is then added directly to maleic acid diethyl ester under reflux with the influence of catalytic quantities of alkali (Rouy, 1983).
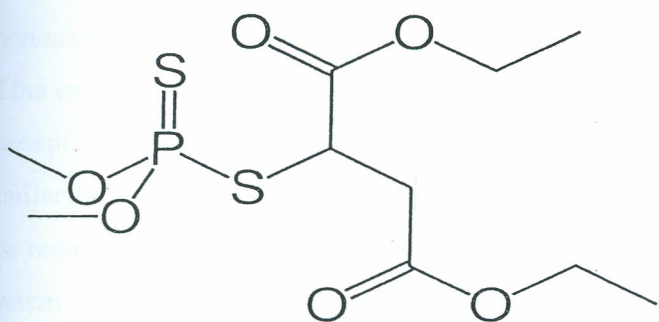
Figure 7: Chemical structure of Malathion

Source: www.en.wikipedia.org/wiki/File:malathion accessed on 1st Sept 2012.

The chemical and physical properties of Malathion have been documented as summarized in Table 4.

Table 4: The physical and chemical properties of Malathion

Property	Value
Boiling point	156-157°C
Melting point	2.9^{o}C
Molecular weight	330.36
Log $K_{o/w}$	2.36
Water solubility	143ppm at 20°C(deionized water)
Vapour pressure	7.9 x 10^{-6} mmHg at 20°C
Density	1.23 g/ml
Henry's law constant	2x10^{-8}atm m^{-3}/mol
Acute oral LD$_{50}$ for rats	2800 mg/kg

$K_{o/w}$ – Octanol-water partition coefficient

Source :(Howard, 1991).

The high margin of safety of malathion as compared to other pesticides to mammals and its selectivity against target insects, coupled with its amenability at ultra-low volume applications make it a good general purpose contact insecticide employed in controlling insects of household, home, garden, stored grains, greenhouse, agriculture, forestry and public health (Mulla & Mian, 1981).Malathion has low mammalian toxicity in spite of its strong insecticidal properties. Although it has little or no cholinesterase activity, like many other organophosphates, malathion is activated by monooxygenase attack to produce the potent anticholinesterase inhibitor malaoxon. Malathion and malaoxon are rapidly detoxified in mammals by carboxylesterase attack (but not in insects) to produce their respective monoacids referred to as malathion monocarboxylic acid and malaoxon monocarboxylic acid. If the carboxylesterase detoxification pathway is inhibited, mammals may be made almost as susceptible to malathion as insects (Caldwell, 1984). Effects of malathion on human are similar to those observed for other organophosphates, except that larger doses of malathion are required to produce them. Single dose of 30 mg/day malathion may affect the immune system response of man (Gallo & Lawryk, 1991). Symptoms of acute exposure to the organophosphate may include numbness, in coordination, headache, tremor, nausea, abdominal cramps, blurred vision, and difficulty in breathing or respiratory depression (ATSDR, 2005). One of the major problems related to hazardous nature of malathion is the presence of impurities in the formulated material. These impurities may arise either as by

30

products or they may form as degradation products (see Table 5) during storage of the technical product (Ware, 1992). Pure malathion is not very toxic but crude malathion and its formulations contain impurities which are toxic to mammals (Breck, 1974).

Table 5: Toxicity of Malathion and its degradation products through oral routes in rats

Compound	Oral LD$_{50}$ (mg/kg)
Malathion	1375
Malaoxon	215
DMPT	694
DMDTP	4510
MCA	5615
DCA	5544

Source: Mehlhorn& Armstrong, 2001

Malathion comes in a variety of formulations depending on factors such as nature of the target species, the desired persistence and the method of application. It is formulated as dust, wettable powders and emulsifiable concentrate and as aerosols; it has low thermal and alkaline stability (Ware, 1992).Thus due to its branched chemical structure and intermediate molecular size malathion was a model pesticide in this study. The interactions of the extensively branched chemical structure of malathion with the various channels and cages of mordenite, (MOR), ferrierite (FER), ZSM-5(MFI) and USY (FAU) zeolites are not yet documented.

2.5.2.1 Malathion Degradation in Water

Degradation of malathion in water is pH dependent as it degrades quickly in water with pH >7.0(Newhart, 2006). Hydrolysis is the main route of degradation in alkaline aerobic conditions. The half-life of malathion in water ranges from 0.2 weeks at pH 8.0 to 21 weeks at pH 6.0. Metabolites resulting from hydrolysis include malaoxon, malathion alpha and beta monoacid, diethyl fumarate, diethyl thiomalate, O, O-dimethylphosphorodithioic acid, diethylthiomalate, and O, O-dimethylphosphorothionic acid (see figure 8). Biodegradation also plays a role when pH <7.0 and the rate of hydrolysis is slow relative to the rate of biodegradation. Breakdown constituents of biodegradation include beta monocarboxylic acid, dicarboxylic acid, and diethyl thiomalate (Neal, McCool, & Younglove, 1993). Malathion is also readily oxidized in water to malaoxon by a variety of mild oxidizing reagents. Thus, it is generally recognized that malathion is easily oxidized to malaoxon by swimming pool chlorine concentrations (Scharf, 2003). For instance, malaoxon has greatest persistence when pool water is acidic, and malathion is stable in oxygen saturated water at a pH 5 for up to two

weeks (ATSDR, 2005). Sunlight shortens both malathion and malaoxon half-lives in pools to 3 days. These data suggest that little accumulation of malathion or malaoxon in swimming pools occurs, but does indicate that they can persist at low levels for a considerable period of time (Howard, 1991). In river water, the half-life of malathion is generally less than one week. For example, in the Suwanee River USA, with large amounts of tannins, malathion was 50% degraded by sunlight within 16 hours. However, malathion may remain stable in distilled water for three weeks and its photolysis half-life is 41 days. Applied at up to 2.7 kg per acre in logged ponds for mosquito control, it is generally effective for 2.5-6.0 weeks. In seawater, degradation increases with salinity. Breakdown products in acidic water are mono- and dicarboxylic acids such as dimethyl phosphorothionic acid and 2-mercaptodiethyl succinate (Wolfe, Gordon, & Zepp, 1975). The degradation mechanisms of malathion in water therefore depend on the type and composition of the solvent water. No kinetics and degradation products of malathion in the presence of these zeolites have been reported.
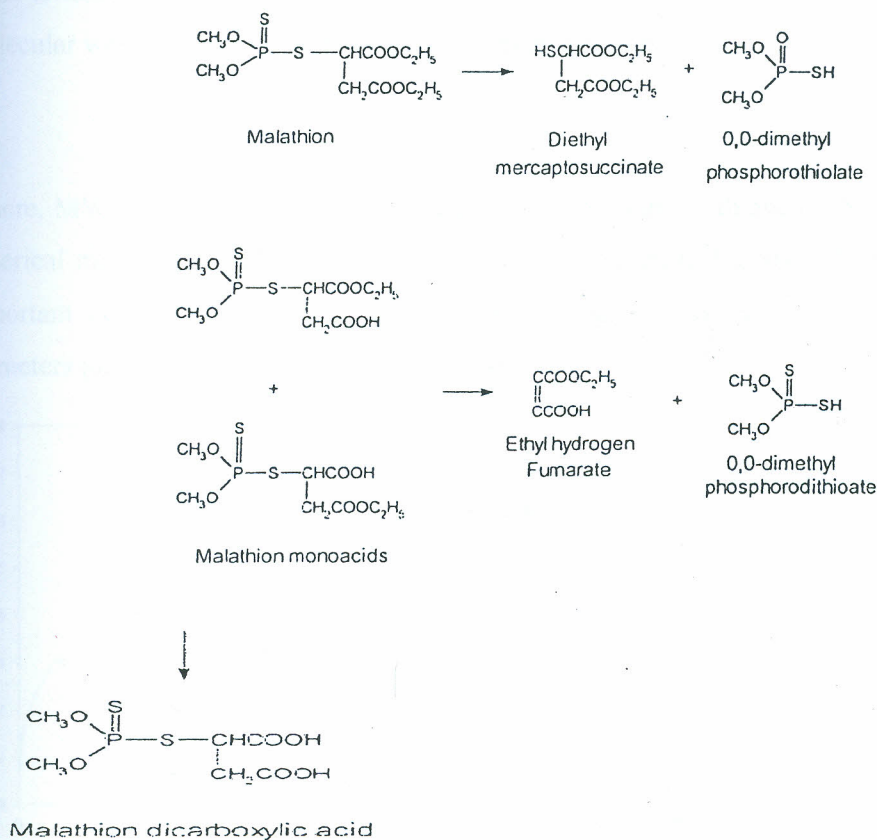
Figure 8: Degradation pathway of Malathion through hydrolysis

Source: Wolfe *et al.*, 1975.

2.6 Determining kinetic diameter of a molecule

Critical diameters are computed as the internuclear distance between the two nuclei that intersected the surface of the smallest possible cylinder containing all nuclei plus an estimate of the van der Waals radii of the hydrogen (1.2 Å) or oxygen (1.52 Å) atoms involved. Molecule (*maximum*) ''lengths'' are calculated as the distance between the two farthest-apart atoms along a line orthogonal to the critical diameter, plus an estimate of the atoms' radii.

However, the *kinetic diameter* (r) is estimated from the properties of the fluid at the critical point (c), shown in Eqs. (2) and (3). (Jungho *et al.*, 2011).

$$r = 0{:}841 V_c^{1/3} \qquad\qquad [2]$$

$$r = 2{:}44 (T_c/P_c)^{1/3} \qquad\qquad [3]$$

Where V_c is the critical volume in $cm^3\ mol^{-1}$, T_c is the critical temperature in Kelvins and P_c is the critical pressure in atmospheres. The kinetic diameter has also been correlated with the molecular weight using Eq. (4) for aromatic hydrocarbons.

$$r = 1.234 (MW)^{1/3} \qquad\qquad [4]$$

Where, MW is the molecular weight in $g\ mol^{-1}$. This kinetic diameter estimation assumes a spherical molecule, and hence the critical mass is related to the size of the sphere. Equally important is that, molecular weights have been shown to be closely related to kinetic diameters (as shown in Figure 9 and Table 6).
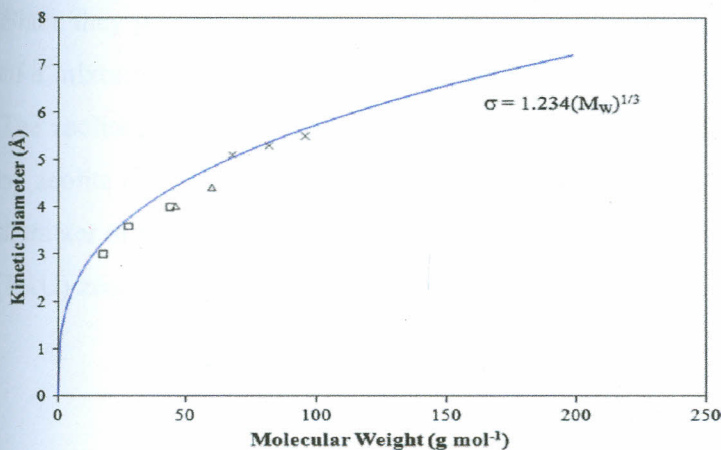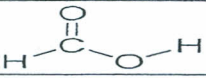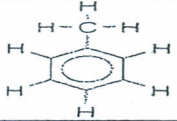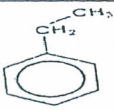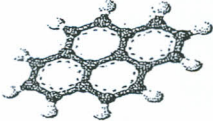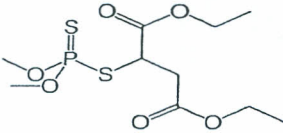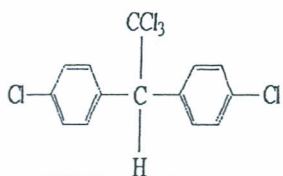
Figure 9: Showing the variation of kinetic diameter verses the molecular weight (Jungho et al., 2011).

33

Table 6: Molecular dimensions (adopted from Jungho et al, 2011).

Molecule	Chemical Structure	Critical diameter (width) (Å)	Maximum diameter (length) (Å)	Kinetic diameter (r) (Å)
Water (RMM = 18)		1.80	n.d	3.00
Formic acid (MM =		4.60	4.60	4.00
Toluene (RMM =		6.70	8.70	5.85
Ethyl benzene (RMM =		6.70	9.20	6.00
Pyrene (RMM =		7.36	9.80	7.24
Malathion (RMM= 330.36)		7.00	11.00	8.60
1, 1, 1-trichloro-2, 2-bis-(p-chlorophenyl) ethane. (DDT) (RMM; 354.5)		5.00	11.00	7.20

Since they possess pore sizes of several angstroms, zeolites are able to separate components of a mixture on the basis of a difference in molecular size (that is, molecular sieving effect). The zeolite pore size is mainly determined by its unique structure, but it can also be affected by zeolite chemical composition (Blagica et al., 2006).Specifically, the effects of molecular diameter of malathion on zeolite mordenite (MOR), ferrierite (FER), ZSM-5 (MFI) and USY (FAU) zeolites has not been documented.
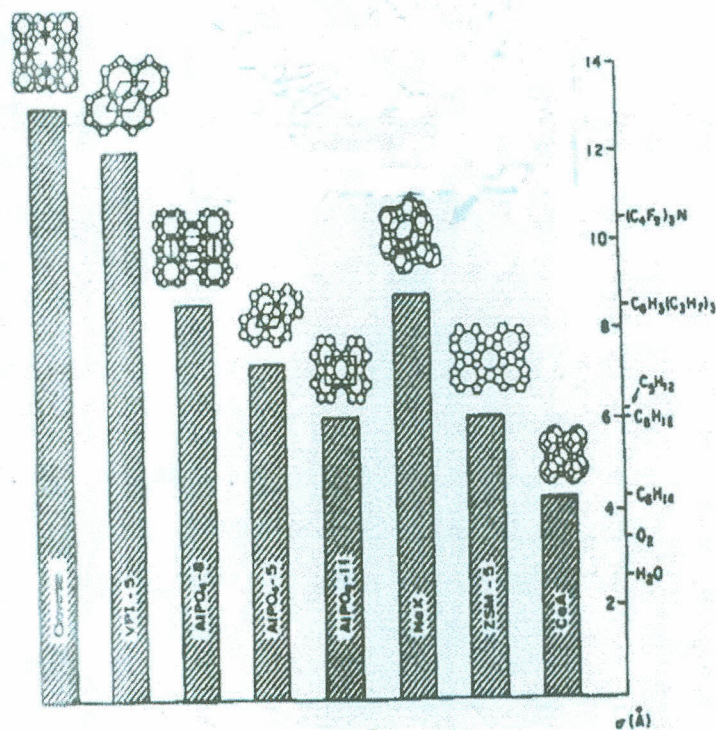
Figure 10: matching of the molecular sizes with the openings of the various zeolites. (Wilkinson, 2014)

2.6.1 Window opening (pore size) and internal surface area

For environmental pollutants especially those of organic origin, ability to estimate their size is important. Mainly, *critical diameter* is the diameter of the smallest cylinder inside which the molecule will fit, while the *maximum diameter* is defined as the longest dimension of the molecule (Jungho, et al., 2011)the effect of window opening on pesticide removal has not been documented.

CHAPTER THREE

MATERIALS AND METHODS

3.1.1 Materials and Instruments

This section shall outline the materials and instruments used during experimental work applied in the acquisition of data and all the experimental measurements were done at room temperature, unless stated otherwise.

3.1.1 Materials

The solvents: n-hexane, dichloromethane and acetone used were supplied by Sigma Aldrich Brazil ltd and were all AR grade. Analytical grade anhydrous Na_2SO_4, and NaCl(both99%pure), and Whatman filter papers were also obtained from Sigma Aldrich Brazil Ltd.Malathion and DDT analytical standard and zeolite mordenite, Ferrierite, USY and Faujasite were purchased from Sigma- Aldrich Inc. (Brazil).

3.1.2 Instruments

Instruments used included; Vulcan oven (modelA-550,Dentsply International, USA),analytical balance (SartoriusBP210S,Germany),suction pump(model 7049-05,Chicago,USA),rotary evaporator (EyelaN-100,Japan),gas Chromatograph (Varian chrompack, Japan),FT-IR spectrometer (Equinox55,Japan) and X-ray diffractometer (Scintag XDS 2000, Germany),NMR-Bruker Avance III-4000,SEM-aphilips XL30 FEG EDS-a Philips XL30 FEG.

3.2 Sodium exchange of zeolites

Twenty (20) grams of each zeolite sample (FERR, MOR, USY and ZSM-5), in a 250 ml beaker were exchanged by soaking them in 100 mls of 0.5M, $NaNO_3$. Later the zeolites were heated using a Agitador Magnetico C/Aquecimento MA085/CT hot plate at $80^{\circ}C$ for 60 minutes while stirring with magnetic stirrer. The separation was achieved by centrifuging the mixture in Revan Centrifuge Ciclo C.T at 3000 rpm for 3 mins. The decantant was washed using distilled water. This process was repeated three times and finally the decantant was dried in Fanem hot air oven model 315SE kept at $100^{\circ}C$ for 10hrs.The zeolites were then considered totally exchanged and were ready for activation.

3.3 Activation of zeolites

With a view to promoting the stabilization of physical, chemical and catalytic properties of the material, samples of zeolite (FERR, MOR, USY and ZSM-5), were subjected to activation, by a procedure in two stages. Initially, the sample was subjected to a heating ramp rate of 5°C / min from ambient temperature to reach 500°C in an inert atmosphere of nitrogen (flow rate 100 mL / min) after the temperature reached 500°C, maintained the system under these conditions for 1 hour, then the N_2 flow is replaced by dry air at a flow rate of 100 mL / min and temperature of 500°C for 4 hrs. This activation procedure aimed at removing matrix water and any ammonia which could still be held up in the zeolite structure.

3.4 Sample collection and treatment

Fifteen(15) l of surface water was collected from Monjolinho River, which is located near Federal University of Sao Carlos in Brazil, (22°01′04″S47°53′27″W22.01778°S 47.89083°W), at the source by scooping the surface waters. The physical-chemical characteristics of the water was determined at the Department of chemistry of UFScar; after which the water was filtered under pressure into a glass container using Whatman filter paper to remove the suspended particles. This was done three times in the order of decreasing pore sizes that is, 1.2μm, 0.7μm then finally 0.45μm. scooping

3.5 Preparation of stock solution of Malathion

Stock solutions of malathion was prepared by dissolving 100mg of malathion into 250mL of acetone to make a concentration of 400ppm.It was then transferred into a dark amber bottle which was corked and kept in a fridge at -4 °C.

3.6 Experimental Design

The research was set up at University of Sao Carlos laboratory of catalysis (LABCAT), with fourteen set-ups of three replicates each at 27°C as described below.

A 100mLwater sample was measured and transferred into a150mL glass beaker. Into the beaker, 2.5 mL of malathion earlier dissolved in 250 mL of acetone was added to make10ppm of malathion this was used as a control.

In another set up, 100mL water sample was measured and transferred into a150mL glass beaker. Into the beaker, 2.5 mL of malathion earlier dissolved in 250mL of acetone was added

to make10 ppm of malathion. One gram of ZSM-5 zeolite was weighed and added to the jar then stirred. This was repeated for each and every type of zeolite used to come up with 13 sets. The data obtained were in each case were analyzed and reported as Mean ± Standard error.

3.7 Analysis of water samples

After 30minsfrom the start time of treatment, 20 mLeach was transferred to clean label amber bottles from each of the beakers in the three setups and the pH measured. The specific time intervals for sampling were 30 mins, 60 mins, 90 mins, 8 hrs, 24 hrs, 48 hrs and 72 hrs, after the beginning of the treatment.

3.8 Extraction of analytes

Solvent extraction was done following the method of Zweig and Devine (1969) where20 mL sample was transferred into 100 ml separating funnel. One gram sodium chloride was added to the sample to salt out the pesticide from the aqueous phase.A10mLvolume of dichloromethane was then added to the mixture and shaken for 5mins, with periodic venting to release pressure. The mixture was allowed to stand for 5mins until aqueous and organic layers clearly separated out. The organic layer was transferred into a clean 50mLbeaker containing 2 g anhydrous sodium sulphate to dry the extract.Another10mLof analytical grade dichloromethane was added to the separation funnel, shaken for 5mins and allowed to stand for separation to occur. The process was repeated three times for each sample. Theextractswerepooledanddriedwith2gramsof anhydrous sodium sulphate and allowed to stand. Filtration using a funnel and Whatman No.1 filter paper was done to remove the clumped sodium sulphate crystals from the extract. The dried sample was concentrated to dryness using an Eyela N-1000 rotary evaporator in a water bath temperature at 40°C. One milliliter of HPLC grade n-hexane was used to reconstitute the analyte which was then transferred to a clean amber vial awaiting GC-MS analysis.

3.9 Gas Chromatographic analysis of the samples

GC analysis was done at standard conditions using Varian Chrompack with MS.The capillary column was RTX-1MS, length 30m, id 0.25mm and 0.25μm films. The carrier gas was helium with a 16.2mL/min flow rate, pressure 89.7Kpa, total flow 16.2 mL/min, column flow 1.20mL/min, linear velocity 40.7cm/sec, purge flow 3.0 mL/min and split ratio 10.0.2.0μL of

the sample was injected at a temperature of $200^{\circ}C$. The oven temperature was kept at $100^{\circ}C$ with a hold time of 0 minutes, and then from $100^{\circ}C$ to $300^{\circ}C$ at a rate of $10^{\circ}C/min$ with a hold time of 5minute. The detector was maintained at $300^{\circ}C$.

Full scan mode was used for qualitative analysis that is for positive identification of target analyte which is based on the mass spectra and retention time of the malathion. Once the fragmentation ions of malathion were identified, 3 quantification ions were selected for SIM mode analysis. The concentration of malathion residue was determined using external calibration and the formula below:

Concentration in $\mu g /L = ABV_t V_i W_s$

Where:

A= Response factor (1/slope from calibration curve)

B = Peak area

V_t= Extract volume in μL

V_i= Volume injected in μL

W_s= Weight of water sample (kg)

The control and blank samples were used to calculate the recovery percentage after extraction and clean up processes as shown below:

$$\%Recovery= \frac{Amount\ found - Amount\ from\ unspiked\ sample}{Amount\ spiked} \times 100$$

Where

Amount found is the calculated concentration from the response of the spiked sample. Amount from unspiked sample is the original concentration of the blank.

3.10 Characterization of zeolite

At the end of the experiment the zeolites were dried by pressing the cake in between Whatman No.1 filter papers and were taken for XRD, FTIR, SEM, NMR and EDS for characterization.

3.10.1 Infrared measurements (IR)

Fourier Transform Infrared (FTIR) analysis offers quantative and qualitative studies for organic and inorganic samples. It identifies chemical bonds in molecule by producing an infra-red absorption spectrum. The spectra produce a profile of the sample, a distinctive molecular fingerprint that can be used to screen and scan samples for many different components. It is an effective analytical instrument for detecting functional groups and characterizing covalent bonding information.

A mixture of 1% sample and 99% IR grade KBr (to dilute the sample for better resolution) was ground in a glass mortar to fineness. For air sensitive samples, the weighing and grinding were both performed under inert (argon gas) atmosphere in the glove box. Then ca. 0.10 gram of the ground mixture were fixed in FT-IR MB-102 Bomen – Michelson at a nominal resolution of 2 cm^{-1}. However, the actual amount of zeolite materials may differ from pellet to pellet depending on how much adsorbate and exchanged cation are in the sample. A total of 128scans were collected for each sample spectrum. The spectrometer was purged with nitrogen gas for 30 minutes before and after pellet insertion, after which the spectrum was recorded over the 4000 – 400 cm^{-1} range. The FTIR spectrometer was calibrated by checking the deviation between the literature and experimental polystyrene spectral band positions. The root mean square deviation (rmsd) for the two spectra was 1.32 cm^{-1}. (Blocki, 1993).

3.10.2 X-ray diffraction measurements (XRD)

The X-ray diffractograms was used for identification of the material (type of crystalline structure) and also in checking the presence of contaminants phases by comparison with published data (Robson, 2001; Treacy, Higgins, & Ballmoos, 1996) Another property that could be obtained from X-ray diffraction was the degree of crystallinity of the material by comparing with a standard sample diffractograms obtained under the same analytical conditions. The degree of crystallinity of the material under study was determined by comparing the sum of peak areas of the most intense diffraction pattern with the sum of the areas of a standard sample.

The samples were characterized by X-ray diffraction (XRD) analysis on a Shimadzu equipment model XRD-6000 using a radiation source of Cu K α with voltage of 30 kV and current 30 mA, Ni-filter. Data were collected in the 2θ range of 5-50 degrees with a goniometer speed of 2 ° / min with a step of 0.02 degree.

3.10.3 Scanning Electron Microscopy (SEM)

The scanning electron microscope (SEM) uses a focused beam of high-energy electrons to generate a variety of signals at the surface of solid specimens. The SEM is routinely used to generate high-resolution images of shapes of objects and to show spatial variations in chemical compositions by acquiring elemental maps or spot chemical analyses using EDS, discrimination of phases based on mean atomic number (commonly related to rel ative density) using BSE, and compositional maps based on differences in trace element "activators" (typically transition metal and Rare Earth elements) using CL. The SEM is also widely used to identify phases based on qualitative chemical analysis and/or crystalline structure. Precise measurement of very small features and objects down to 50 nm in size is also accomplished using the SEM. Backscattered electron images (BSE) can be used for rapid discrimination of phases in multiphase samples. SEMs equipped with diffracted backscattered electron detectors (EBSD) can be used to examine micro fabric and crystallographic orientation in many materials (Egerton, 2005). Scanning Electron Microscopy (SEM) analysis was performed using a Philips XL 30 FEG microscope installed at the Structural Characterization Laboratory Department of Materials Engineering – UFSCAR.

3.10.4 Energy Dispersive X-ray Spectroscopy (EDS)

Interaction of an electron beam with a sample target produces a variety of emissions, including x-rays. An energy-dispersive (EDS) detector is used to separate the characteristic x-rays of different elements into an energy spectrum, and EDS system software is used to analyze the energy spectrum in order to determine the abundance of specific elements. EDS was used to find the chemical composition of materials down to a spot size of a few microns, and to create element composition maps over a much broader raster area. Together, these capabilities provide fundamental compositional information for a wide variety of materials. A typical EDS spectrum is portrayed as a plot of X-ray counts vs. energy (in keV). Energy peaks correspond to the various elements in the sample. Generally they are narrow and readily resolved, but many elements yield multiple peaks. For example, iron commonly shows strong K_α and K_β peaks. Elements in low abundance will generate x-ray peaks that may not be resolvable from the background radiation (Kowenje &Osewe 2015).

41

Energy dispersive X-ray spectroscopy analysis were performed using a Philips XL 30 FEG microscope installed at the Structural Characterization Laboratory – Department of Materials Engineering – UFSCAR.

3.10.5 Nuclear Magnetic Resonance (NMR)

Nuclear magnetic resonance (NMR) is a physical phenomenon in which magnetic nuclei in a magnetic field absorb and re-emit electromagnetic radiation. This energy is at a specific resonance frequency which depends on the strength of the magnetic field and the magnetic properties of the isotope of the atoms; NMR allows the observation of specific quantum mechanical magnetic properties of the atomic nucleus. All isotopes that contain an odd number of protons and/or of neutrons (see Isotope) have an intrinsic magnetic moment and angular momentum, in other words a non-zero spin, while all nuclides with even numbers of both have a total spin of zero. A key feature of NMR is that the resonance frequency of a particular substance is directly proportional to the strength of the applied magnetic field. It is this feature that is exploited in imaging techniques; if a sample is placed in a non-uniform magnetic field then the resonance frequencies of the sample's nuclei depend on where in the field they are located. The resolution of the imaging technique depends on the magnitude of magnetic field gradient. By studying the peaks of nuclear magnetic resonance spectra, chemists can determine the structure of many compounds. It can be a very selective technique, distinguishing among many atoms within a molecule or collection of molecules of the same type but which differ only in terms of their local chemical environment (Lynam & Keeler, 2005). The solid-state NMR was performed by Bruker Avance III-400 operating at 9.4T magnetic field. Two channels MAS-4mm probe head was used. Samples were packed into 4mm zirconia rotors (about 60mg). Rotors was spun at 5 kHz of spinning speed for running the carbon-13 experiments. In ^{27}Al rotors were spun at 10khz. For ^{13}C-CPMAS experiments were done by using recycle delay of 3s and contact time of 3ms. For ^{27}Al spectrum, a MAS experiment were done by using 1s as recycle delay.

For liquid state NMR was performed by Bruker Avance III-400 operating at 9.4T magnetic field, an inverse two channel 1H-X probe head was used. Samples were dissolved in 500µL acetone-d6. Numbers of scans were 64, acquisition time 4.0s and recycle delay was 2.0s.

3.10.6 Thermal Gravimetric Analysis (TGA)

Thermal treatment of compounds results in weight loss due to drying and production of volatile substances by chemical reactions. Thermal gravimetric analysis was performed to determine weight loss upon thermal treatment of zeolite as a function of time or heating temperature. During the operation of the TGA, the signals are relayed to the computer connected to it for data recording. Themograms were produced from the recorded data as graphical plots of percentage of residual weight against the temperature (Javed *et al.*, 20 1 5).

3.11 Reaction Kinetics

3.11.1 Kinetics Studies

Here, 14set-ups of three replicates each at 27 °C was used in which 100 mL of water sample was measured and transferred into a 150 mL glass beaker. Into the beaker, 2.5 mL of malathion earlier dissolved was added to make a concentration of 10 ppm which was used as a control. In another set up, 100 mL water sample was measured and transferred into a150 mL glass beaker. Into the beaker, 2.5 mL of malathion was likewise added to make a concentration of 10 ppm. 1 g of ZSM-5 zeolite was weighed and dispersed into the jar with stirring and was repeated for each type of zeolite used to come up with 13 sets. For each case, the operational pH of the solutions was measured. At pre-determined time intervals (30 mins, 60 mins, 240 mins, 8 hrs 24 hrs, 48 hrs and 72 hrs); aliquots were obtained from the reaction vessels for residual pesticide analysis. Solvent extraction was done following the protocol described in (Ogunah, et al., 2013) and residual malathion determined by GC-MS. The amount adsorbed (q_t) at time *t*, was obtained by the mass balance equation:

$$q_t = \frac{(c_o - c_1)}{m} V \qquad (1)$$

To obtain the kinetics parameters, the data was modeled using pseudo-first-order and pseudo-second-order equations below.

$$\text{Pseudo-first-order model: } \log(q_e - q_t) = \log q_e - \frac{k_1}{2.303} t \qquad (2)$$

$$\text{Pseudo-second-order model: } \frac{t}{q_t} = \frac{1}{k_2 q_e^2} + \frac{t}{q_e} \qquad (3)$$

3.11.2 Equilibrium studies

To obtain the equilibrium adsorption isotherms, 0.1 g of each zeolite was separately, in triplicate vessels, dispersed into reaction flasks containing 50 mL of various concentrations of (20,10,5

ppm) of malathion and magnetically stirred at 300 rpm and 300 K. After equilibration, residues and degradation products of the malathion and were quantified. The amount adsorbed (%) was obtained by the relation:

$$\%adsorbed = \frac{c_0 - c_e}{c_0} \times 100 \qquad (4)$$

The equilibrium adsorption capacity, q_e, at different adsorbate concentration levels was obtained by the equation: $q_e = V\frac{(c_0 - c_e)}{m} \qquad (5)$

The equilibrium adsorption data was then fitted for two widely used adsorption isotherm equations, namely, Langmuir, and Freundlich. The linearized version of the isotherm equations are given by:

Langmuir isotherm: $\frac{1}{q_e} = \frac{1}{Q_0} + \frac{1}{Q_0 K_L C_e} \qquad (6)$

Freundlich isotherm: $\log q_e = \log K_1 + \frac{1}{n}\log C_e \qquad (7)$

CHAPTER FOUR

RESULTS AND DISCUSSIONS

4.1 Introduction

The data in this section were obtained primarily from XRD, FTIR, SEM, TGA, DTGA, EDS, and NMR measurements of Na exchanged zeolites(mordenite (MOR), ferrierite (FER), ZSM-5 (MFI) and USY (FAU) and malathion treated Na exchanged zeolites(mordenite (MOR), ferrierite (FER), ZSM-5 (MFI) and USY (FAU). All measurements were taken at room temperature, unless otherwise stated. In addition the identification of metabolite and their residual concentration was done through GC-MS analysis

4.2 Characterization of zeolites

Characterizations of zeolites were done by use of XRD, FTIR, SEM and EDS to check for the manufacturer's specifications. From the XRD spectra (Figures 15-20), it is observed that the zeolite spectra conformed to the other spectra of zeolites obtained from international zeolite authority data base thus confirming that the materials used were actually the named zeolites. They all showed partial amorphous nature in the region from 40-50 degrees 2Θwith full crystallinity and high intensities. Sodium exchange did not affect the structure of the zeolites for the patterns were still similar though with high intensities (Figures 29-34). FTIR confirmed the said stability as all the spectra obtained were also similar with the ones reported earlier (Figures 31-36). For the morphology observed from SEM images they were similar to the ones reported earlier in the literature (Yang, 2006;Leardini, Martucci, Braschi, Blasioli, & Quartieri, 2014; Pérez*et al.*, 2013).EDS analysis confirmed the presence of elements and was used to calculate the Si/Al ratio as was indicated by the manufacturer's. The calculated values matched the ones indicated by the manufactures as shown in the Table 7 below.

Table 7: Si/Al ratio of different types of zeolites

ZEOLITE TYPE	Calculated Si/Al ratio (a.u)	Manufacturers Si/Al ratio(a.u)
FERR	9.94 ±00	9.94
MOR	10.57 ±00	10.57
MOR	6.42 ±00	6.42
MFI	22.97 ±00	22.97
MFI	12.86 ±00	12.86
FAU-Y	2.77 ±00	2.77

4.2.1 Characterization of sodium exchanged zeolites

The zeolite materials obtained were characterized by X-ray diffraction then compared to a standard sample (Robson, 2001; Treacy *et al*., 1996) as shown in Figures 11 to 16 below. The results show that the samples that were ion exchanged then activated fit standard sample of zeolite USY, MOR, FER and ZSM-5, identified as pure with intensities somewhat lower than those obtained from the standard sample. The higher intensities imply a gradual gain of crystallinity possibly caused by Na^+ relocation within the zeolite matrix (Kowenje *et al*., 2006).

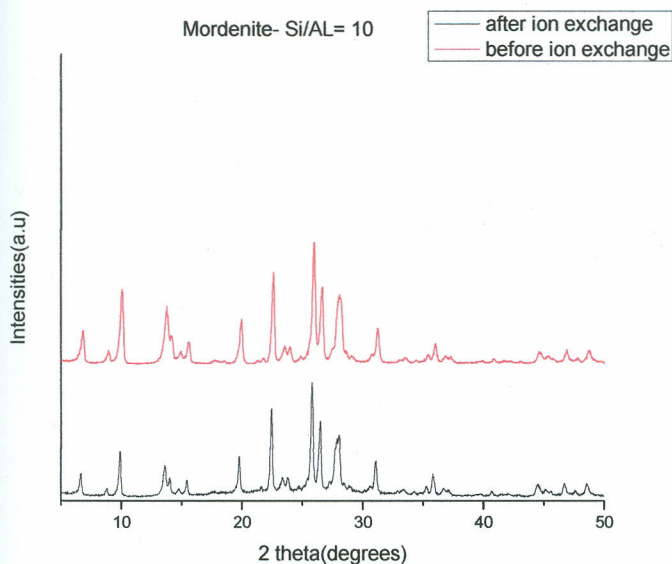## 4.2.2 X-ray diffraction for the synthesized Na-exchanged zeolites
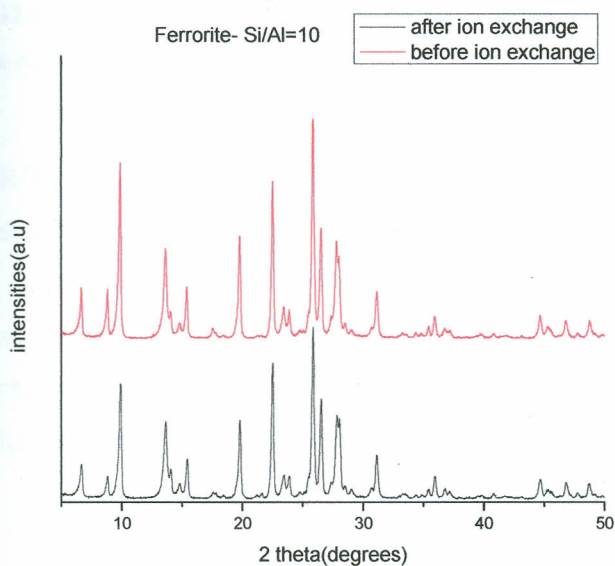
Figure 11:X-rays of two samples of Ferrierite zeolite (Si/Al=10), wherein (1) the experimental product 1, after Na exchange (2) sample standard

The XRD pattern of nanocrystalline ferrierite before and after Na-exchange was similar (Figure 11). Synthesized nanocrystalline sample shows the partial amorphous nature in the region from 40-50 degrees 2Θ. However, the activated sample indicated the full crystallinity. It was also noted that the intensity of nanocrystalline ferrierite before was higher than after ion exchange. The higher intensities imply a gradual gain of crystallinity possibly caused by Na^+ relocation within the zeolite matrix (Kowenje *et al*., 2006).
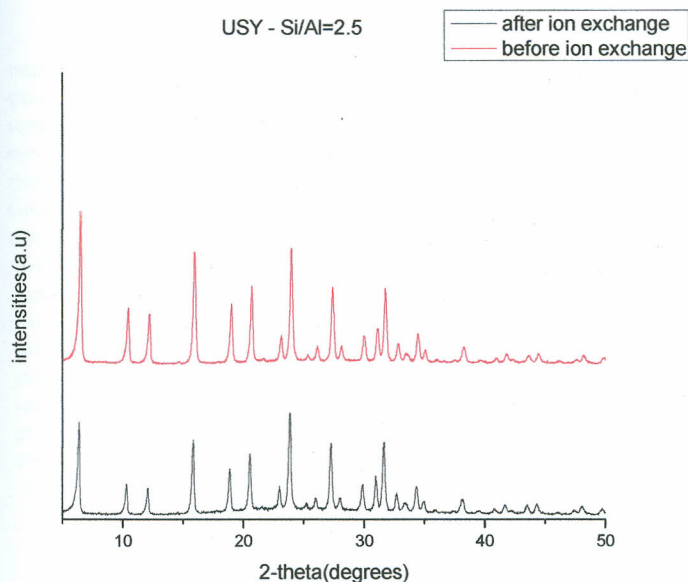
46
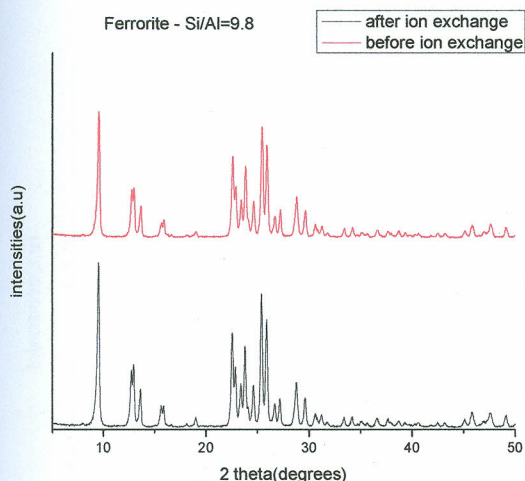
Figure 12:X-rays of two samples of Ferrierite zeolite (Si/Al=9.8), wherein (1) the experimental product 1, after Na exchange (2) sample standard

The XRD pattern of nano crystalline ferrierite before and after was similar (Figure 12). As-synthesized nano crystalline sample shows the partial amorphous nature in the 40 degrees region from 30-40 degrees 2Θ. However, the calcined sample indicated full crystallinity. It was also noted that the intensity of nanocrystalline ferrierite before was higher than after the ion exchange. The higher intensities imply a gradual gain of crystallinity possibly caused by Na^+ relocation within the zeolite matrix (Kowenje *et al.*, 2006).
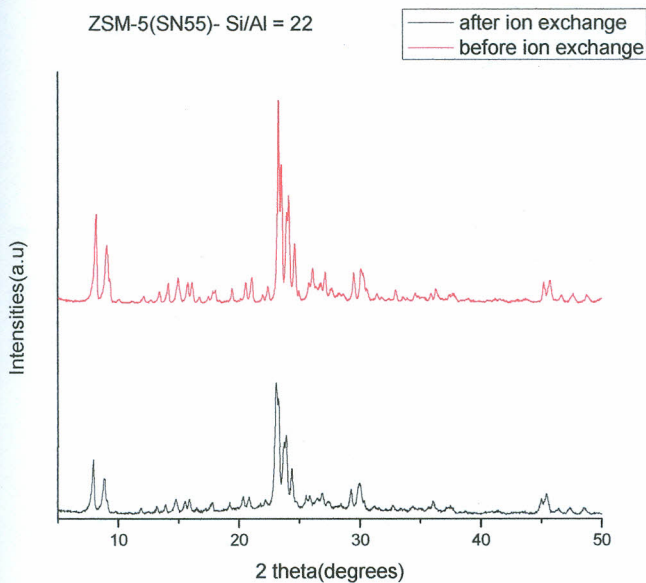
Figure 13:X-rays of two samples of ZSM-5zeolite (Si/Al=22), wherein (1) the experimental product 1, after Na exchange (2) sample standard

The XRD pattern of nano crystalline ZSM-5 before and after was similar (Figure 13). Synthesized nano crystalline sample shows the partial amorphous nature in the 30 region from 30-40 degrees 2Θ. However, the calcined samples indicated the full crystallinity. It was also noted that the intensity of nano crystalline ZSM-5 before was higher than after ion exchange. The higher intensities imply a gradual gain of crystallinity possibly caused by Na^+ relocation within the zeolite matrix (Kowenje *et al.*, 2006).
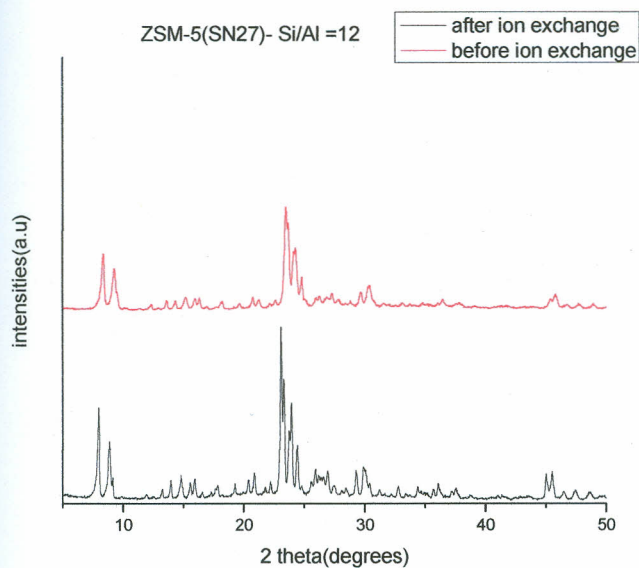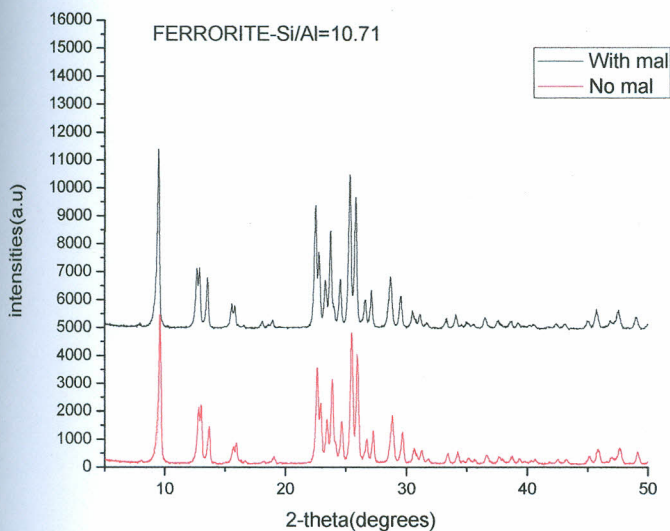
Figure 14:X-rays of two samples of ZSM-5zeolite (Si/Al=12), wherein (1) the experimental product 1, after Na exchange (2) sample standard

The XRD pattern of nano crystalline ZSM-5 before and after was similar (Figure 14). As-synthesized nano crystalline sample shows the partial amorphous nature from 10-20 degrees 2Θ and region from 30-40 degrees 2Θ. It was also noted that the intensity of nano crystalline ZSM-5 before was higher than after ion exchange. The higher intensities imply a gradual gain of crystallinity possibly caused by Na^+ relocation within the zeolite matrix (Kowenje *et al.*, 2006).
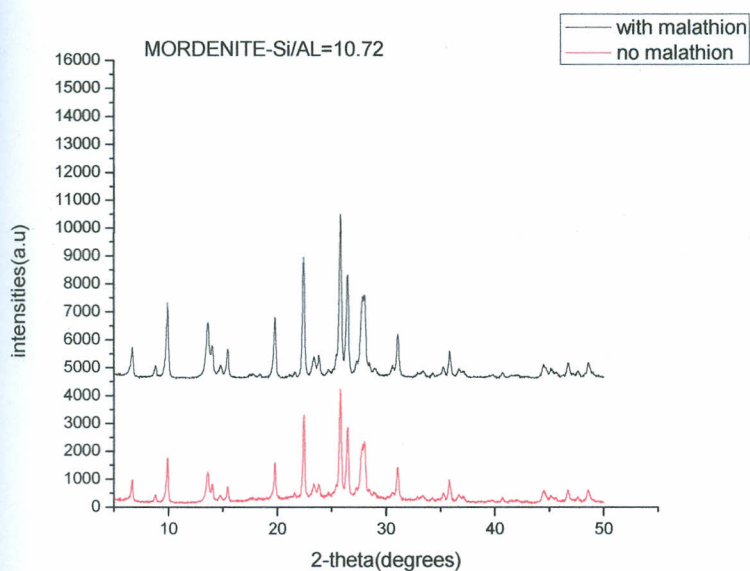
Figure 15:X-rays of two samples of mordenite zeolite (Si/Al=10), wherein (1) the experimental product 1, after Na exchange (2) sample standard

The XRD pattern of nano crystalline mordenite before and after was similar (Figure 15). As-synthesized nano crystalline sample shows the partial amorphous nature in the 30 region from 30-40 degrees 2Θ. However, the calcined sample indicated the full crystallinity. It was also noted that the intensity before was higher than after ion exchange. The higher intensities imply a gradual gain of crystallinity possibly caused by Na^+ relocation within the zeolite matrix (Kowenje *et al.*, 2006).
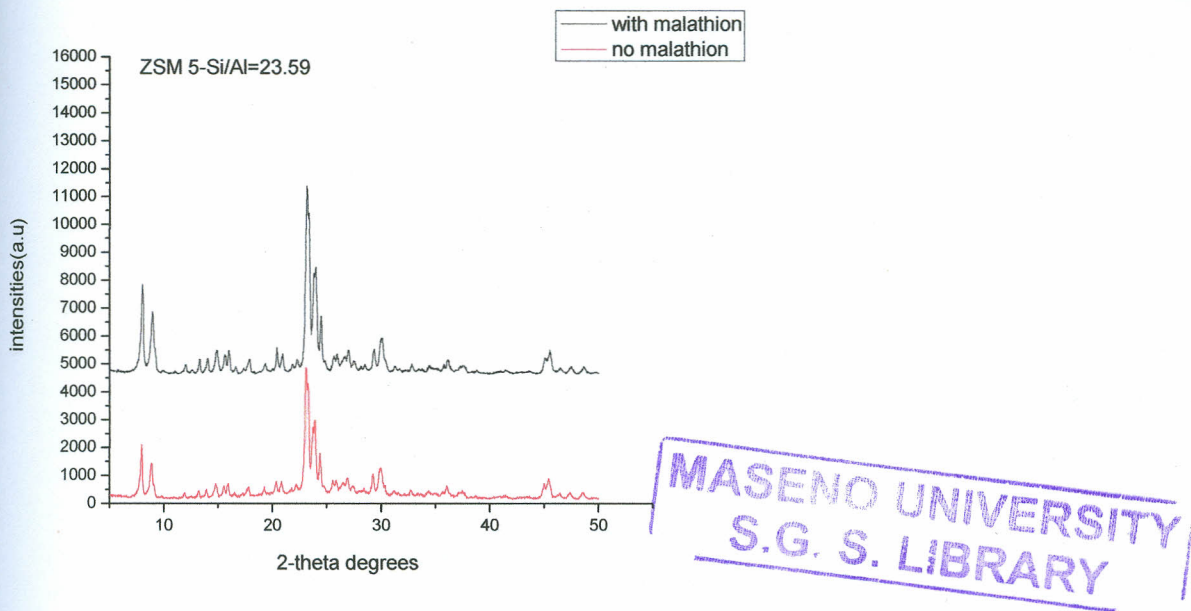
Figure 16: X-rays of two samples of USY zeolite (Si/Al=2.5), wherein (1) the experimental product 1, after Na exchange (2) sample standard

The XRD pattern of nano crystalline USY before and after was similar (Figure16). As-synthesized nano crystalline sample shows the partial amorphous nature in the 40 region from 40-50 degrees 2Θ. However, the calcined sample indicated the full crystallinity. It was also noted that the intensity before was higher than after ion exchange. The higher intensities imply a gradual gain of crystallinity possibly caused by Na^+ relocation within the zeolite matrix (Kowenje *et al.*, 2006).

4.1.3 X-ray diffraction for Na-zeolite treated with Malathion

The material obtained was characterized by X-ray diffraction then compared to Na-exchanged standard sample as shown in Figures 17 to 22 below. The results show that the samples that were Malathion treated fits Na-exchanged standard sample of zeolite USY, MOR, FER and ZSM-5, with intensities higher than those obtained from the standard sample. The higher intensities imply a gradual gain of crystallinity possibly caused by Na^+ relocation within the zeolite matrix (Kowenje *et al.*, 2006).

51

Figure 17:X-rays of two samples of Ferrierite zeolite (Si/Al=10.71), wherein (1) the experimental product 1, after Na exchange (2) sample treated with Malathion

The XRD analysis of the malathion treated ferrierite zeolite (Figure 17) revealed that after the treatment procedure, no substantial changes were observed in the ferrierite pattern probably due to the high dispersion of the pesticide. However, the peak intensities of the samples were higher than those of the starting material (ferrierite), showing the gradual gain of crystallinity possibly caused by Na^+ removal from the zeolite matrix. Because the cell parameters were not considerably changed, the increase in the degree of crystallinity could be explained in part due to the X-ray absorption of malathion molecules. These data demonstrated that the structure of ferrierite was not affected by malathion adsorption and the process of absorption is Na^+ mediated.
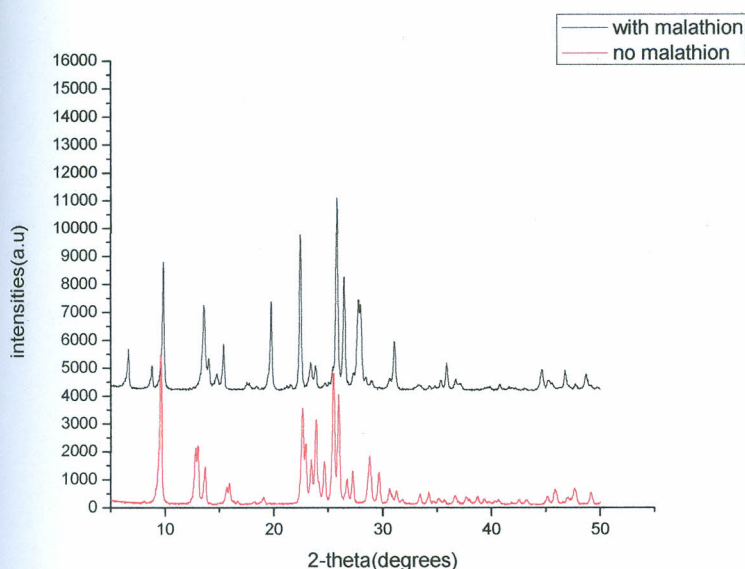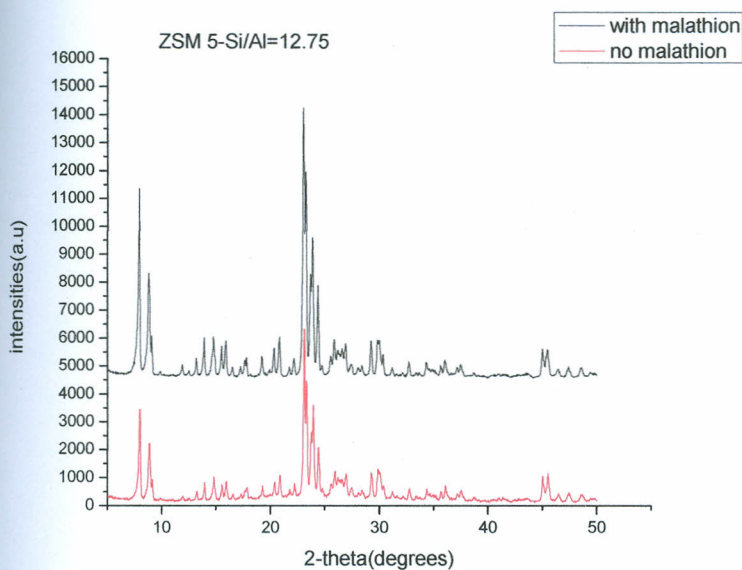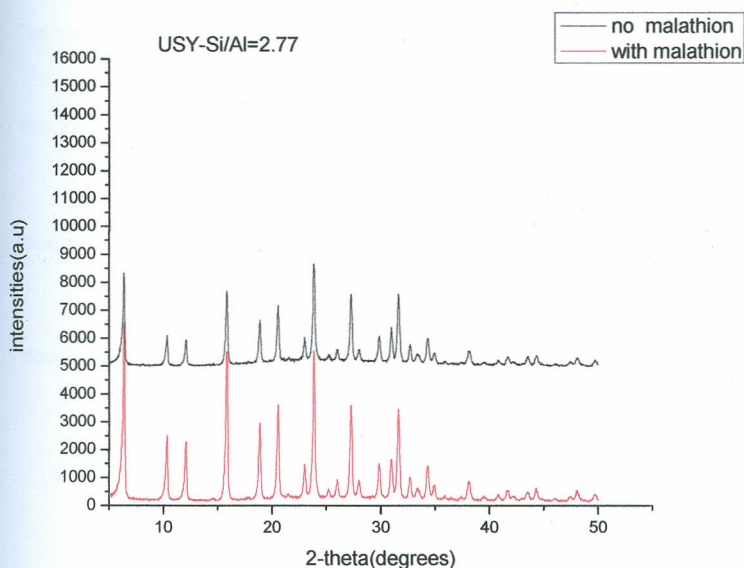
Figure 18: X-rays of two samples of mordenite zeolite (Si/Al=10.72), wherein (1) the experimental product 1, after Na exchange (2) sample treated with malathion

The XRD analysis of the malathion treated mordenite zeolite (Figure 18) revealed that after the treatment procedure, no substantial changes were observed in the mordenite pattern probably due to the high dispersion of the pesticide. However, the peak intensities of the samples were higher than those of the starting material (mordenite), showing the gradual gain of crystallinity probably caused by Na^+ removal from the zeolite surface. Because the cell parameters were not considerably changed, the increase in the degree of crystallinity could be explained in part due to the X-ray absorption by the malathion molecules. These data demonstrated that the structure of mordenite was not affected by malathion adsorption (Barrer, 1985).

Figure 19: X-rays of two samples of ZSM-5 zeolite (Si/Al=23.59), wherein (1) the experimental product 1, after Na exchange (2) sample treated with malathion

The XRD analysis of the malathion treated ZSM-5 zeolite (Figure19) revealed that after the treatment procedure, no substantial changes were observed in the ZSM-5 pattern probably due to the high dispersion of the pesticide. However, the peak intensities of the samples were higher than those of the starting material (ZSM-5), showing the gradual gain of crystallinity caused by Na^+ removal from the zeolite surface. The increase in the degree of crystallinity could be explained in part due to the X-ray absorption by the malathion molecules because the cell parameters were have not considerably changed,. These data demonstrated that the structure of ZSM-5was not affected by malathion adsorption (Barrer, 1985).

Figure 20: X-rays of two samples of mordenite zeolite (Si/Al=6.83), wherein (1) the experimental product 1, after Na exchange (2) sample treated with malathion

The XRD analysis of the malathion treated mordenite zeolite (Figure 20) revealed that after the treatment procedure, no substantial changes were observed in the mordenite pattern probably due to the high dispersion of the pesticide. However, the peak intensities of the samples were higher than those of the starting material (mordenite), showing the gradual gain of crystallinity caused by Na^+ removal from the zeolite surface. Because the cell parameters were not considerably changed, the increase in the degree of crystallinity could be explained in part due to the X-ray absorption of malathion molecules. These data demonstrated that the structure of mordenite was not affected by malathion adsorption (Barrer, 1985).

Figure 21: **X-rays of two samples of ZSM-5 zeolite (Si/Al=12.75), wherein (1) the experimental product 1, after Na exchange (2) sample treated with Malathion**

The XRD analysis of the malathion treated ZSM-5 zeolite (Figure 21) revealed that after the treatment procedure, no substantial changes were observed in the ZSM-5 pattern probably due to the high dispersion of the pesticide. However, the peak intensities of the samples were higher than those of the starting material (ZSM-5), showing the gradual gain of crystallinity caused by Na^+ removal from the zeolite surface. Because the cell parameters were not considerably changed, the increase in the degree of crystallinity could be explained in part due to the X-ray absorption by the malathion molecules. These data demonstrated that the structure of ZSM-5 was not affected by malathion adsorption (Barrer, 1985).

56

Figure 22: X-rays of two samples of USY zeolite (Si/Al=2.77), wherein (1) the experimental product 1, after Na exchange (2) sample treated with malathion

The XRD analysis of the malathion treated USY zeolite (Figure 22) revealed that after the treatment procedure, no substantial changes were observed in the USY pattern probably due to the high dispersion of the pesticide. However, the peak intensities of the samples were higher than those of the starting material (USY), showing the gradual gain of crystallinity caused by Na^+ removal from the zeolite surface. Because the cell parameters were not considerably changed, the increase in the degree of crystallinity could be explained in part due to the X-ray absorption of malathion molecules. These data demonstrated that the structure of USY was not affected by malathion adsorption (Barrer, 1985).

4.2 Characterization of treated zeolites using Energy Dispersive X-ray Spectroscopy (EDS) analysis

Figures 23 and 24 show EDS of the prepared sample. The results showed the presence of Si, Al, Na and O in the synthesized sample. The Si/Al molar ratio equals to what was stated by the manufacturers that is sigma Aldrich Brazil which supplied the zeolites but again after the treatments sulphur and phosphorous elements can be detected in the matrix.
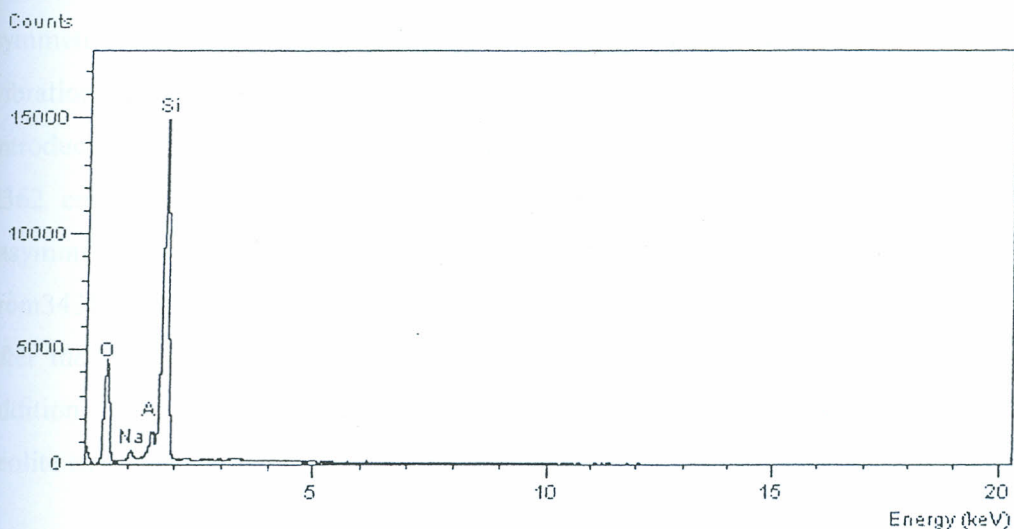
57

Figure 23: EDS spectrum showing elements in zeolite before treatment
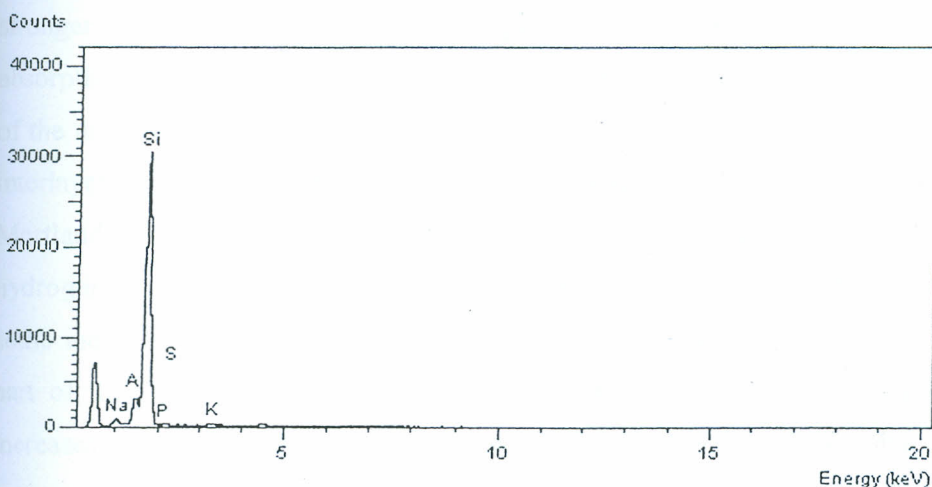

Figure 24: EDS of zeolite showing elements after treatment with Malathion

4.3 Na- zeolites treated with Malathion

4.3.1 Infrared spectra of USY (Si/Al=2.77) exposed to 10ppm Malathion

Figures 25 shows FTIR spectrum of USY (Si/Al=2.77) exposed to 10 ppm malathion. A representative FTIR spectrum of USY (Si/Al=2.77) showed bands related to O–H stretching vibration modes (asymmetric and symmetric) between 3438 cm^{-1}, 2362 cm^{-1}, 2455 cm^{-1} and 2338 cm^{-1}, and O–H bending vibrations at 1652 cm^{-1} associated with coordinated water molecules. The presence of the bands at 1151 cm^{-1} and 1030 cm^{-1} were assigned to internal

58

tetrahedral asymmetrical stretch while the band at 790 cm^{-1} might have been vibrations for symmetrical stretch, the band at595 cm^{-1}, 536 cm^{-1} and 515 cm^{-1} were due to double ring vibrations and finally the band at 473 cm^{-1} was assigned pore opening vibration. Upon introduction of malathion the most noticeable changes were the increase of band intensities at 2362 cm^{-1} and 2338 cm^{-1} which were related to O–H stretching vibration modes (asymmetric and symmetric), shifting of bands to higher wave numbers for instance band from3438 cm^{-1} to 3598 cm^{-1} and band at 1038 cm^{-1} to 1050 cm^{-1}. In all the bands obtained after the treatment there was reduction in intensity as shown in figure 25 after malathion addition. These changes were attributed to the malathion molecules interacting with the zeolite structure.

Lack of new bands shows that there was no formation of new chemical bonds between the malathion atoms and zeolite and that the only possibility was attraction of the molecules with stronger electrostatic forces during adsorption. The formation of the 1629 cm^{-1} to 1636 cm^{-1} absorption band is believed to be indicative of hydrogen bonding between a carbonyl group of the malathion molecule and some water molecules associated with the sodium ion on the interlayer surface. Similar hydrogen bonding reactions have been reported by Parfitt and Mortland(1968). The frequency shift shown to be less than 10 cm^{-1} suggests that the hydrogen bonding energies involved were small. The strength of such a hydrogen bond gives some indication of the acidity or the degree of dissociation of a proton forming an integral part of the hydration sphere of a saturating cation. As the positive charge of the cation increases (that is, monovalent vs. divalent), its ability to polarize the hydration water increases, making the hydrogen ion more labile. Hence the small perturbation observed for hydrogen bonding in the Na-USY-malathion system was consistent with the idea that the sodium tends to hydrate to only a limited extent on the interlayer surface. The persistence of the 1629 cm^{-1} band after exposure to water vapour indicated that there were carbonyl groups present in excess of the hydrogen bonding capacity of the Na-USY system (Gallo & Lawryk, 1991)
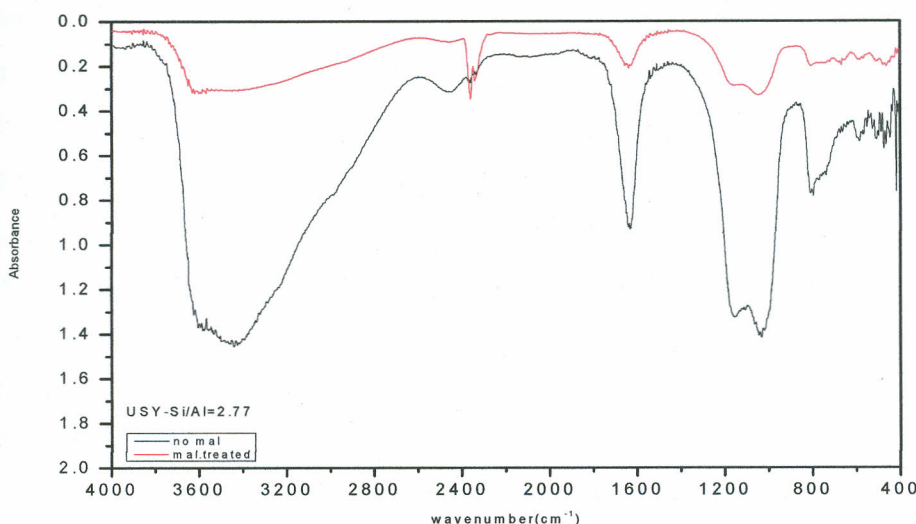
Figure 25: Infrared spectra of USY (Si/Al=2.77) before and after Malathion addition

4.3.2 Infrared spectra of Ferrierite (Si/Al=10.71) exposed to 10ppm Malathion

A representative FTIR spectrum of Ferrierite (Si/Al=10.71) showed bands related to O–H stretching vibration modes (asymmetric and symmetric) between 3636 cm^{-1}, 2972 cm^{-1}, 2894 cm^{-1},2364 cm^{-1} and2333 cm^{-1}, and O–H bending vibrations at 1982 cm^{-1},1848 cm^{-1}, 1652 cm^{-1},1625 cm^{-1} and 1384 cm^{-1} were associated with coordinated water molecules. The presence of the bands at 1202 cm^{-1} was assigned to internal tetrahedral asymmetrical stretch, band at1072 cm^{-1} was for asymmetric stretch and the band at 800 cm^{-1} and 759 cm^{-1} might have been vibrations for symmetrical stretch pore vibration, the band at 669 cm^{-1} and 528 cm^{-1}could be due to double ring vibrations and finally the band at 460 cm^{-1} was assigned pore opening vibration. Upon introduction of malathion the most noticeable changes were introduction of a band at1711 cm^{-1} which was due to carbonyl stretching of the ester group, 1419 cm^{-1} for CH$_3$ and CH$_2$ and finally 1364cm^{-1} for terminal CH$_3$ from malathion molecules. There was a decrease of band intensities at 2364 cm^{-1} and 2333 cm^{-1} which were related to O–H stretching vibration modes (asymmetric and symmetric), shifting of bands to higher wave numbers. For example, band from1848 cm^{-1} to 1862 cm^{-1}. There was also disappearance of three bands that is bands at 2972 cm^{-1} and 2894 cm^{-1}. In most of the bands obtained after the treatment, there was reduction in intensity as shown in figure 26. These

60

changes were attributed to the malathion molecules interacting with the zeolite structure. The formation of the 1711 cm^{-1}absorption band is believed to be indicative of hydrogen bonding between a carbonyl group of the malathion molecule and some water molecules associated with the sodium ion on the interlayer surface. Similar hydrogen bonding reactions have been reported by Parfitt and Mortland(1968). The frequency shift was less than 10 cm^{-1} suggesting that the hydrogen bonding energies involved were small. The strength of such a hydrogen bond gives some indication of the acidity or the degree of dissociation of a proton forming an integral part of the hydration sphere of a saturating cation. As the positive charge of the cation increases (that is monovalent vs. divalent), its ability to polarize the water of hydration increases, making the hydrogen ion more labile. Hence the small perturbation observed for hydrogen bonding in the Na-ferrierite (Si/Al=10.71)-malathion system was consistent with the idea that the sodium tends to hydrate to only a limited extent on the interlayer surface. The persistence of the 1711 cm^{-1} band after exposure to water vapour indicated that there were carbonyl groups present in excess of the hydrogen bonding capacity of the Na-ferrierite (Si/Al=10.71)system (Gallo & Lawryk, 1991).
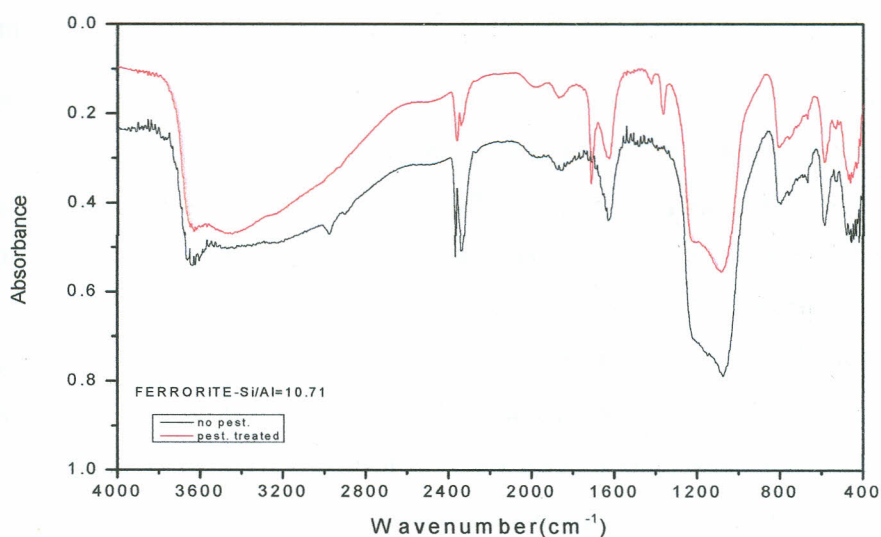

Figure 26: Infrared spectra of Ferrierite (Si/Al=10.71) before and after Malathion addition

61

4.3.3 Infrared spectra of ZSM-5 (Si/Al=23.59) exposed to 10ppm Malathion

Figures 27 shows FTIR spectrum of ZSM-5 (Si/Al=23.59) exposed to 10 ppm malathion. A representative FTIR spectrum of ZSM-5 (Si/Al=23.59) showed bands related to O–H stretching vibration modes (asymmetric and symmetric) between 3648 cm^{-1}, 2976 cm^{-1}, 2903 cm^{-1}, 2362 cm^{-1} and 2331 cm^{-1}, and O–H bending vibrations at 1994 cm^{-1}, 1871 cm^{-1}, 1652 cm^{-1}, 1625 cm^{-1} and 1384 cm^{-1} were associated with coordinated water molecules. The presence of the bands at 1219 cm^{-1} was assigned to internal tetrahedral asymmetrical stretch, band at 1050 cm^{-1} was for asymmetric stretch while the band at 873 cm^{-1} and 800 cm^{-1} might have been vibrations for symmetrical stretch pore vibration. The bands at 681 cm^{-1} and 535 cm^{-1} were due to double ring vibrations while finally the band at 455 cm^{-1} was assigned pore opening vibration. Upon introduction of malathion the most noticeable changes were introduction of a band at 1715 cm^{-1} which was due to carbonyl stretching of the ester group from malathion, increase of band intensities at 2362 cm^{-1} and 2336 cm^{-1} which were related to O–H stretching vibration modes (asymmetric and symmetric), shifting of bands to higher wave numbers. For example, band from 3648 cm^{-1} to 3651 cm^{-1} and band at 2331 cm^{-1} to 2339 cm^{-1}. There was also disappearance of three bands that is bands at 2976 cm^{-1}, 2903 cm^{-1} and 873 cm^{-1}.

In most of the bands obtained after the treatment there was reduction in intensity as shown in figure 27. These changes were attributed to the malathion molecules interacting with the zeolite structure. The formation of the 1715 cm^{-1} absorption band was believed to be indicative of hydrogen bonding between a carbonyl group of the malathion molecule and some water molecules associated with the sodium ion on the interlayer surface. Similar hydrogen bonding reactions have been reported by Parfitt and Mortland(1968). The frequency shift was less than 10 cm^{-1} suggesting that the hydrogen bonding energies involved were small. The strength of such a hydrogen bond gives some indication of the acidity or the degree of dissociation of a proton forming an integral part of the hydration sphere of a saturating cation. As the positive charge of the cation increases (that is, monovalent vs. divalent), its ability to polarize the hydration water increases, making the hydrogen ion more labile. Hence the small perturbation observed for hydrogen bonding in the Na- ZSM-5 (Si/Al=23.59) -malathion system was consistent with the idea that the sodium tends to hydrate to only a limited extent on the interlayer surface. The persistence of the 1715 cm^{-1} band after exposure to water vapour indicated that there were carbonyl groups present in

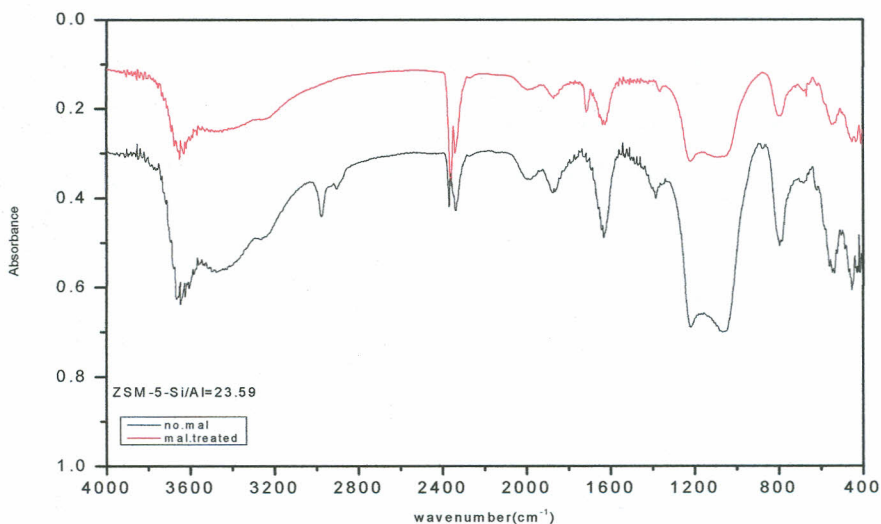excess of the hydrogen bonding capacity of the Na- ZSM-5 (Si/Al=23.59) system (Gallo & Lawryk,1991).

Figure 27: Infrared spectra of ZSM-5(Si/Al=23.59) before and after Malathion addition

4.3.4. Infrared spectra of mordenite (Si/Al=6.83) exposed to 10ppm Malathion

Figures 28 shows FTIR spectrum of mordenite (Si/Al=6.83) exposed to 10 ppm malathion. A representative FTIR spectrum of mordenite (Si/Al=6.83) showed bands related to O–H stretching vibration modes (asymmetric and symmetric) between 3621 cm^{-1}, 2976 cm^{-1}, 2903 cm^{-1}, 2366 cm^{-1} and 2339 cm^{-1}, and O–H bending vibrations at 1843 cm^{-1} and 1628 cm^{-1} was associated with coordinated water molecules. The presence of the bands at 1217cm^{-1} was assigned to internal tetrahedral asymmetrical stretch, band at 812 cm^{-1} might have been vibrations for symmetrical stretch pore vibration, while the bands at 630 cm^{-1} and 558 cm^{-1} were due to double ring vibrations. Finally the band at 463 cm^{-1} was assigned pore opening vibration. Upon introduction of malathion the most noticeable changes were increase of band intensities at 2366 cm^{-1} and 2339 cm^{-1} which were related to O–H stretching vibration modes (asymmetric and symmetric), shifting of band wave numbers for instance, band from3621 cm^{-1} to 3617 cm^{-1} and band at 1628 cm^{-1} to 1634 cm^{-1}. There was also disappearance of two bands that is, bands at 2976 cm^{-1} and 2903 cm^{-1}.In most of the bands obtained after the treatment there was reduction in intensity as shown in figure 28. These changes were attributed to the malathion molecules interacting with the zeolite structure. The fact that frequency shift was less than 10 cm^{-1}suggests that the hydrogen bonding energies

63

involved were small. The strength of such a hydrogen bond gives some indication of the acidity or the degree of dissociation of a proton forming an integral part of the hydration sphere of a saturating cation. As the positive charge of the cation increases (that is monovalent vs. divalent), its ability to polarize the hydration water increases, making the hydrogen ion more labile. Hence the small perturbation observed for hydrogen bonding in the Na-mordenite (Si/Al=6.83) -malathion system was consistent with the idea that the sodium tends to hydrate to only a limited extent on the interlayer surface.
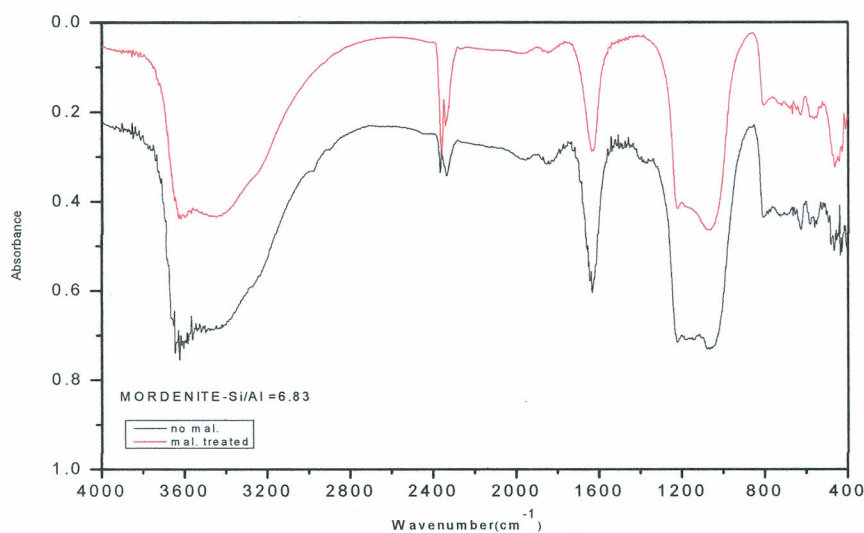

Figure 28: Infrared spectra of mordenite (Si/Al=6.83) before and after Malathion addition

4.3.5 Infrared spectra of mordenite (Si/Al=10.72) exposed to 10ppm Malathion

Figures 29 shows FTIR spectrum of mordenite (Si/Al=10.72) exposed to 10 ppm malathion. A representative FTIR spectrum of mordenite (Si/Al=10.72) showed bands related to O–H stretching vibration modes (asymmetric and symmetric) between 3644 cm^{-1}, 2976 cm^{-1}, 2897 cm^{-1}, 2373 cm^{-1} and 2340 cm^{-1}, and O–H bending vibrations at 1839 cm^{-1} and 1626 cm^{-1} was associated with coordinated water molecules. The presence of the bands at 1217cm^{-1} and 1069 cm^{-1} were assigned to internal tetrahedral asymmetrical stretch, band at 807 cm^{-1} might have been vibrations for symmetrical stretch pore vibration, while the bands at 663 cm^{-1}, 636 cm^{-1}, 631 cm^{-1} and 568 cm^{-1} were due to double ring vibrations and finally the band at 463 cm^{-1} was assigned pore opening vibration. Upon introduction of malathion the most noticeable changes were decrease of band intensities at 2373 cm^{-1} and 2340 cm^{-1} which were

64

related to O–H stretching vibration modes (asymmetric and symmetric), shifting of band wave numbers. For example, band from 3644 cm^{-1} to 3647 cm^{-1} and band at 1069 cm^{-1} to 1079 cm^{-1}. There was also disappearance of two bands that is bands at 2976 cm^{-1} and 2897 cm^{-1}. In most of the bands obtained after the treatment there was reduction in intensity as shown in figure 29. These changes were attributed to the malathion molecules interacting with the zeolite structure. The frequency shift was less than 10 cm^{-1} implying the hydrogen bonding energies involved was small. The strength of such a hydrogen bond gives some indication of the acidity or the degree of dissociation of a proton forming an integral part of the hydration sphere of a saturating cation. As the positive charge of the cation increases (that is monovalent vs. divalent), its ability to polarize the hydration water increases, making the hydrogen ion more labile. Hence the small perturbation observed for hydrogen bonding in the Na-mordenite (Si/Al=10.72) -malathion system was consistent with the idea that the sodium tends to hydrate to only a limited extent on the interlayer surface.
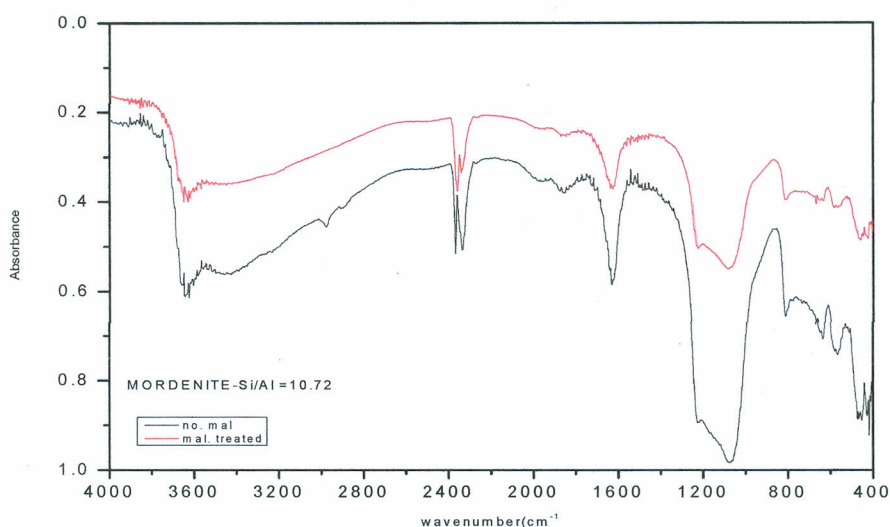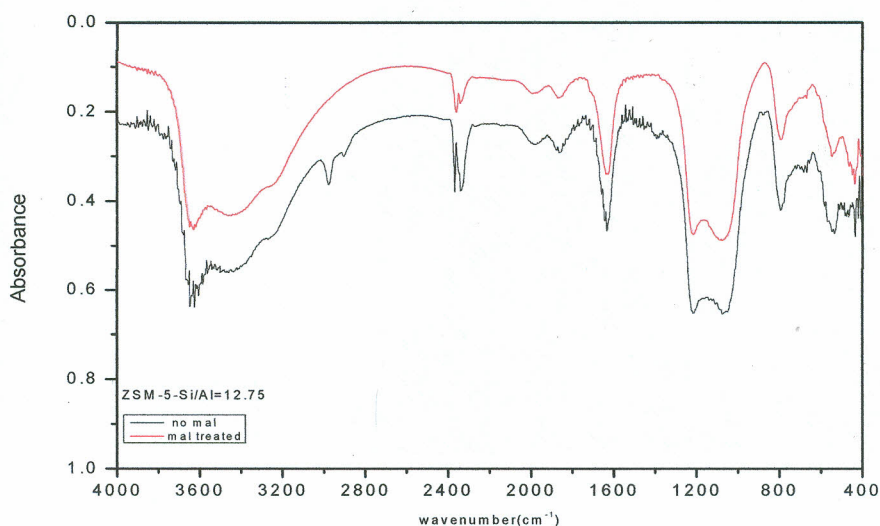

Figure 29: Infrared spectra of mordenite (Si/Al=6.83) before and after Malathion addition

4.3.6 Infrared spectra of ZSM-5(Si/Al=12.75) exposed to 10ppm Malathion

Figures 30 shows FTIR spectrum of ZSM-5(Si/Al=12.75) exposed to 10 ppm malathion. A representative FTIR spectrum of ZSM-5(Si/Al=12.75) showed bands related to O–H stretching vibration modes (asymmetric and symmetric) between 3628 cm^{-1},2977 cm^{-1},2902cm^{-1},2368 cm^{-1} and 2335 cm^{-1}, and O–H bending vibrations at 1983 cm^{-1},1861 cm^{-1},

65

1633 cm^{-1} was associated with coordinated water molecules . The presence of the bands at 1217 cm^{-1} was assigned to internal tetrahedral asymmetrical stretch, band at 1062 cm^{-1} was for asymmetric stretch and the band at 794 cm^{-1} might have been vibrations for symmetrical stretch pore vibration, while the bands at 669 cm^{-1} and 539 cm^{-1} were due to double ring vibrations and finally the band at 438 cm^{-1} was assigned pore opening vibration. Upon introduction of Malathion the most noticeable changes were the decrease of band intensities, shifting of bands to higher wave numbers. For example, band from 3628 cm^{-1} to 3631 cm^{-1} and band at 1983 cm^{-1} to 1986 cm^{-1}. There was also disappearance of two bands that is bands at 2977 cm^{-1} and 2902 cm^{-1}. In most of the bands obtained after the treatment there was reduction in intensity as shown in figure 30. These changes were attributed to the malathion molecules interacting with the zeolite structure. The frequency shift was less than 10 cm^{-1} suggesting the bonding energies involved was small. The strength of such a bond gives some indication of the acidity or the degree of dissociation of a proton forming an integral part of the hydration sphere of a saturating cation. As the positive charge of the cation increases (that is monovalent vs. divalent), its ability to polarize the hydration water increases, making the hydrogen ion more labile. Therefore, the small perturbation observed for hydrogen bonding in the Na- ZSM-5(Si/Al=12.75) -malathion system was consistent with the idea that the sodium tends to hydrate to only a limited extent on the interlayer surface.

Figure 30: Infrared spectra of ZSM-5(Si/Al=12.75) before and after Malathion

4.4 Stability of Na-zeolite matrix upon exposure to Malathion

The morphology analysis of the synthesized zeolites in the presence of malathion was carried out with SEM at different magnifications. Shapes and surface smoothness were compared with the available information as discussed below.

4.4.1 SEM of mordenite zeolite exposed to 10ppm Malathion

Figure 31 shows SEM images of MOR zeolite at various magnifications. The images in are rectangular in shape and this is typical for the MOR zeolites and therefore the observed morphology implies that the exposure to malathion does not compromise the stability of MOR structure. Due to this assertion, it can be said with confidence that since the structure is intact, and then it can asserted that any other changes are the only interactions between the absorbent and the adsorbate (Chen *et al.*, 2009).The SEM micrographs for mordenite (Figure 31) showed no appreciable morphological evolution relative to pure untreated mordenite. The surface appeared rough but homogenous and circular in shape. Though structural changes may not be ascertained through the inspection of the micrographs, possible deviations in topological symmetry and unit cell parameters in MOR after adsorption could not be ruled out (Leardini, Martucci, Braschi, Blasioli, & Quartieri, 2014).
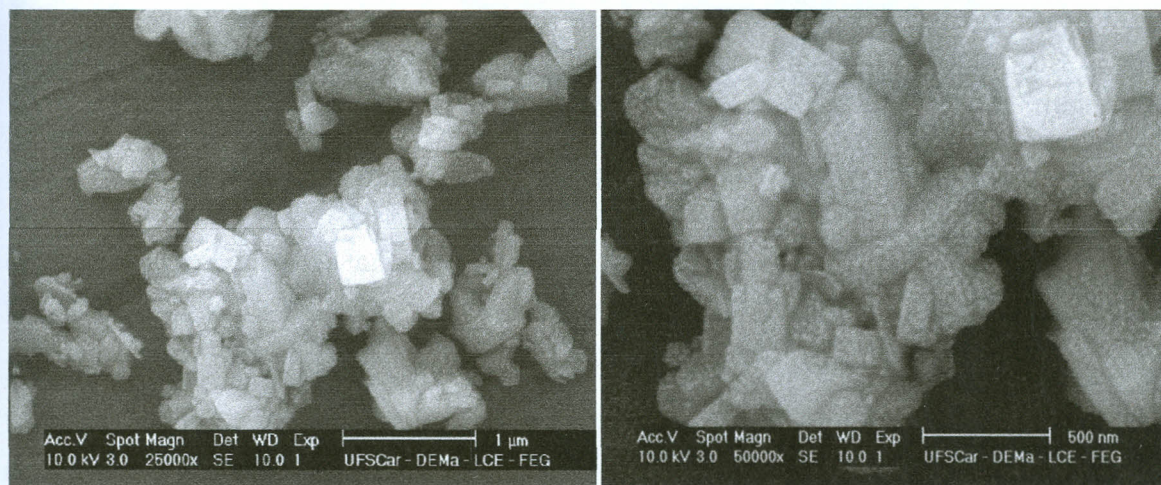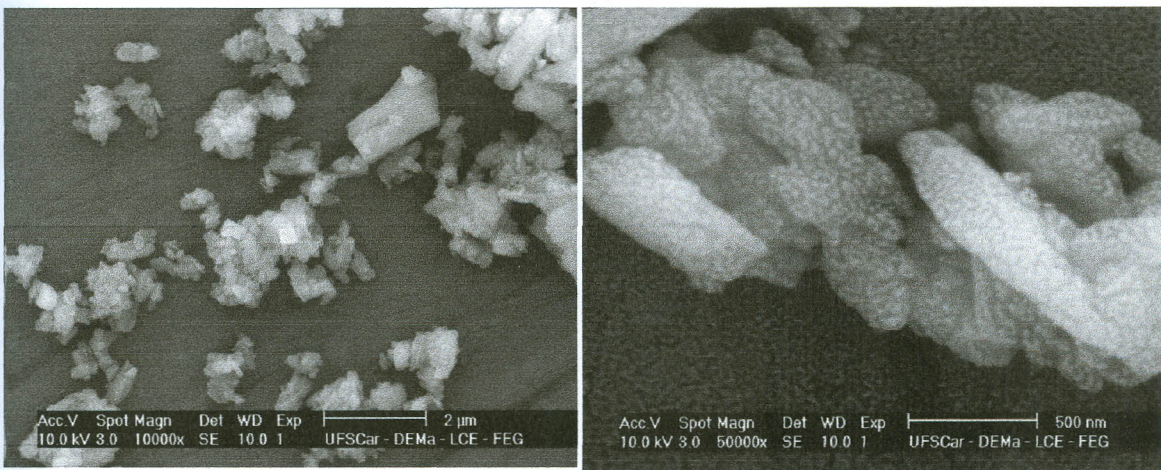

Figure 31: SEM image of MOR zeolite at different magnifications

4.4.2 SEM of ZSM-5 zeolite exposed to 10ppm Malathion

Figure 32 (below) shows SEM images of ZSM-5 zeolite at various magnifications. The SEM images for ZSM-5 were relatively similar to those reported in literature for conventional ZSM-5 (Blocki, 1993). The ZSM-5 particles seemed rounded in shape; there was no observable change in morphology relative to standard ZSM-5 depicting that adsorption of malathion by ZSM-5 results in no structural modification of the zeolite surface. The SEM images at high magnification also suggested the presence of hierarchical porosity and with the small crystal sizes of the particles, the zeolite is imbued with a high mass transfer potential; a desirable property for application as an adsorbent. The results suggest the adsorbate largely diffused into the zeolite pores.

Figure 32: SEM image of ZSM-5 zeolite at different magnifications

4.4.3 SEM of Ferrierite zeolite exposed to 10ppm Malathion

Figure 33 (below) shows SEM images of ZSM-5 zeolite at various magnifications. The ferrierite malathion matrix showed a course heterogeneous surface analogous to the bare untreated Ferrierite zeolites from previous (Pérez*et al.*, 2013) implying no morphological modification resulting from the zeolite malathion interactions. The results are consistent with physisoption mechanism and diffusion into zeolitic channels and not chemical transformations.
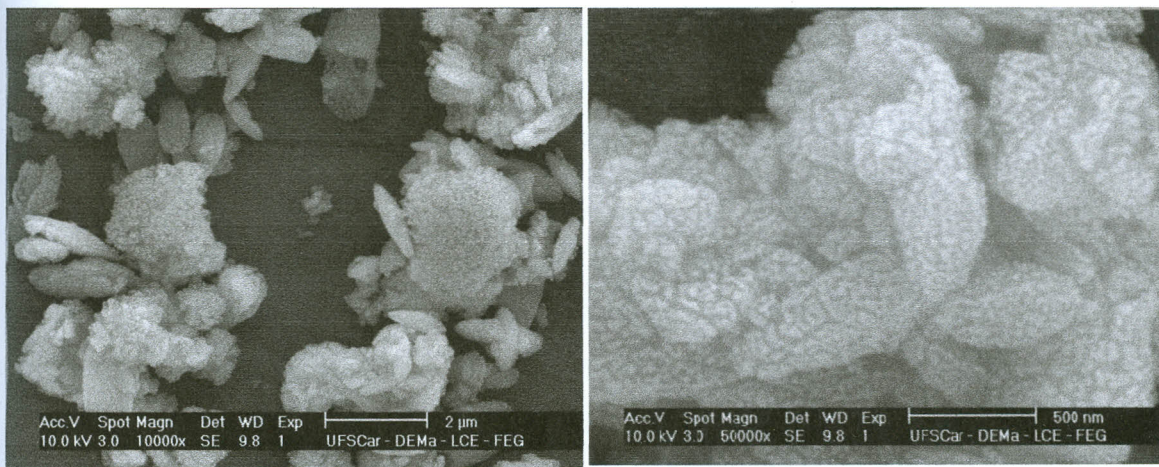
68

Figure 33: SEM images of FERR zeolite at different magnifications

4.4.4 SEM of faujasite-Y zeolite exposed to 10ppm Malathion

Figure 34 shows SEM images of FAU-Y zeolite at different magnifications. The shape and size of synthesized USY particles after adsorption of malathion were studied by SEM and images with a scale bar of 2 μm displayed in Figure 34. The SEM images show, the USY-malathion contained a blend of multi-faced spherules crystals with sharp edges observed in untreated USY zeolites (Kowenje &Osewe, 2015). The images also depict absence of any amorphous phase. The similarity implies that occupancy of malathion species in the zeolite cavities do not result in any surface morphological changes.
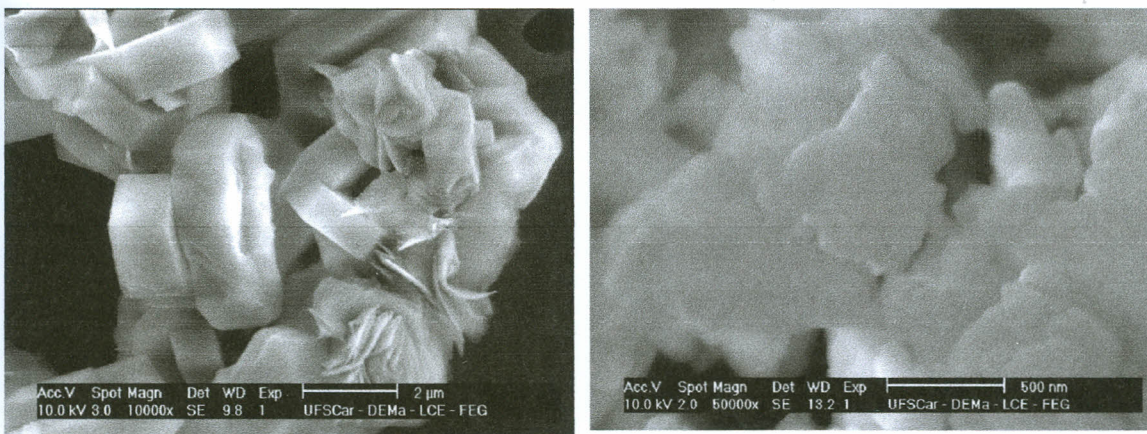

Figure 34: SEM images of FAU-Y zeolite at different magnifications

4.5 Nature of adsorption of zeolite after exposure to Malathion

In order to understand the adsorption behaviour of malathion in zeolites, the nature of the attached Al in the matrix was explored using the ^{27}Al NMR. Here the position of ^{27}Al NMR signal is indicative of the nature of its chemical and sometimes physical environments.

4.5.1 Solid state ^{27}Al NMR for zeolite after exposure to Malathion

The incorporation of malathion structures in zeolite samples was confirmed by ^{27}Al NMR spectra, as shown in Figure 35.The spectrum of the zeolite, showed an intense peak centered at 56.3ppm, attributed to coordinated aluminum tetrahedral Al^{4+} in crystalline structure of zeolite, indicating that practically aluminum was present in the zeolite structure. In the samples exposed to malathion, besides the dominant peak observed around 56ppm, another low intensity peak also observed, centered at about 0 ppm for sample USY and MFI, thus indicating the presence of aluminum species in octahedral environment(Jacobsen, Madsen, Houzvicka, Schmidt, & Carlsson, 2000).The signal at 0 ppm suggests that a small amount of aluminum exists as extra-framework aluminum, which is considered to be formed during calcination, and such post treatment accelerates the de-allumination from the framework of aluminum-rich zeolites (Humplik $et\ al.$, 2014). The shifting of the peak at 56ppm shows a direct attachment of Na^+ to the site while the reduction of the peak intense at 100ppm may imply an interaction of the adsorbate via their paramagnetic oxygen atoms.
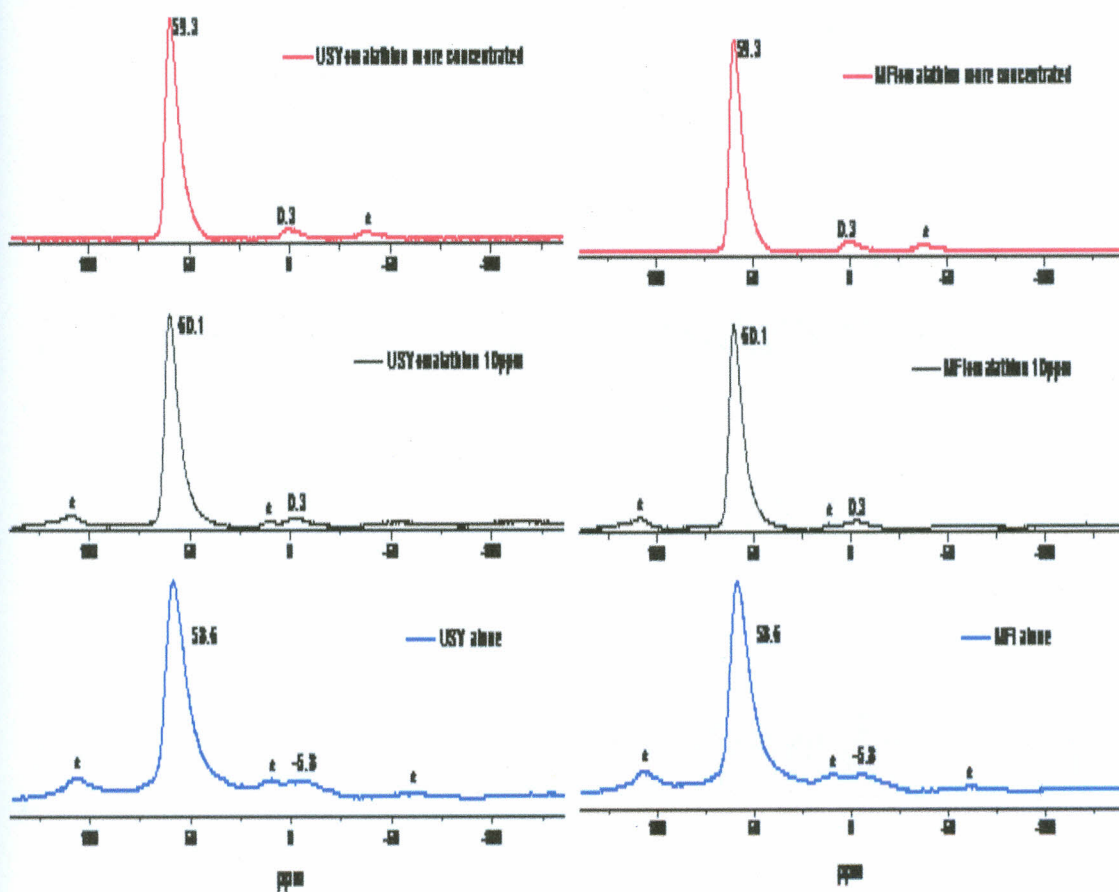
70

Figure 35:[27]**Al NMR spectra of zeolites exposed to different concentration of Malathion**

The signal observed in figure 35 only confirmed the presence of Al^{3+} within the zeolite structure which is always at the points though the interaction with malathion is not observed or if it is there then the interaction is very low as compared to the one in the zeolite structure. This shows that there is no chemical bond formed between the metabolites of malathion and the zeolite because the possible bond formation can only take place at the aluminum site which is considered the Lewis site. However, the absence of the metabolites in the solution of zeolite, water and malathion explains that the metabolites are adsorbed and may be held together with a strong electrostatic forces due to the presence of phosphorus which is more electronegative than oxygen.

4.5.2 Solid state[13]**C NMR for zeolite after exposure to Malathion**

Due to their inherent low intensities, the ^{13}C solid state NMR signal may not show the desired details. Therefore the sample adsorbates were extracted from the zeolite matrix then the ^{13}C NMR was done for the solution. The signals are presented in figure 36, but very low and as

can be seen from the spectrum, the noise also immerses the signals and this could have been attributed to the low concentration of the pesticide leading to low concentration of ^{13}C.

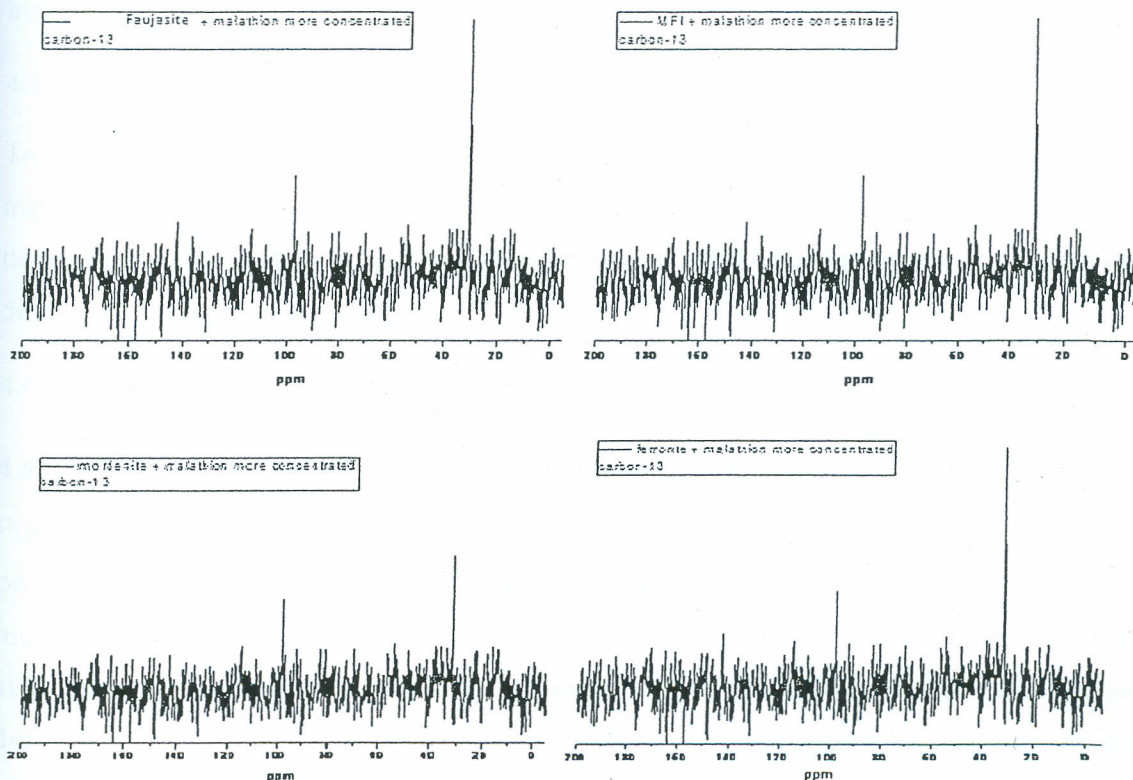**Figure 36:** ^{13}C NMR spectra of zeolites extracts exposed to different concentration of Malathion

The read signals were at 31.25ppm, 53.94ppm, 97.72ppm, 114.05ppm, 142.66ppm, 22.44ppm and finally14.34ppm while the other signals are considered to be noise of the instrument.

4.6 Thermal analysis of Na-zeolite samples

To understand and infer both the strength of attachment of the adsorbates in the zeolite matrix and the possible attachment position, the thermogravimetry (TG), derivative thermogravimetry (DTG), differential thermal analysis (DTA) and temperature-programmed desorption (TPD) were performed.

4.6.1 Thermal Gravimetric and Thermal Differential Analyses

4.6.1.1 Thermal Gravimetric and Thermal Differential Analyses for mordenite

Figure 37 shows TGA/TDA graph for mordenite. In the figure, the black curve represents the percentage mass loss while the blue curve is for differential temperature. In TGA, the molecules are expected to be lost at temperature in the neighbourhood of their boiling points at room temperature and pressure. On analyzing the TG/DTA experimental data, thermal desorption of a solid mordenite zeolite treated with solution of malathion was observed to take place in three distinct steps, the first endothermic loss at 90^0C (5.2%) is consistent with the loss of physisorbed water. The subsequent losses are exothermic steps at 200^0C (4.8 %) which may imply the loss of malathion molecules and 360^0C (2.5%) is due to loss of Malathion dicarboxylic acid adsorbed in the cages. Given that MOR zeolite is one dimensional (1D), and the cage opening is about 0.29 x 0.58 nm, while the active molecular diameter of the malathion is ca. 0.7 nm the chances are that inner cages attachments are possible though limited. In addition, it can be noted that for MOR, the Al atoms are not evenly distributed within the matrix but are concentrated at the interconnections between the cages as was evidenced by the ^{27}Al NMR. Since the molecule cannot wholly access the cages but may only do so via its branches, the chemical environment resulting from such a fussy interaction is broad. This means, possibly one part of the molecule or very few molecules gain access to the inner cages of the zeolite. Due to the somewhat wider openings, therefore the confinement effect is less and this explains the low percentage loss of what is adsorbed and low heat requirement during its removal. The broadened shape of the curve is also worthy to note. Such a broad shape is indicative of arrangement of energies which implies a varied attachment chemical environment of the molecule to the zeolite mostly. Physically,

73

such a varied environment may only mean that the pesticide molecule is attached on the surface and in the inner spaces of the zeolite at the same time in a situation christened "reputation" behavior. (Barrer, 1985).
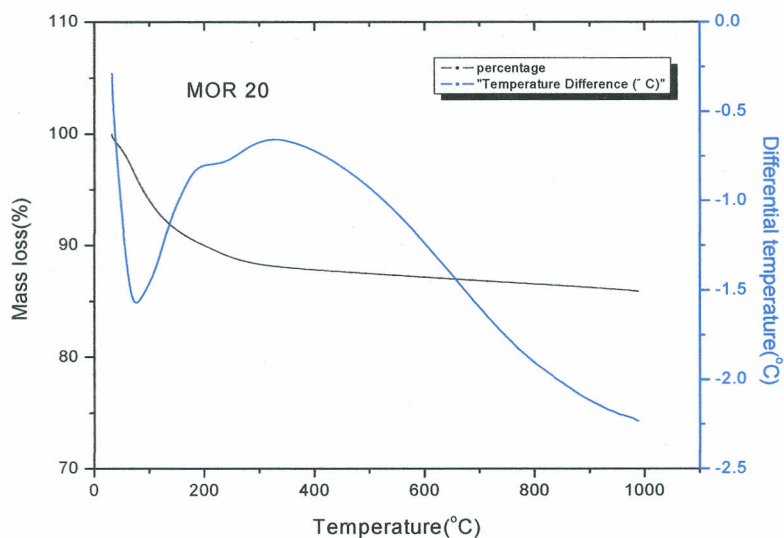

Figure 37: TGA/DTA graph for mordenite

4.6.1.2 Thermal Gravimetric and Thermal Differential Analyses for ferrierite

In Figure 38, the black curve represents the percentage mass loss while the blue curve is for differential temperature. In TGA, the molecules are expected to be lost at temperature in the neighbourhood of their boiling points at room temperature and pressure. On analyzing the TG/DTA experimental data, thermal decomposition of a solid ferrierite zeolite treated with solution of malathion was observed to take place in two distinct steps, the first endothermic loss at 86^0C (2.6%) was due to the loss of physisorbed water the second exothermic step at 350^0C (7.4%) was due to loss of malathion dicarboxylic acid adsorbed at the surface and cages. It is a two dimensional zeolite thus explaining high percentage of what is adsorbed by the cages compared to a one dimensional zeolite. Here, the spectra are sharper as compared to the MOR situation. The FER is 0.45 x 0.55 nm meaning a somewhat relatively smaller opening and therefore may not allow any part of the pesticide molecule to access any inner cages. However, the most effect on the surface energetic would come from the fact that in the FER, the Al sites are almost uniformly distributed within the zeolite matrix. Such a situation

74

confines the adsorbate to the outer surfaces of the zeolites which are chemically and energetically homogenous leading to such observed sharp peaks (Breck, 1974).
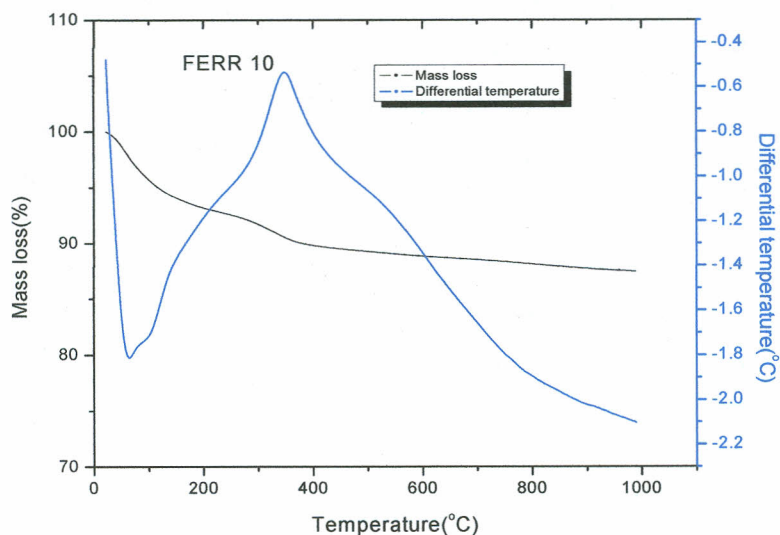

Figure 38: TGA/DTA graph for Ferrierite

4.6.1.3 Thermal Gravimetric and Thermal Differential Analyses for mordenite

In Figure 39, the black curve represents the percentage mass loss while the blue curve is for differential temperature. On analyzing the TG/DTA experimental data, thermal decomposition of a solid mordenite zeolite treated with solution of malathion was observed to take place in three distinct steps, the first endothermic loss at 100^0C (6%) was due to the loss of physisorbed water the second exothermic steps at 191^0C (5.7 %) for loss of malathion and malaxion finally at 375^0C (2.5%) was due to loss of malathion dicarboxylic acid adsorbed within the zeolite matrix. Given that MOR zeolite is one dimensional (1D), and the cage opening is about 0.29 x 0.58 nm, while the active molecular diameter of the malathion is 0.7 nm the chances are that inner cages attachments were possible though limited. In addition, it can be noted that for MOR, the Al atoms are not evenly distributed within the matrix but are concentrated at the interconnections between the cages. Since the molecule cannot wholly access the cages but may only do so via its branches, the chemical environment resulting from such a fussy interaction is broad. This means, possibly on part of the molecule or very few molecules gain access to the inner cages of the zeolite. Due to the somewhat wider openings, therefore the confinement effect is less and this explains the low percentage loss of

75

what is adsorbed and low heat requirement during its removal. The broadened shape of the curve is also worthy to note. Such a broad shape is indicative of arrangement of energies which implies a varied attachment chemical environment of the molecule to the zeolite mostly. Physically, such a varied environment may only mean that the pesticide molecule is attached on the surface and in the inner spaces of the zeolite at the same time in a situation christened "reputation" behaviour (Blocki, 1993).
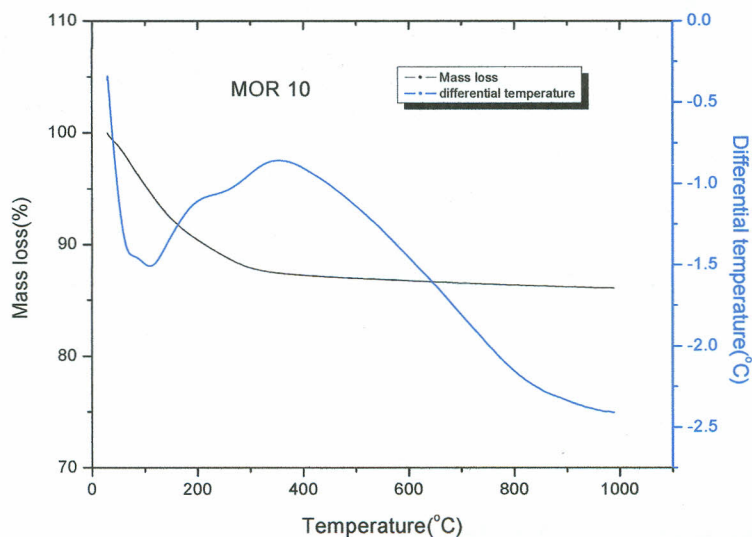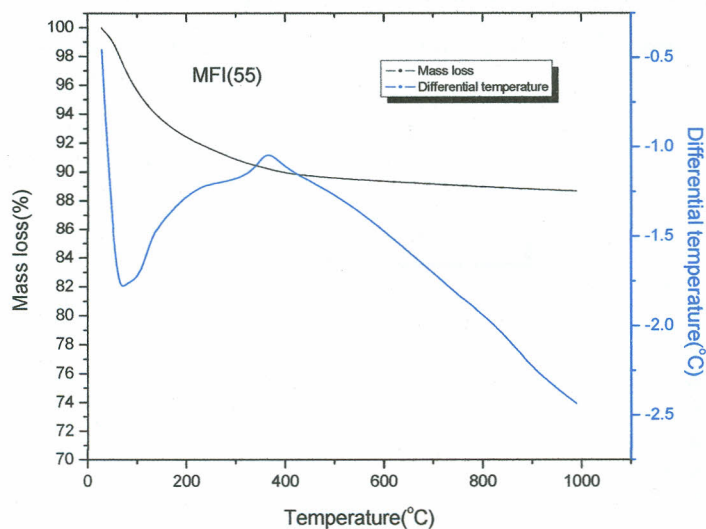

Figure 39: TGA/DTA graph for mordenite

4.6.1.4 Thermal Gravimetric and Thermal Differential Analyses for MFI

In Figure 40, the black curve represents the percentage mass loss while the blue curve is for differential temperature. On analyzing the TG/DTA experimental data, thermal decomposition of a solid MFI zeolite treated with solution of malathion was observed to take place in two distinct steps, the first endothermic loss at 90^0C (3.6%) was due to the loss of physisorbed water the second exothermic step at 400^0C (6.4%) was due to loss of malathion monocarboxylic acid adsorbed within the matrix. Here, the spectra are sharper compared to the MOR situation. The MFI is 0.51 x 0.55 nm meaning a somewhat relatively smaller opening than that of malathion and its metabolites and therefore may not allow any part of the pesticide molecule to access any inner cages. However, the most effect on the surface energetic would come from the fact that in the MFI, the Al sites are almost uniformly distributed within the zeolite matrix. Such a situation confines the adsorbate to the outer

76

surfaces of the zeolites which are chemically and energetically homogenous leading to such observed sharp peaks (Barrer, 1985).
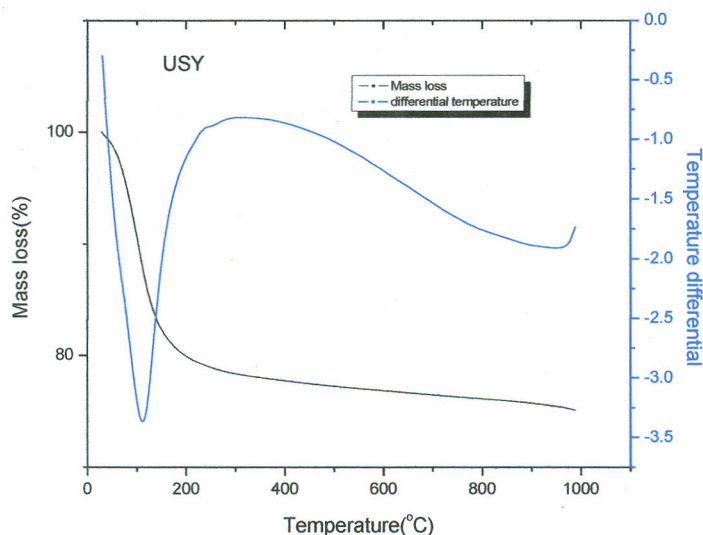

Figure 40: TGA/DTA graph for MFI

4.6.1.5 Thermal Gravimetric and Thermal Differential Analyses for USY

In Figure 41, the black curve represents the percentage mass loss while the blue curve is for differential temperature. On analyzing the TG/DTA experimental data, thermal decomposition of a solid FAU-zeolites treated with solution of malathion was observed to take place in two distinct steps, the first endothermic loss at 100^0C (3%) was due to the loss of physisorbed water the second exothermic step at 192^0C(17%) was due to loss of malathion adsorbed. Given that FAU zeolite is three dimensional (3D), and the cage opening is about 0.74 nm, while the active molecular diameter of the malathion is 0.7 nm the chances are that inner cage attachments are possible. In addition, it can be noted that for FAU, the Al atoms are not evenly distributed within the matrix but are concentrated at the interconnections between the cages. Since the molecule cannot wholly access the cages but may only do so via its branches, the chemical environment resulting from such a fussy interaction is broad. This means, possibly on part of the molecule or very few molecules gain access to the inner cages of the zeolite. Due to the somewhat wider openings, therefore the confinement effect is less and this explains the low percentage loss of what is adsorbed and low heat requirement

77

during its removal. The broadened shape of the curve is also worthy to note. Such a broad shape is indicative of arrangement of energies which implies a varied attachment chemical environment of the molecule to the zeolite mostly. Physically, such a varied environment may only mean that the pesticide molecule is attached on the surface and in the inner spaces of the zeolite at the same time in a situation christened "*reptation*" behaviour (Barrer, 1985).

Figure 41: TGA/DTA graph for USY

4.6.1.6 Thermal Gravimetric and Thermal Differential Analyses for MFI

In Figure 42, the black curve represents the percentage mass loss while the blue curve is for differential temperature. On analyzing the TG/DTA experimental data, thermal decomposition of a solid MFI zeolite treated with solution of malathion was observed to take place in two distinct steps, the first endothermic loss at 90 ^{0}C (5%) was due to the loss of physisorbed water the second exothermic step at 425 ^{0}C (5.4%) was due to loss of malathion monocarboxylic acid adsorbed at the cages. Here, the spectrum is, again, sharper compared to the MOR situation. The MFI is 0.51 x 0.55 nm meaning a somewhat relatively smaller opening and therefore may not allow any part of the pesticide molecule to access any inner cages. However, the most effect on the surface energetic would come from the fact that in the MFI, the Al sites are almost uniformly distributed within the zeolite matrix. Such a situation

confines the adsorbate to the outer surfaces of the zeolites which are chemically and energetically homogenous leading to such observed sharp peak (Baerlocher *et al.*, 2007).
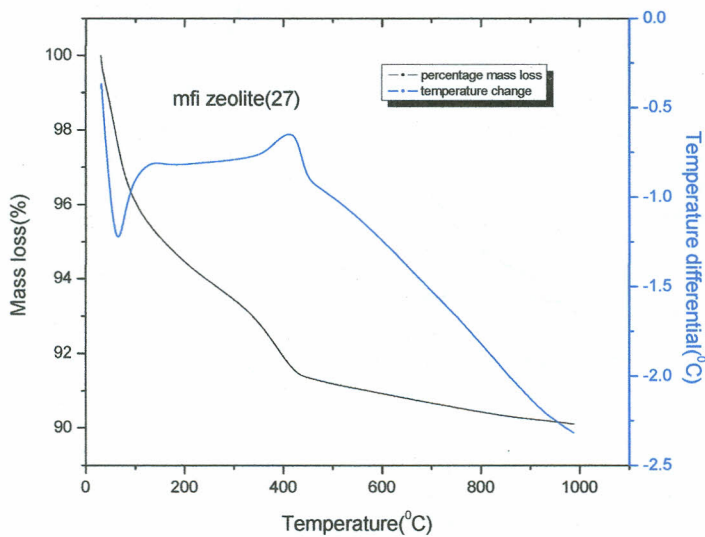
Figure 42: TGA/TDA graph for MFI.

4.6.2 Differential thermal Gravimetric and Differential Thermal Analyses

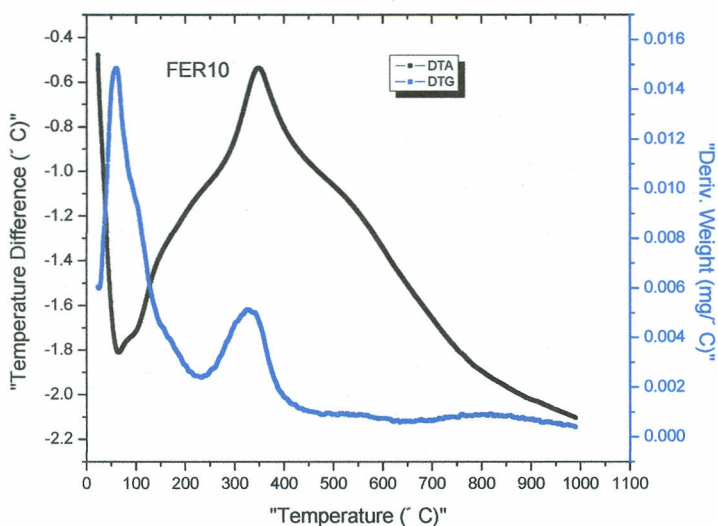## 4.6.2.1 Differential thermal Gravimetric and Differential Thermal Analyses for Ferrierite

In Figure 43, the black curve represents the temperature difference while the blue curve is for derivative weight. In DTG/DTA, the masses of lost molecules can be calculated by simply multiplying their peak readings. On analyzing the DGA/DTA experimental data, desorption of malathion and its metabolites from a solid ferrierite zeolite treated with solution of malathion was observed to be accompanied by two major weight losses. The endothermic weight loss at 56 ^{0}C for water is 0.0252 mg while exothermic loss related to DCA at 340 ^{0}C is 0.003mg. The FER is 0.45 x 0.55 nm meaning a somewhat relatively smaller opening and therefore may not allow any part of the pesticide molecule to access any inner cages. However, the most effect on the surface energetic would come from the fact that in the FER, the Al sites are almost uniformly distributed within the zeolite matrix. Such a situation confines the adsorbate to the outer surfaces of the zeolites which are chemically and energetically homogenous leading to such and observed sharp peaks (Blocki, 1993).

79

Figure 43: DTG/DTA graph for Ferrierite

4.6.2.2 Differential thermal Gravimetric and Differential Thermal Analyses for USY

In Figure 48, the black curve represents the temperature difference while the blue curve is for derivative weight. In DTG/DTA, the masses of lost molecules can be calculated by simply multiplying their peak readings. On analyzing the DGA/DTA experimental data, desorption of malathion and its metabolites from a solid FAU-Y zeolite treated with solution of malathion is accompanied by one major endothermic weight loss at 100 ^{0}C for water which was 0.175mg. Given that FAU zeolite is three dimensional (3D), and the cage opening was about 0.74 nm, while the active molecular diameter of the malathion is 0.7 nm the chances are that inner cages attachments are possible. Due to the somewhat wider openings, therefore the confinement effect is less and this explains the low percentage loss of what is adsorbed and low heat requirement during its removal. Physically, such a varied environment may only mean that the pesticide molecule is attached on the surface and in the inner spaces of the zeolite at the same time in a situation christened "reputation" behaviour (Blocki, 1993).

Figure 44: DTG/DTA graph for USY

4.6.2.3 Differential thermal Gravimetric and Differential Thermal Analyses for MFI

In Figure 45, the black curve represents the temperature difference while the blue curve is for derivative weight. In DTG/DTA, the masses of lost molecules can be calculated by simply multiplying their peak readings. On analyzing the DGA/DTA experimental data, desorption of malathion and its metabolites from a solid MFI zeolite treated with solution of malathion was observed to be accompanied by two major weight losses. The endothermic weight loss at 75^0C for water was 0.0189mg while exothermic loss related to MCA at 400^0C was 0.001875 mg. The MFI was 0.51 x 0.55 nm meaning a somewhat relatively smaller opening and therefore may not allow any part of the pesticide molecule to access any inner cages. However, the most effect on the surface energetic would come from the fact that in the MFI, the Al sites are almost uniformly distributed within the zeolite matrix (Barrer, 1985).

Figure 45: DTG/DTA graph for MFI

4.6.2.4 Differential thermal Gravimetric and Differential Thermal Analyses for mordenite

In Figure 46, the black curve represents the temperature difference while the blue curve is for derivative weight. In DTG/DTA, the masses of lost molecules can be calculated by simply multiplying their peak readings. On analyzing the DGA/DTA experimental data, desorption of malathion and its metabolites from a solid mordenite zeolite treated with solution of malathion was observed to take place in two major weight losses accompanied by two types of enthalpy changes where one is exothermic and the other endothermic. The endothermic weight loss at 100^0C for water was 0.0225mg while exothermic loss related to MCA at 400^0C was 0.000015mg. Given that MOR zeolite is one dimensional (1D), and the cage opening is about 0.29 x 0.58 nm, while the active molecular diameter of the malathion is 0.7 nm the chances are that inner cages attachments are possible though limited. This means, possibly on part of the molecule or very few molecules gain access to the inner cages of the zeolite. Due to the somewhat wider openings, therefore the confinement effect is less and this explains the low percentage loss of what is adsorbed and low heat requirement during its removal. Physically, such a varied environment may only mean that the pesticide molecule is attached on the surface and in the inner spaces of the zeolite at the same time in a situation christened "*reptation*" behaviour.
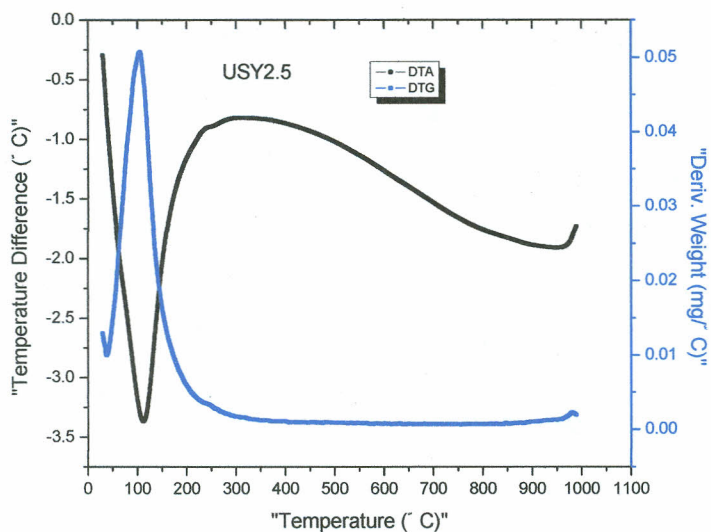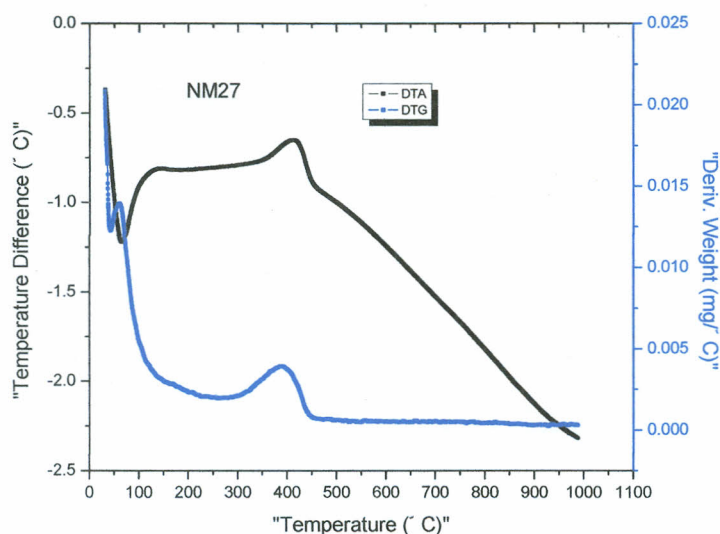
82

Figure 46: DTG/DTA graph for mordenite

4.6.2.5 Differential thermal Gravimetric and Differential Thermal Analyses for mordenite

In Figure 47, the black curve represents the temperature difference while the blue curve is for derivative weight. On analyzing the DGA/DTA experimental data, desorption of malathion and its metabolites from a solid mordenite zeolite treated with solution of malathion is observed to take place in two major weight losses accompanied by two types of enthalpy changes where one is exothermic and the other endothermic. The endothermic weight loss at $90^{0}C$ for water was 0.036mg while exothermic loss related to DCA at $350^{0}C$ was 0.00075mg. Given that MOR zeolite is one dimensional (1D), and the cage opening is about 0.29 x 0.58 nm, while the active molecular diameter of the malathion is 0.7 nm the chances are that inner cage attachments are possible though limited. This means, possibly one part of the molecule or very few molecules gain access to the inner cages of the zeolite. Due to the somewhat wider openings, therefore the confinement effect is less and this explains the low percentage loss of what is adsorbed and low heat requirement during its removal. Such low attachments are consistent with the minimum deviations observed by the FT-IR presented in section4.3.Physically; such a varied environment may only mean that the pesticide molecule is attached on the surface and in the inner spaces of the zeolite at the same time in a situation christened "reptation" behaviour.
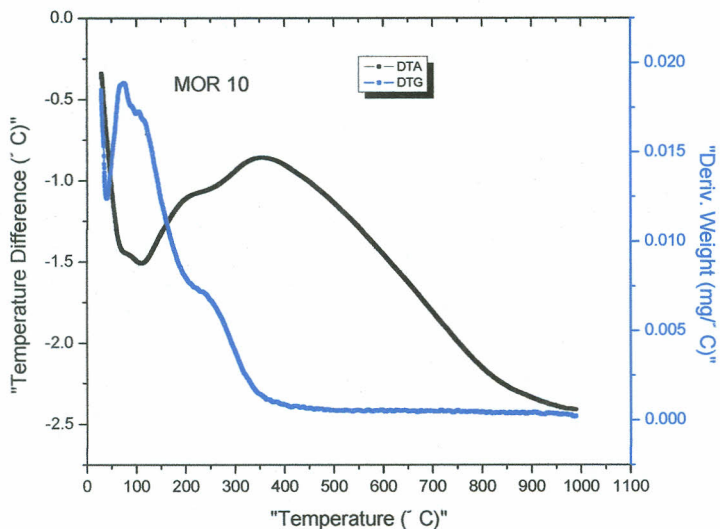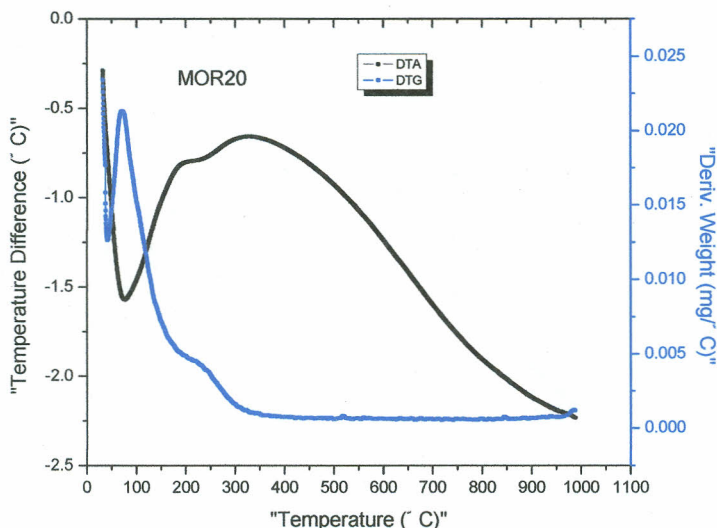
Figure 47: DTG/DTA graph for mordenite

4.6.2.6 Differential thermal Gravimetric and Differential Thermal Analyses for MFI

In Figure 48, the black curve represents the temperature difference while the blue curve is for derivative weight. On analyzing the DGA/DTA experimental data, desorption of malathion and its metabolites from a solid MFI zeolite treated with solution of malathion was observed to take place in two major weight losses accompanied by two types of enthalpy changes where one was exothermic and the other endothermic. The endothermic weight loss at 80^0C for water is 0.02975mg while exothermic loss related to MCA at 400^0C was 0.002mg. The MFI was 0.51 x 0.55 nm meaning somewhat relatively smaller openings and therefore may not allow any part of the pesticide molecule to access any inner cages. However, the most effect on the surface energetic would come from the fact that in the MFI, the Al sites are almost uniformly distributed within the zeolite matrix (Arnold, 1996).
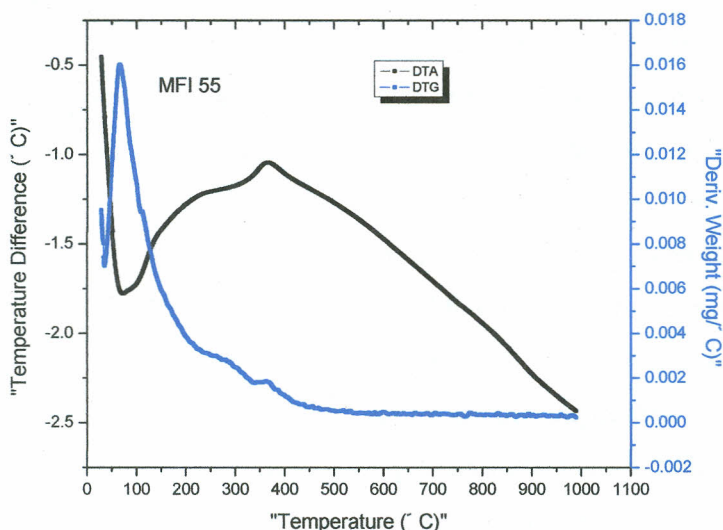
Figure 48: DTG/DTA graph for MFI

4.7 TG/DTG/DTA study

On analyzing the TG/DTG/DTA experimental data, thermal decomposition of a solution of malathion and its metabolites adsorbed in faujasite and mordenite zeolite was observed to take place in one distinct step that includes dehydration of the zeolite from the composition of water and carbon derivatives from the malathion. The step indicated the presence of two sub steps as seen from the DTG/DTA curves. The DTA curves showed that dehydration was an endothermic reaction represented by a sharp peak, whereas decomposition in nitrogen is an exothermic reaction indicated with a broad hump. The exothermic reaction of decomposition is confirmed by separately recording DTA's for the samples with different zeolites.

The corresponding onset and termination temperature for these steps observed from TG/DTG/DTA curves remain the same. DTA curves also indicate the type of reaction occurring in these temperature ranges. On the other hand analyzing the TG/DTG/DTA experimental data, thermal decomposition of a solution of malathion and its metabolites adsorbed in MFI and ferrierite zeolite was observed to take place in two distinct steps that includes dehydration of the zeolite from the composition of water and malathion its

85

metabolites. And the final step was the thermal decomposition of malathion this is shown by a weight loss due to removal of deposited malathion. The change in colour of the catalysts during the TG experiment is a good indication of carbon removal. For example, a used ZSM-5 sample was black and turned white during the TG procedure. However, as indicated by the TG curve of the sample reacted for 40 min, the amount of malathion deposition on the surface of the catalyst is relatively low. The decrease in weight below $500^{\circ}C$ is a result of malathion thermal decomposition and desorption. According to the DTG profiles, the temperature for weight loss rises with on-stream time, indicating the type of molecules deposition varied with reaction time. Malathion species such as DCA and MCA were deposited on the zeolite. According to the suggestion of Barrer (1985) the deposited malathion species burnt at low temperature are mainly those formed on the cages, while the species burnt at high temperature is primarily deposited on the Brønsted acid sites and responsible for the gradual deactivation of the zeolite (Barrer, 1985).

4.8 Effect of zeolite on water pH

Malathion mainly undergoes hydrolysis in water (Wolfe *et al.*, 1975)with a pH value of 4 or greater. Transformation of malathion essentially depends on the pH; as such the metabolites differ in acidic and alkaline conditions (Ogunah *et al.*, 2013). Therefore it is important to investigate the effect of different types of zeolites on the solution pH as they have different Si/Al ratio in their make ups.

## 4.8.1 Effects of Malathion treatment on pH

From Table 8, it can be seen that when the malathion and zeolites were introduced in water the pH of the solution increased with time up to three hours then started decreasing for all the treatments. When malathion is introduced in water with pH<7 it quickly forms monocarboxylic acid (MCA), dicarboxylic acids (DCA) and diethylthiomalate (Neal*et al*, 1993).

Table 8: pH variation with time for water treated with zeolite and Malathion (±0.05)

Time hrs	MFI Si/Al = 23.59	MOR Si/Al = 10.72	FERR Si/Al=1 0.71	MFI Si/Al=12.75	MOR Si/Al=6.83	FAU-Y Si/Al=2.77
0.5	10.33	4.3	5.3	9.1	8.6	7.68
1	10.35	4.9	5.4	9.1	8.6	7.63
3	10.26	5.2	5.7	9.2	8.9	7.53
8	10.23	5.4	5.7	8.8	8.5	7.12
24	9.98	2.9	5.6	8.8	8.39	8.1
48	9	3.6	4.8	7.61	8.33	8.02
72	8.4	2.2	4.19	7.52	8.31	7.6

Carboxylic acids are weak acids with pK_a values ~ 4-5. The carboxylic acid in water forms carboxylate ion which is a resonance stabilized carbanion
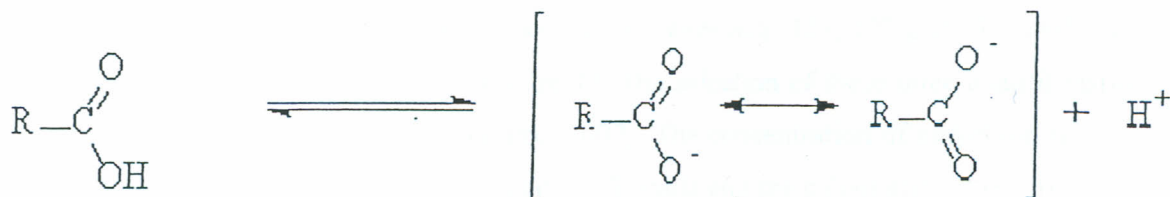
R = H, alkyl, aryl   resonance stabilised carboxylate anion

The above process introduces a proton in the solution and as a result the pH values reduce. But with the introduction of Na-zeolite into the solution, Na^+ ions go into the solution forming dilute aqueous sodium hydroxide solution which in turn reacts with Carboxylic acids to form the water soluble carboxylate ion. The H^+ balances the Al charge of the zeolite to make it neutral and as a result the pH will increase (Ogunah et al., 2013) according to the equation;

insoluble in cold water   soluble in cold water
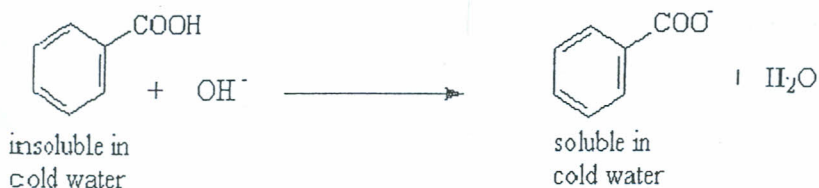
A carboxylic acid and an alcohol used in the dissolution of pesticide will react to form an ester and water. The reaction is at equilibrium and catalyst, usually H^+, is required and this is provided by H^+ produced during carboxylate ion formation as shown in the equation;

$$CH_3\overset{O}{\overset{\|}{C}}-OH \quad + \quad CH_3CH_2OH \quad \rightleftharpoons \quad \overset{H^+}{} \quad CH_3\overset{O}{\overset{\|}{C}}-OCH_2CH_3 \quad + \quad H_2O$$
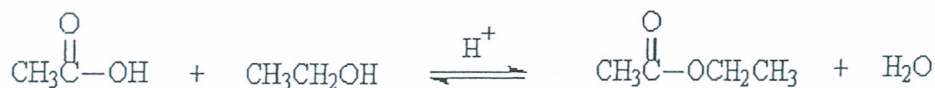
4.9 Dissipation of Malathion pesticides under different water treatments with zeolites

Dissipation of malathion can be done through quantifying the amounts of malathion and its metabolites present at any specific given time after the extraction from the bulk solution using the best method with the highest percentage recovery. The extract is then injected into a GC machine and fragments are determined based on their molecular masses and retention times.

4.9.1 Quantitative and qualitative analysis of Malathion under different treatments

The GC-MS analysis was done and the peaks selected were m/z: 125, 127 and 173 (with m/z: 127 being based peak ion) as shown in Figure 49. The selection of these three quantification ions followed the level suggested by Rissato, (2007). The concentration of malathion residue was determined using external calibration and the formula and the calculated values are listed in the Table 12 below.
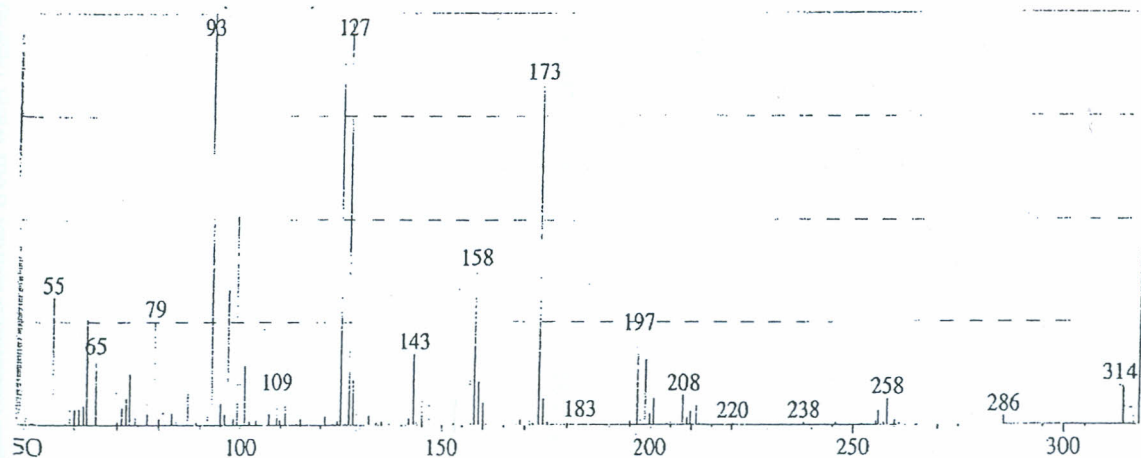

Figure 49: GC-MS Fragment ions of Malathion

88

Table 9: Residual concentration with time for Malathion extract from water treated with Malathion and six different types of Na-zeolite at 27°C at different times(nd-not detected,NA-not applicable)

Pesticide	Zeolite type	Si/Al(a.u)	pH(a.u)	Residual concentration at different times (h)						
				8h	12h	16h	20h	24h	48h	72h
Malathion	Faujasite-3D	2.77±0.05	7.68±0.05	0.912± .044	0.854 ± 0.027	0.663 ± 0.036	0.565 ± 0.014	0.484 ± 0.033	n.d	n.d
	Mordenite-1D	10.72±0.05	4.1±0.05	1.163± .027	0.986 ± 0.018	0.942 ± 0.045	0.875 ± 0.011	0.807 ± 0.043	0.743 ± 0.046	0.565 ± 0.014
	Mordenite-1D	6.83±0.05	8.6±0.05	1.210± .041	1.190 ± 0.024	0.988 ± 0.033	0.907 ± 0.012	0.877 ± 0.053	0.679 ± 0.044	n.d
	ZSM-53D	23.59±0.05	10.33±0.05	0.991± .034	0.847 ± 0.025	0.728 ± 0. 032	0.699 ± 0.027	0.614 ± 0.04	n.d	n.d
	ZSM-53D	12.75±0.05	9.1±0.05	0.996± .036	0.928 ± 0.055	0.872 ± 0.046	0.743 ± 0.046	0.679 ± 0.044	n.d	n.d
	Ferrierite-2D	10.71±0.05	5.3±0.05	0.987± .026	0.907 ± 0.022	0.853 ± 0.042	0.760 ± 0.043	0.677 ± 0.046	n.d	n.d
	N/A	0.00±0.05	6.6±0.05	1.036± .030	0.923 ± 0.044	0.892 ± 0.034	0.869 ± 0.054	0.853 ± 0.042	0.760 ± 0.043	0.679 ± 0.044

From table 12 it can be seen that the Malathion concentration decreased with time in all the experiments. This was expected since it is the hydrolysis of malathion that leads to formation of MCA and DCA which are the major degradation products of malathion (Lalah&Wandiga, 2002)

4.9.1.1 Degradation products of Malathion in water

The degradation of malathion was investigated at concentrations of 10 ppm without zeolites. malathion monocarboxylic acid and the dicarboxylic acid were the only degradation products detected as shown in Figure50.
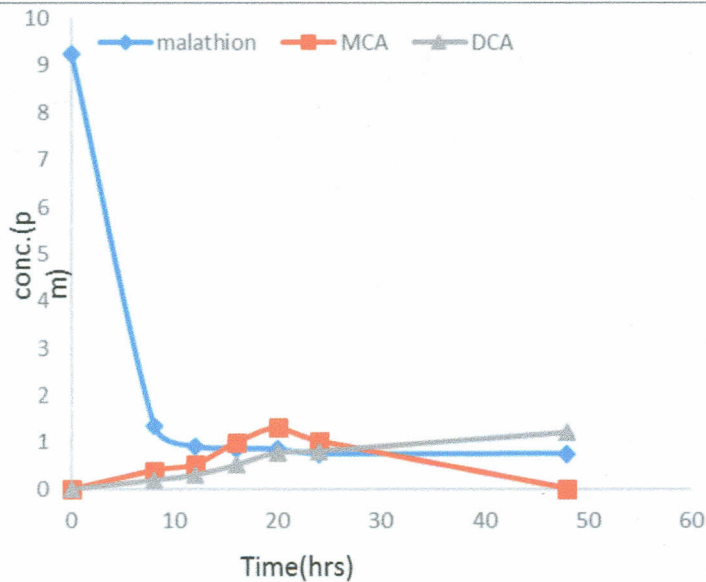
Figure 50: Distribution of degradation products of 10ppmMalathion without zeolites.
Where MCA is malathion monocarboxylic acid, DCA is malathion dicarboxylic acid

From Figure 50 it can be observed that the concentration of malathion dropped sharply within the first 9 hours of the experiment then reached equilibrium after 22 hours while the concentration of DCA and MCA increased but upon reaching 20 hours the concentration of MCA starts decreasing and at the end of the experiments its concentration was the lowest. This shows that the initial hydrolysis product was the malathion mono-carboxylic acid which still underwent further hydrolysis although at a slower rate (Hong, 1998)to form DMDTP and malathion di-carboxylic acids as the other hydrolysis products. Although DMDTP is identified as a product, it is more toxic as compared to the carboxylic acids. In alkaline conditions hydrolysis of malathion yields $(CH3O)_2P(S)Na$ and $(CH_3O)_2P(S)OH$ (Ogunah *et al.*, 2013).

4.9.1.2 Dissipation products of Malathion in water with zeolite

Upon introduction of the zeolites to the solution, degradation products were not detected from the extracts but malathion was detected at low concentrations as compared to the amount detected earlier with no zeolite treatments. Figure 51 illustrates the concentrations of malathion remaining in solutions with time with different treatments.

DISSIPATION OF MALATHION

Legend:
- fau=2.77
- mor=10.72
- mor=6.83
- zsm5=23.59
- zsm5=12.75
- fer=10.71
- water alone
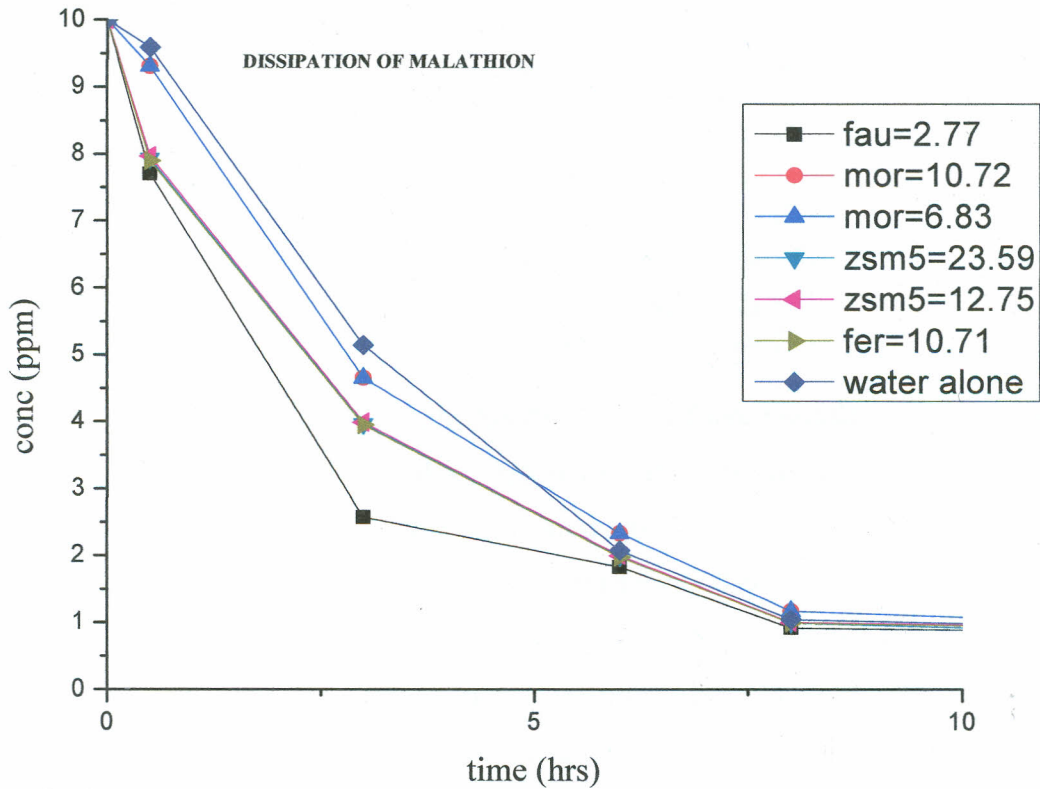
Figure 51: Distribution of 10ppm malathion in water treated with different zeolites

From the figure, it is seen that FAU is the most effective because the concentration of malathion remaining after 3 hours was the lowest as compared to the rest of the treatments followed by FER and then MFI. It can also be seen that what remained in water with no zeolite treatment was the highest as compared to the rest of the treatments which is evidence that zeolites enhance the decomposition of malathion in water.

91

4.9.1.3 Kinetic study of Malathion and effect of zeolites

The study was done within the pH indicated in table 10and the dissipation trend tested against zeroth, first and second order kinetics with respect to the disappearance of malathion based on the concentration of malathion found in water. The dissipation demonstrated pseudo first-order kinetics and by linear regression analysis, the first order plots gave the following reaction rates and constants as presented in the table.

Table 10: Half-lives of Malathion in river water (where K, degradation rate constant; R, regression coefficient; $t_{1/2}$, half-life period)

Pesticide	Zeolite type	Parameters				
		pH (a.u)	Si/Al (a.u)	K(h^{-1})	R^2 (a.u)	$t_{1/2}$(h)
Malathion	Faujasite-3D	7.68	2.77	0.0420	0.979	16.5
	Mordenite-1D	4.1	10.72	0.0213	0.955	32.5
	Mordenite-1D	8.6	6.83	0.0229	0.926	30.3
	ZSM-5(sn27)-3D	10.33	23.59	0.0279	0.964	24.8
	ZSM-5(sn55)-3D	9.1	12.75	0.0247	0.972	28.1
	Ferrierite-2D	5.3	10.71	0.0233	0.986	29.7
	NONE	6.6	NONE	0.0140	0.874	49.5

First-order reaction model, degradation rate constant and half-live periods of the malathion were calculated from the data in Table 9 and are listed in Table 10.The data show that malathion degradation in water was enhanced by the introduction of zeolites. Among the zeolites investigated were faujasite, mordenite MFI and ferrierite. There were two MFI and two mordenite with different Si/Al ratio. The results show that FAU exhibited more acceleration on the degradation of malathion than other types of zeolites used. More interesting, the applied zeolites showed different impacts on malathion degradation in terms of Si/Al. When the same class of zeolite was used the rate was affected by the amount of aluminum in the zeolite with its increase lowered the half-life. Mordenite (Si/Al=6.83) exhibited stronger acceleration on the degradation of malathion than mordenite (Si/Al=10.72), as it led to the increase in rate constant and also the pHs. Ferrierite exhibited stronger acceleration on the degradation of malathion with a half-life of 29.7 hrs compared to 32.5hrs for mordenite. This shows that other parameters such as dimensionality may play more roles in the elimination process. Ferrierite has 2D while mordenite has 1D and this leads to faster rate of diffusion of malathion and its metabolites into ferrierite than in mordenite.

4.10 Effects of Si/Al ratio on degradation of Malathion

The Si/Al ratio of a zeolite cage is the most important factor affecting its chemical stability, hydrophilic properties, and occurrence of inter-crystalline defects. Zeolites have a structure that allows the creation of active sites, such as acid sites, whose strength and concentration can be controlled according to the desired application (Gates & Schuit, 1979). The concentration of Al in the structure plays a crucial role in the acidity of zeolites. Purely siliceous zeolites, materials not containing Al^{3+} or another trivalent metal are not acidic. The Bronsted acid sites in zeolites occur when the negative charge of the crystal structure is balanced by a hydrogen ion (Smith, 1993).

4.10.1 Effects of Si/Al on resultant reacting solution pH

Introduction of zeolites in water solution had some effects on the pH of the resultant medium. The effect of the solution pH upon introduction of the zeolites FAU, MOD, and ZSM-5 is depicted in Figure 52.

The plot shows pH values in water solution (y-axis, ranging from 6 to 11) versus Si/Al ratio (x-axis, ranging from 0 to 25) with a fitted curve:

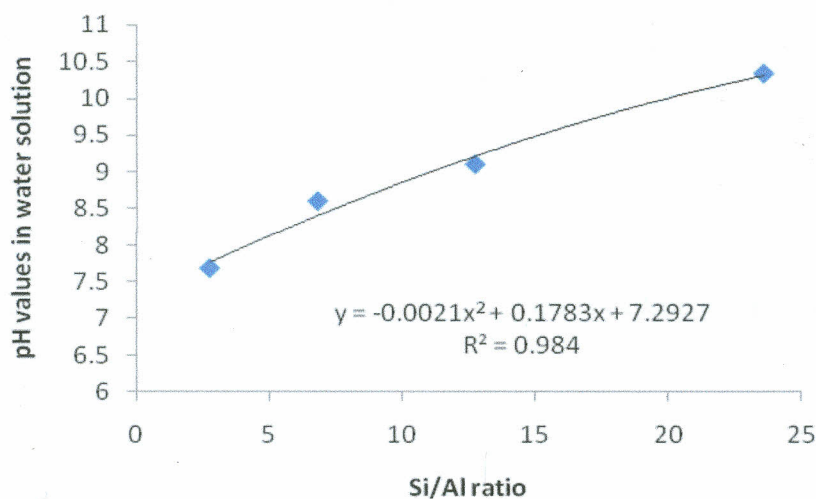$$y = -0.0021x^2 + 0.1783x + 7.2927$$
$$R^2 = 0.984$$

Figure 52: Variation of solution pH with Si/Al ratio of the zeolite.

The Si/Al ratio has a direct/polynomial relationship with the pH of the resulting solution in which the zeolite is dispersed. Thus it is important to note the resultant pH of a reaction media as

93

this will enhance or impede adsorption process. The overall result shows that malathion degradation in water was highly enhanced by the introduction of zeolites. The results were consistent with higher Si/Al ratio exhibiting accelerated degradation of malathion than other types of zeolites used. However, the zeolitic Si/Al ratio was not very significant in determining the half-life of malathion degradation in the waters.

4.10.2 Effects of Si/Al on Malathion dissipation half-life

The data show that malathion degradation in water was totally enhanced by the introduction of zeolites. The results show higher Si/Al ratio exhibited somewhat accelerated degradation of malathion than other types of zeolites used. Somehow, the indirect effect of the resulting pH may be investigated especially during evaluation of the degradation of dissipation mechanism.

The chart shows HALF-LIFE (H) on the y-axis (range 20 to 34) versus SI/AL RATIO on the x-axis (range 0 to 25), with trend line equation:
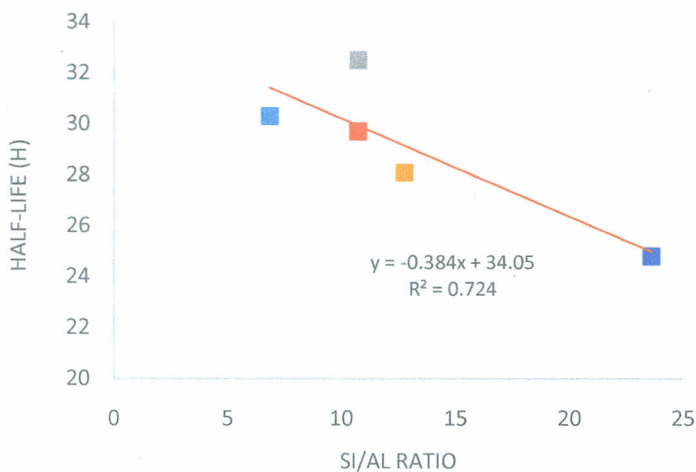
$$y = -0.384x + 34.05$$
$$R^2 = 0.724$$

Figure 53: Relationship between the half-lives of the Malathion dissipation and the Si/Al of the zeolites used.

4.10.3 Effects of solution pH on Malathion dissipation half-life

Table 54 shows the effect of solution pH on malathion dessipation half-lives.
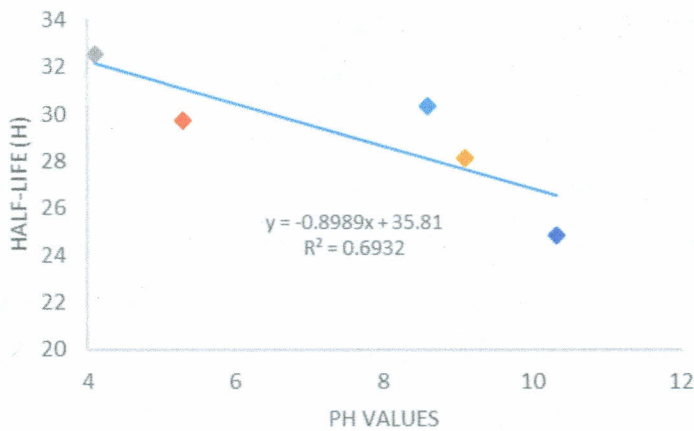

Figure 54: Effect of pH values on dessipation half-lives.

It is seen that pH, to some extent, does not affect the half-life values as much as the Si/Al ratio.Kowenje &Osewe (2015) similarly reported that ionic strength and pH had little effect on hydrocarbon sorption. Transformation of malathion essentially depends on the pH; as such the metabolites differ in acidic and alkaline conditions (Ogunna *et al.,* 2013).

The change of pH with addition of zeolite could have led to the experiments. Montgomery (2007) reported that hydrolysis products are dependent on pH.In alkaline solutions malathion hydrolyses to form diethyl fumarate and dimethyl phosphorodithioic acid(Bender & Davidson, 1969).

4.10.4 Effect of Channel, cage or cavity dimensionality on dissipation of Malathion

Dimensionality (D), whether 1D, 2D, or 3D, can also be applied to separate molecules and to purify the environment. The channel dimensions of the zeolites are another important aspect affecting solute removal. Besides size exclusion effects, it was also been observed that solutes, which do fit in the channels of ZSM5, MOR or Y zeolite, are removed more effectively when they fit tightly, because of larger van der Waals interactions. It has been reported that the

drawback of employing MFI-type zeolites in porous membranes is that the crystals must be oriented with respect to the permeation direction.

The interconnected inner channel in LTA offers the opportunity for simplified membrane fabrication since crystal alignment is unnecessary (Kowenje &Osewe, 2015; Blagica *et al.*, 2006). Because zeolite impact caging effects on adsorbates, some workers offer a different explanation of the differentiated adsorption by zeolites. Kowenje &Osewe(2015), offered an alternative or additional explanation that in the small channels of ZSM5 zeolite (about 5.5 Å) water is unable to form a structure which is typical for its liquid form and is actually present as vapour, making it easier for solutes to transport through the channels of ZSM5. In the larger cages of Y zeolite, water is still present in its liquid form. In Figure 55, shows the effects of 1D, 2D, and 3D orientations of zeolitic channels and cavities on the half-life of malathion degradation in waste waters.
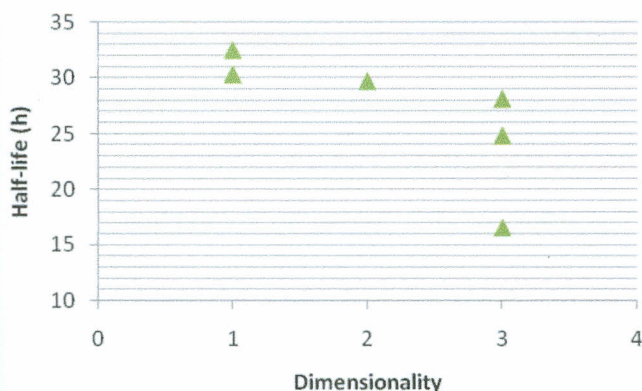
Figure 55: The variation of Malathion dissipation half-life with zeolite dimensionality

According to Figure 55, Faujasite (3D) exhibited stronger acceleration on the dissipation of malathion with a half-life of ca.16 hrs compared to 32.5hrs for mordenite (1D). This shows that dimensionality is a factor when it comes to pollutants elimination process. Ferrierite which possess 2D structure has somewhat intermediate half-life of ca. 29 hrs.

4.10.5 Effects of internal surface area and window opening on dissipation of Malathion

Solutes with a diameter closer to the zeolite pore dimension showed higher adsorption ("close fit mechanism"). An important consideration for applying zeolites in drinking water treatment practice is that their size exclusion and close fit adsorption mechanism makes them effective for the removal of specific solutes (Kowenje &Osewe, 2015).Because the Si:Al ratio allows for tuning of the surface properties and the resultant electrostatic double layer such membranes could also be tuned for specific ion selective applications. However, further work is needed to fully understand the connection between zeolite chemistry and membrane performance. In this study the dissipation half-life of malathion as affected by the largest window opening for FAU, MOR, and ZSM-5s zeolites was investigated and the relationship is as shown in the figure below.
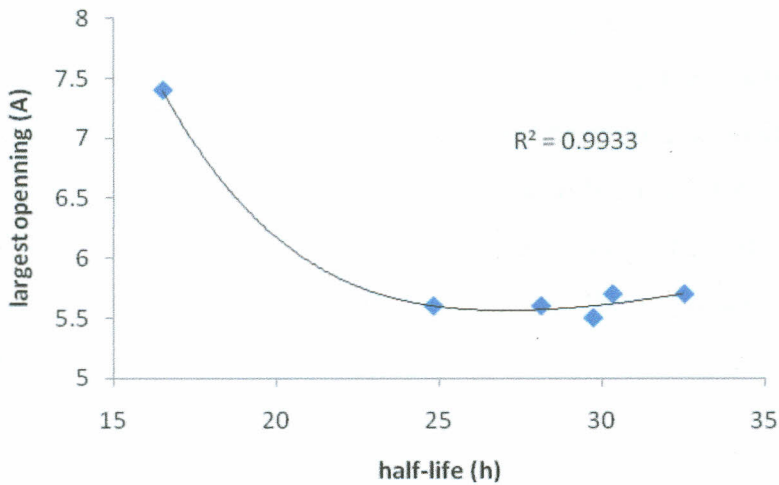
Figure 56: The relationship between the largest zeolite channel opening with half-life of the malathion.

The pesticide used in this study has critical diameter of ca. 7.0 Å. There are also branches of the molecule that are "straight chains" with critical diameters of ca. 4.0 Å (see Table 1). Because the zeolites have channel openings ranging from 5.5 – 7.4 Å, the pesticide would 'snake/reptate' through or just get half-way adsorbed in the channels. Whatever the mechanism, the above figure indicates that larger chenneled zeolites enhance the dessipation of the malathion faster in water. Specifically, Blagica *et al.*, (2006) quantified the amount of propanol adsorbed on silicalite was

about 70% of the pore volume. This observation is consistent with the fact that zeolites with bigger internal voids would ordinarily adsorb more adsorbates.

4.11 Efficiency of zeolites in the degradation of Malathion

Faujasite (3D) exhibited stronger acceleration on the degradation of malathion with a half-life of ca.16 h compared to 32.5 hrs for mordenite (1D). This shows that dimensionality is a factor when it comes to pollutants elimination process. Ferrierite, which possesses 2D structure, had somewhat intermediate half-life of ca. 29 hrs.

The pesticide used in this study has critical diameter of ca. 7.0 Å. There are also branches of the molecule that are "straight chains" with critical diameters of ca. 4.0 Å (see Table 1). Since the zeolites have channel openings ranging from 5.5 – 7.4 Å, the pesticide would 'snake/reptate' through or get half-way adsorbed in the channels. Irrespective of the mechanism, the Figure 56indicates that larger chenneled zeolites enhance the dessipation of the malathion faster in water. Specifically, Blagica et al. (2006) quantifiedthe amount of propanol adsorbed on silicalite was about 70% of the pore volume. This observation is consistent with the fact that zeolites with bigger internal viods would ordinarily adsorb more adsorbates. It is evident that water treated with the zeolite had malathion degrading faster than that without. On comparison, faujasite seemed to be more efficient in enhancing the degradation of malathion than the other five remaining zeolite.

4.12 Adsorption isotherm studies

The adsorption of malathion on different types of zeolite was studied for initial concentration 10ppm and contact time (0-70hrs) at 25 °C as shown in Figure 57below. It can be seen that adsorption capacity of the zeolites reached equilibrium in approximately 7 h for six different types of zeolites.
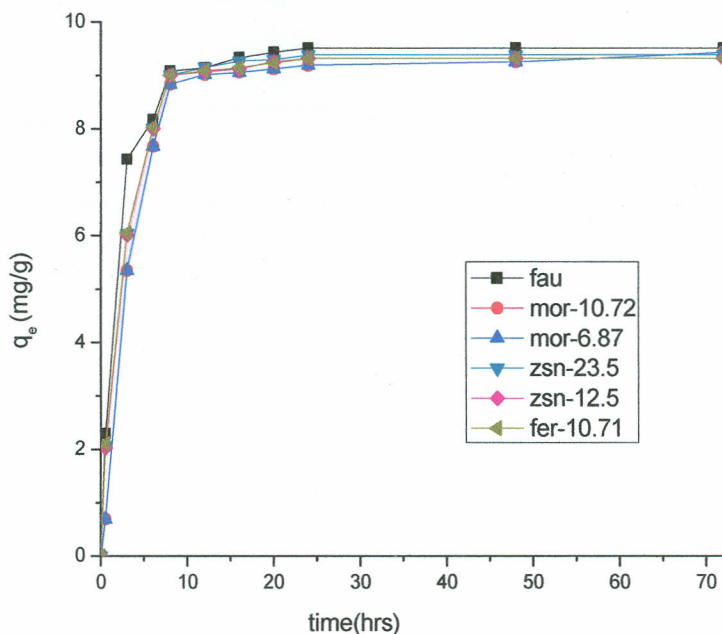
Figure 57: Effect of contact time on the adsorption of Malathion from aqueous solution by different types of zeolite at initial concentration of 10ppm

The graph of log q_e verses log C_e showing Freundlich adsorption isotherm of malathion on zeolites and a graph of C_e against C_e/q_e showing Langmuir adsorption isotherm of malathion on zeolite were drawn for each treatment. The Langmuir model is based on the assumption that the maximum adsorption occurs when a saturated monolayer of solute molecules is present on the adsorbent surface, the energy of adsorption is constant and there is no migration of adsorbate molecules in the surface plane. The Freundlich isotherm model is an empirical relationship describing the adsorption of solutes from a liquid to a solid surface and assumes that different sites with several adsorption energies are involved. Langmuir and Freundlich adsorption constants are tabulated in Table 11.

99

Table 11: Studied Langmuir and Freundlich parameters for Malathion adsorption (mmol/g) by zeolites from aqueous solution at 25°C

Zeolites	Langmuir Isotherm			Freundlich Isotherm		
	q_{max}(mg/g)	K_L (L/mol)	R^2	n	K_F	R^2
Ferrierite(Si/Al=10.71)	2.079	0.921	0.914	1.934	8.723	0.814
Mordenite (Si/Al=10.72)	0.722	1.138	0.847	1.314	8.551	0.727
Mordenite (Si/Al=6.83)	0.722	1.138	0.847	1.314	8.551	0.727
MFI(Si/Al=23.59)	2.070	0.886	0.911	2.016	8.472	0.800
MFI (Si/Al=12.75)	2.012	1.835	0.912	1.901	8.750	0.810
USY(Si/Al=2.81)	3.300	1.000	0.952	7.299	8.723	0.944

It can be seen that Langmuir isotherm exhibits higher correlation coefficient values (R^2), which implies considerably better fit compared to Freundlich isotherm. Maximum adsorption capacity of MFI (12.75)-zeolite (2.012 mg.g^{-1}) and higher K_L value (1.85 L.mol^{-1}) were obtained at 27°C. Higher K_L value also implied strong bonding of malathion to zeolite at this temperature.

CHAPTER FIVE

SUMMARY, CONCLUSIONS AND RECOMMENDATIONS

5.1 Summary

This study sought to establish the effects of the Na-zeolites on the degradation and elimination of the pesticide malathion from fresh water. The study investigated four types of zeolites, FAU, FERR, MFI and MOR under different Si/Al ration and dimensionality (1D, 2D and 3D) on malathion spiked in water. From the data presented in this report and those from literature elsewhere, the following summary can be made.

I.   Malathion degradation in water was highly enhanced by the introduction of Na-zeolites

II.   The half-life of malathion in fresh water was found to be49.5hrs and upon introduction of the Faujasite zeolites half-life was 16.5 hrs, mordenite 30.3 hrs ZSM 24.8 hrs ferrierite 29.7 hrs respectively.

III.   Dimensionality is a factor when it comes to pollutants elimination process that is 3D is more effective followed by 2D then finally 1D.

IV.   Larger channeled zeolites enhance the dissipation of malathion faster in water.

V.   Major degradation products of malathion in water alone were malathion mono and dicarboxylic acids but upon introduction of zeolite the products are eliminated

VI.   Mechanism for degradation of malathion is hydrolysis of two ethyl ester groups attached to S-C and P-S-C bonds.

VII.   From XRD analysis the increase in crystallinity is evidence that malathion is adsorbed in the zeolite structure and lack of new peaks show that the structure of zeolite is not affected as there is no formation of new bonds.

VIII. From IR analysis, the reduction in intensity at 2362 and 2338cm^{-1} and shifting of bands to higher wave numbers for example 3438 to 3598 cm^{-1}and band 1038 to 1050 cm^{-1}show that there's interaction of malathion molecules with the zeolite structure.

IX.   From IR studies, lack of new bands shows that there's no formation of new chemical bonds between malathion and zeolite and only possibility is the attraction of molecules with stronger electrostatic forces during adsorption.

X.   From IR analysis the formation of the $1629 cm^{-1}$ to $1636 cm^{-1}$ absorption bands indicate the formation of hydrogen bonding between carbonyl group of malathion molecules associated with the sodium ion on the interlayer surface.

XI.   From the solid state NMR analysis there's an intense peak at 56.3 ppm attributed to coordinated aluminum tetrahedral Al^{+4} indicating presence of aluminum and a low peak centered at 0 ppm showing presence of aluminum in octahedral environment. Upon introduction of malathion the interaction is absent showing that there's no chemical bond formed between the metabolites of malathion and the zeolite. The possible bond can only be formed in the aluminum sites and their absence indicate that they are adsorbed and held together by strong electrostatic forces due to presence of phosphorus which is more electronegative than oxygen.

XII.   From the EDS analysis the presence of phosphorus and sulphur in the zeolite after exposure to malathion confirms the introduction of malathion in the zeolite structure.

XIII.   Malathion degradation in fresh water was found to undergo *pseudo*-first order kinetics ($R^2=0.996$) with rate constant of-$0.144\pm0.010 hr.^{-1}$.On addition of both Na-zeolites the kinetics was also found to be pseudo-first order but with different R^2 values and rate constants.

XIV.   Faujasite was found to have the highest percentage in the degradation of malathion in this study.

XV.   High Si/Al ratio exhibit accelerated degradation of malathion.

XVI.   Si/Al ratio had direct multiple relationship with the pH of the resulting solution.

XVII.   Ionic strength and pH had little effect in the half-life values for the degradation of malathion but they influences the type of metabolites formed.

5.2 Conclusions

With the respect to the summary above, the null hypothesis was adopted and the conclusions therefore are;

I.   Si/Al ratio had direct multiple relationships with the pH of the resultant solution.

II. High Si/Al ratio exhibited accelerated degradation of malathion while pH had little effect on half-life values for degradation malathion.

III. Larger channeled zeolites enhanced the dissipation of malathion in water and dimensionality of zeolite also had effect on dissipation half-life.

IV. Malathion degradation in fresh water and in the absence of zeolites produced malathion mono-and malathion di-carboxylic acids as well but upon introduction of zeolites the metabolites were not detected

V. Malathion degradation, in fresh water and fresh water with zeolites, underwent pseudo-first order kinetics.

VI. Malathion adsorption did not affect the structure of the zeolite.

5.3 Recommendations

In this work, it has been successfully shown that malathion dissipation was enhanced in Na-zeolites and followed pseudo-first order kinetics. High Si/Al ratio encouraged dissipation of malathion while the solution pH only influenced the type of metabolites formed. Effectiveness of dimensionality decreased in the order of 3D, 2D then 1D. Larger channeled zeolites also enhanced the dissipation of malathion in water. Further efforts, arising the following require further investigation::

I. The effect of the different molecular sizes of pesticide on different types of zeolites,

II. To understand the nature of the interactions, if any, between channel size and the molecular size of the other pesticides

REFERENCES

Arnold, R. B. (1996). Update: ASTM/ISR Paper Aging Research Program . *The Abbey Newsletter, 20(3)*, 29-30.

ATSDR. (2005). *Toxicological information about malathion used for eradicating mosquitoes (West Nile Virus Control).* ATSDR.

Baerlocher, C., McCusker, L. B., and Olson, D. H. (2007). Atlas of zeolite framework types. *Elsevier.*

Barrer, R. M. (1985). Synthesis of zeolites . *Studies in Surface Science and Catalysis, 24*, 1-26.

Bender, C. F., and Davidson, E. R. (1969). *Studies in configuration interaction: The first-row diatomic hydrides.*

Blagica, C., Kocev, D., Kolcakovska, E., and Stojanova, D. (2006). Zeolites as alcohol adsorbents from aqueous solutions. . *APTEFF, 37*, 83-87,.

Blocki, S. W. (1993). Hydrophobic Zeolite Adsorbent: A Proven Advancement in Solvent Separation Technology. *Environmental Progress 12(3)*, 226-230.

Breck, D. W. (1974). *Zeolites Molecular Sieves, Structure Chemistry and Use.* New York: Wiley

.

Caldwell, J. (1984). Xenobiotic acyl-coenzymes A: critical intermediates in the biochemical pharmacology and toxicology of carboxylic acids.

Chen, G. J., McDonald, J. W., and Newton, W. E. (1976). Synthesis of molybdenum (IV) and molybdenum (V) complexes using oxo abstraction by phosphines Mechanistic implications. *Inorganic Chemistry, 15(11)*, 2612-2615.

Chen, Y. L., Analytis, J. G., Chu, J. H., Liu, Z. K., Mo, S. K., Qi, X. L., and Zhang, S. C. (2009). Experimental realization of a three-dimensional topological insulator. *Bi2Te3. Science, 325(5937), ,* 178-181.

Clark, G., & Phillips, A. (2014). *Inside book publishing.* Routledge.

Corma, A., Corell, C., and Pérez-Pariente, J. (1995). Synthesis and characterization of the MCM-22 zeolite. *Zeolites, 15(1)*, 2-8.

Egerton, R. F. (2005). *Physical principles of electron microscopy*. New York: Springer.

Flanigen, E. M. (1980). Molecular sieve zeolite technology — the first Twenty-five years. *Pure & Appl.Chem., 52*, 2191—2211.

Gadekar, L. S., Katkar, S. S., Vidhate, K. N., Arbad, B. R., and Lande, M. K. (2008). *Modification characterization and catalytic potency of modified natural zeolite for Knoevenagel condensation reaction.* Bulletin of the Catalysis Society of India.

Gallo, M. A., and Lawryk, N. J. (1991). Organic phosphorus pesticides. *Handbook of pesticide toxicology, 2*, 917-1123.

Gates, B. R., and Schuit, G. C. (1979). *Chemistry of catalytic process.* New York.: McGraw – Hill.

Hong, F., (1998). Hydrolysis of phorate using simulated environmental conditions: rates, mechanisms, and product analysis. *Journal of agricultural and food chemistry, 46(3)*, 1192-1199.

Howard, P. H. (1991). *Handbook of environmental fate and exposure data for organicChemicals vol 3:pesticides.* . Chelsea : Lewis Publishers.

Humplik, T., Raj, R., Maroo, S. C., Laoui, T., and Wang, E. (2014). Effect of hydrophilic defects on water transport in MFI zeolites. *Langmuir. 30(22)*, 6446-53.

Jacobsen, C. J., Madsen, C., Houzvicka, J., Schmidt, I., and Carlsson, A. (2000). Mesoporous zeolite single crystals. *Journal of the American Chemical Society, 122(29)*, 7116-7117.

Javed, S., Aslam, U., Kazmi, M., Rustam, M., Riaz, S. and Munir, Z. (2015). Studies on Thermal Degradation Behavior of Siliceous Agriculture Waste (Rice Husk, Wheat Husk and Bagasse). *Polish Journal of Chemical Technology, 17(1)*, 47–51.

Jonam, L. K., Diuna, T., Stanic, T., and Pfend. (2006). Institute for technology of nuclear and other mineral raw materials. *Water Research (Water Res.)*.

Jungho, J., Tompsett, G. A., Foster, A. J., Hammond, K. D., Auerbach, S. M., and Lobo, R. F. (2011). Investigation into the shape selectivity of zeolite catalysts for biomass conversion. *Journal of Catalysis 279 (2011)* , 257–268.

Kanyi, C. E., (2006). "Linear, Primary Monohaloalkne Chemistry in NaX and NaY Faujasites with and without NaO . *Activation. Zeolites as Nucleophilic Reactions II" Microporous and Mesoporous Materials, 92,*, 295 –302.

Karmen, L. M., Nataša, Z., Šiljeg, M., and Farkaš, A. (2013. *Natural Zeolites in Water Treatment – How Effective is Their Use.* Retrieved from http://dx.doi.org/10.5772 /50738. 2013.

Kazemimoghadam, M., and Mohammadi, T. (2007). Synthesis of MFI zeolite membranes for water desalination. *Desalination, 206(1-3)* , 547-553.

Kowenje, C., Jones, B. R., Doetschman, D., Yang, S., and Kanyi, C. (2006). "Effects of cation siting and spin-spin interactions on the electron paramagnetic resonance (EPR) OF Cu2+ exchanged X faujasite zeolite" paper in press in chemical physics.

Lala, J. O., Acholla, F. V., and Wandiga, S. O. (1994). The fate of 14C-p,p'-DDT in Kenya tropical soils. *J.Environ. Sci. Health B 29*, 57-64.

Lalah, J. O., and Wandiga, S. O. (2002). The effect of boiling on the removal of persistent malathion residues from stored grains. *Journal of stored products research, 38(1)*, 1-10.

Lalah, J., Yugi, P., Jumba, I., and Wandiga, S. (2003). Organochlorine pesticide residues in Tana and Sabaki rivers in Kenya. *Bull Environ. Contam. Toxicol. 71*, 298-307.

Leardini, L., Martucci, A., Braschi, I., Blasioli, S., and Quartieri, S. (2014). Regeneration of high-silica zeolites after sulfamethoxazole antibiotic adsorption: a combined in situ high-temperature synchrotron X-ray powder diffraction and thermal degradation study. *Mineralogical Magazine, 78(5)*, 1141-1160.

Luna, F. J., Ukawa, S. E., Wallau, M., and Schuchardt, U. (1997). Cyclohexane oxidation using transition metal-containing aluminophosphates (MAPO-VFI). *Journal of Molecular Catalysis A: Chemical, 117(1-3)*, 405-411.

106

Lynam, M. M., and Keeler, G. J. (2005). Automated speciated mercury measurements in Michigan. *Environmental science & technology, 39(23)*, 9253-9262.

Mehlhorn, H., and Armstrong, P. M. (2001). Encyclopedic Reference of Parasitology: Diseases, Treatment. *Therapy, 2,* , 363.

Meier, W. M., and Olson, D. H. (1970). Zeolite frameworks. Molecular Sieve Zeolites-I. *Advances in Chemistry Series, 101*, 155-170.

Montgomery, D. R. (2007). Soil erosion and agricultural sustainability. *Proceedings of the National Academy of Sciences, 104(33)*, (pp. 13268-13272).

Mulla, M. S., and Mian, L. S. (1981). Biological and environmental impacts of the insecticides malathion and parathion on nontarget biota in aquatic ecosystems. In Residue Reviews . *Springer New York*, 101-135.

Neal, R., McCool, P., and Younglove, T. (1993). *Assessment of malathion and malaoxon concentration and persistence in water, sand, soil and plant matrices under controlled exposure conditions.* Riverside CA: California department of pesticide regulation, environmental hazards assessment program.University of California, .

Newhart, K. (2006). *Environmental fate of malathion. .* California Environmental Protection Agency.

Occelli, M. L., and Robson, H. E. (1989). *Zeolite synthesis.* American Chemical Society.

Ogunah, J. A., Kowenje, C. O., Osewe, E. T., Lalah, J. O., Jaoko, D. A., and Koigi, R. N. (2013). Effects of zeolites X and Y on the degradation of malathion in water. . *Science, 1(1)*, 7-13.

Papageorgiou, S. K., Katsaros, F. K., Kouvelos, E. P., Nolan, J. W., Le Deit, H., and Kanellopoulos, N. K. (2006). Heavy metal sorption by calcium alginate beads from Laminaria digitata. *Journal of Hazardous Materials, 137(3)*, 1765-1772.

Parfitt, R. L., and Mortland, M. M. (1968). Ketone adsorption on montmorillonite . *Soil Science Society of America Journal, 32(3)*, 355-363.

Pérez, L. L., Ortiz-Iniesta, M. J., Zhang, Z., Agirrezabal-Telleria, I., Santes, M., Heeres, H. J., and Melián-Cabrera, I. (2013). Detemplation of soft mesoporous silica nanoparticles with structural preservation. *Journal of Materials Chemistry A, 1(15)*, 4747-4753.

Quantities, P. (1991). *Handbook, Ed. by IS Grigor'ev and EZ Meilikhov* . Moscow,: Énergoatomizdat.

Rabo, J. A. (1976). Zeolite chemistry and catalysis. *Amer Chemical Society, 171*.

Rissato, S. R. (2007). Multiresidue determination of pesticides in honey samples by gas chromatography–mass spectrometry and application in environmental contamination. *Food Chemistry, 101(4)*, 1719-1726.

Robson, H. (2001). *Verified synthesis of zeolitic materials.* Gulf Professional Publishing.

Rouy, N. (1983). *U.S. Patent No. 4,367,180* . Washington, DC: U.S: Patent and Trademark Office.

Scharf, J. E. (2003). *Dermal absorption of a dilute aqueous solution of malathion.* Masters Thesis, University of South Florida, U.S.A.

Shoumkova, A. (2011). *Zeolites for water and wastewater treatment: An overview. Research Bulletin of the Special Issue on Global Fresh Water Shortage, 2(10).* Australian Institute of High Energetic Materials,.

Smith, J. V. (1993). *Origin and structure of zeolite in zeolite chemistry and catalysis.* . Chemical Society.

Spence, K. (2007). *Preparation of high-silica zeolite beads from silica gel. Worcecter Polytechnic Institute.* Unpublished Masters Thesis.

Treacy, M. M., Higgins, J. B., and Ballmoos, R. (1996). Collection of simulated XRD powder patterns for zeolites. *Zeolites, 5(16)*, 330-802.

Vartuli, J. C., Shih, S. S., Kresge, C. T., and Beck, J. S. (1998). *Potential applications for M41S type mesoporous molecular sieves.*

Wabule, M. N., Ngaruiya, P. N., Kimmins, F. K., and Silverside, P. J. (2004). Registration for biocontrol agents in Kenya.

Wandiga, S. O. (1996). *Organochlorine pesticides: Curse or blessings of the tropical environment, in: Environment and Development in Kenya. Kenya National Academy of Sciences Public Lecture Series.* Nairobi: of Sciences Public Lecture Series, Kenya National Academy of Science.

Wandiga, S. O. (2002). Accumulation, distribution and metabolism of 14C-1,1,1- Trichloro- 2,2-,bis(P-Chlorophenyl)ethane(p,p-DDT) residues in a model Tropical marine Ecosystem,. *Environmental Technology, 23*, 1285-1292.

Wandiga, S., & Mghenyi, J. M. (1988). *Isotope techniques for studying the fate of persistent pesticides in the tropics CRP report,.* Vienna: IAEA.

Ware, W. (1992). *Reviews of environmental contamination and toxicology, Springer-.* New York: Springer - Verlag Inc.

Weitkamp, J. (2000). Zeolites and catalysis. *Solid State Ionics, 131(1)* , 175-188.

Wilkinson, A. P. (2014). *Zeolitic Materials: Ion Exchange and Shape Selective Catalysis.* Retrieved from School of Chemistry and Biochemistry Georgia Institute of Technology Atlanta GA 30332- 0400.

Wolfe, N. L., Gordon, J. A., and Zepp, R. (1975). Kinetic investigation of malathion degradation in water. *Bulletin of Environmental Contamination and Toxicology 13(6),* 707-713.

Worthing, C. R. (1979). The pesticides manuals, a world compendium of British crop protective control.

Yang, S. (2006). "Sodium X-Type Faujasite Zeolite Decomposition of Dimethyl Methylphosphonate (DMMP) to methylphosphonate. Nucleophilic Zeolite Reactions I.". *Microporous and mesoporous materials 92,* 56 – 60.

Zhao, D., Cleare, K., Oliver, C., Ingram, C., Cook, D., Szostak, R., and Kevan, L. (1988). Characteristics of the synthetic heulandite-clinoptilolite family of zeolites. . *Microporous and Mesoporous Materials, 21(4-6),* 371-379.

Zweig, G., and Devine, J. M. (1969). Determination of organophosphorus pesticides in water. *Residue Reviews/Rückstands-Berichte, Springer New York.*, 17-36